# EPoS 2014

## Conference summary

João Alves
Univ. Vienna

37 talks, 4 discussions, 34 posters

***Being invited to do a conference summary talk means your career has reached its end.***

— Neil Evans (via Ted Bergin)

# Outline

- New topics compared to previous EPoS
- The conflicting
- The intriguing
- The lovely

# New topics

# The Milky Way!

## From local to global star formation

***Dobbs**: MW GMCs are "Universal", Extragalactic are not.*
***Molinari**: HiGal - spiral arms as collectors, not triggers*
***Falgarone**: Planck maps (foregrounds + Polarization)*
***Henning**: Large mol. filaments, perpendicular to the plane, not in spiral arms, 1e5Msun, 60-230pc (Orion-like?)*
***Motte**: Herschel HOBYS, super-critical filaments, DR21 (Orion OMC2-OMC3?),MonR2*
***Csengeri**: ATLASGAL is open! short SF time, quiescent SiO*
***Zahorecz**: Planck cold cores*

# THOR


**S. Bihr[1], H. Beuther[1], K. Johnston[1], J. Ott[2], S. Glover[3], P. Carlhoff[4], A. Brunthaler[5], P. Goldsmith[6], P. Schilke[4], F. Motte[7], T. Henning[1] and the THOR team**

[1] Max Planck Institute for Astronomy (MPIA), [2]NRAO Socorro, [3]Institute for Theoretical Astrophysics Heidelberg, [4]University of Cologne, [5]Max Planck Institute for Radioastronomy Bonn, [6]Jet Propulsion Laboratory, [7]Laboratoire AIM, CEA/IRFU - CNRS/INSU - University of Paris


## The HI, OH, Recombination Line Survey of the Milky Way

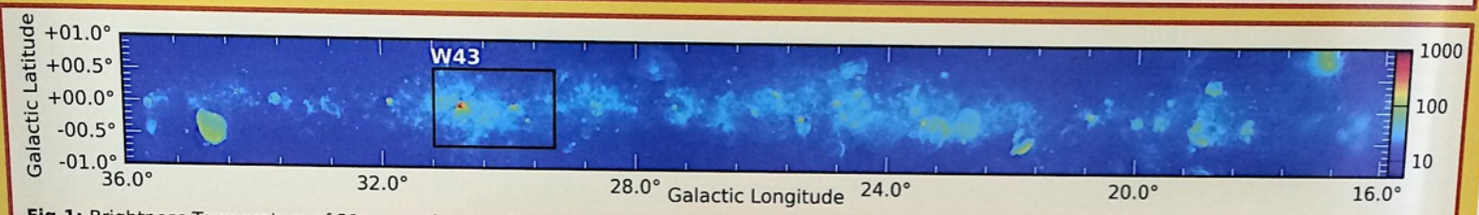


**Fig.1:** Brightness Temperature of 21cm continuum of part of the THOR survey


**Abstract:**

'CO-dark molecular hydrogen' is a well-known problem in molecular cloud observations. On the other hand, neutral atomic hydrogen is directly observable via the well-known 21cm line. Usually, the 21cm line is assumed to be optically thin. Column densities and masses are calculated with this assumption. However, a significant fraction of HI can be hidden by optical depth effects, such as self absorption (HISA - HI self absorption) or contamination of diffuse continuum emission in the background.


**Continuum and optical depth correction of HI data:**

As W43 has a strong continuum source in the center, we are able to measure the HI optical depth. This information can be used to correct for the optical depth as well as for the continuum emission. Fig.4 shows the column density assmuing opically thin emission and a clear correlation between the continuum emission and the column density is noticeable. But this is only an observational and not a physical effect. Fig.5 shows the corrected column density and the correlation vanished. This result is used for the further analysis.

**Fig.4:** HI column density of W43 assuming optically thin emission. Contours show the continuum emission at 21cm.

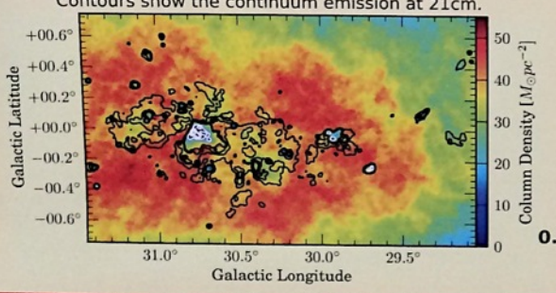


**M = 0.9 x $10^6 M_\odot$**

**Fig.5:** HI column density of W43 with optical depth/continuum corrections. Contours show the continuum emission at 21cm.




**Radial ditribution of HI column density:**

Fig. 4 shows the radial distribution of the HI column density from the center at l=30.5deg and b=0deg. The squares represent the corrected column density and the dots represent the optically thin assumption. Both methods show a clear increase in the column density towards the center. Close to the center the column density stays constant. This is likely due to the transition of HI to $H_2$.

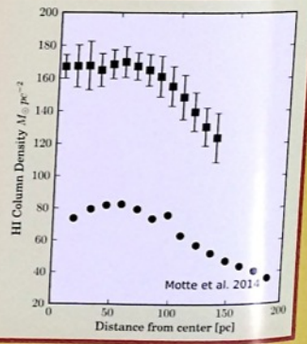


**Comparison to theory and low mass clouds**

The red line in Fig. 5 represents the cloud formation theory of Krumholz et al. 2009. They predict that the HI column density rises towards a certain level before HI can shield itself from the interstellar radiation field after which $H_2$ can form. This critical density is thought to be at ~$10 M_\odot pc^{-2}$. Lee at al. 2012 observed this threshold for the Perseus cloud. Our data is represented by the black dots and shows a much higher critical density of ~$100 M_\odot pc^{-2}$ = $1.25 \times 10^{22} cm^{-2}$. The reason for that could be the OB cluster in the center of W43, which produces a lot of radiation that prevents the formation of $H_2$.

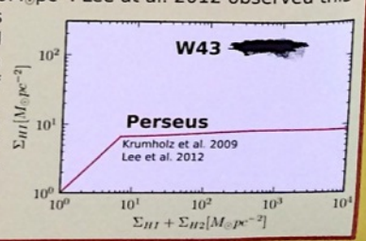



**Simon Bihr - bihr@mpia.de**

PhD student - IMPRS

Max Planck Institute for Astronomy

# Ionized, atomic and molecular carbon in *IRDCs*

H. Beuther[1], S. Ragan[1], H. Linz, Th. Henning[1], M. Nielbock[1], O. Krause[1], V. Ossenkopf[2], J. Stutzki[2], P. Schilke[2], S. Glover[3], and R. Güsten[4]
[1]*MPIA Heidelberg/Germany;* [2]*Uni. Cologne, Germany;* [3]*ITA Heidelberg/Germany;* [4]*MPIfR Bonn/Germany,* email: beuther@mpia.de

**Abstract: How do molecular clouds form out of the atomic phase? And what are the fractions of carbon in the ionized, atomic and molecular phase, respectively?** Using Herschel, Sofia, APEX and the IRAM 30 m telescope, we mapped the ionized, atomic and molecular carbon ([CII]@1901 GHz, [CI]@492 GHz and $C^{18}O$(2–1)@220 GHz) at high spatial resolution ($12'' - 25''$) in four young massive infrared dark clouds (IRDCs).

- Molecular $C^{18}O$ closely follows the dense gas. The atomic [CI] traces the dense gas as well, but extends also to lower column densities. The ionized [CII] exhibits diverse components from diffuse to more compact emission structures
- In at least two (G48.66, IRDC 18223 and maybe IRDC 18454) of the four regions, we find kinematic signatures indicating that the dense gas filaments have formed out of a dynamically active and turbulent atomic/molecular cloud, potentially from converging gas flows.
- The atomic-to-molecular carbon ratio is low (7–12%) with the lowest values toward the most quiescent region (Table 1). The ionized carbon emission depends partly on the radiation field, but [CII] is also strong in a region without significant external sources (G48.66) ⟶ other processes like energetic gas flows can also contribute to the [CII] excitation.

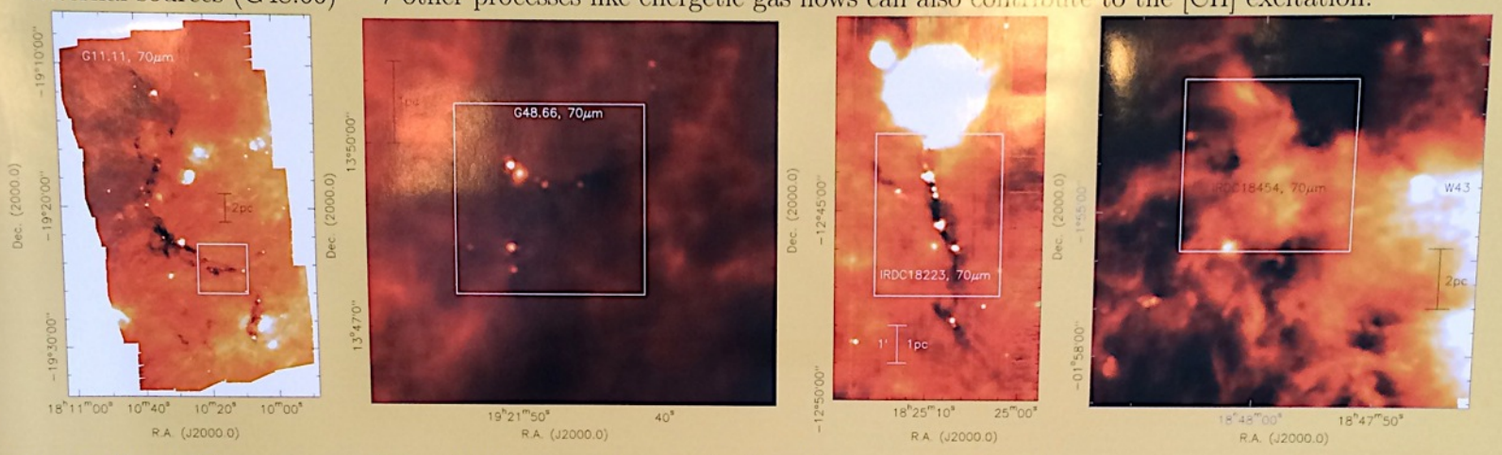


**Fig. 1:** Herschel 70 $\mu$m images of the four IRDCs selected for our study. The white boxes outline the regions mapped in the different carbon lines.

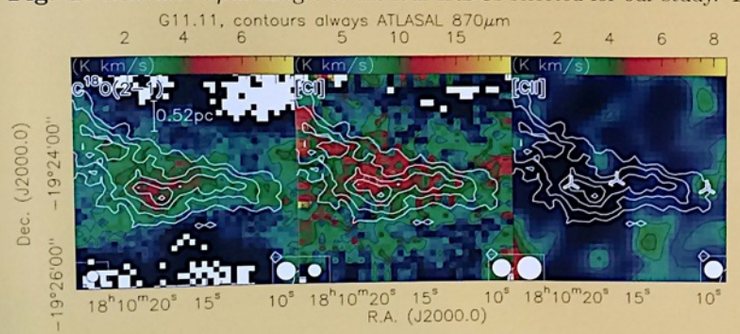


**Fig. 2:** Integrated molecular, atomic and ionized carbon (Herschel) emission for G11.11. The white contours show the ATLASGAL 870 $\mu$m emission. This is the only region where [CII] remains undetected.

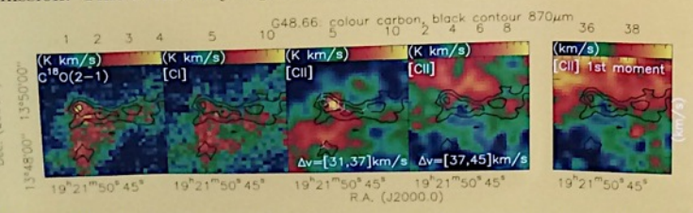


**Fig. 3:** Integrated molecular, atomic and ionized carbon (Herschel) emission for G48.66. The black contours show the ATLASGAL 870 $\mu$m emission. The two [CII] panels represent the different velocity regimes also visible in the spectra in Fig. 6. The fifth right panel presents the [CII] 1st moment map (intensity-weighted velocity) with the clear velocity gradient across the filament. This may be a signature of converging gas flows.

Table 1: Masses of different carbon phases for the 4 regions

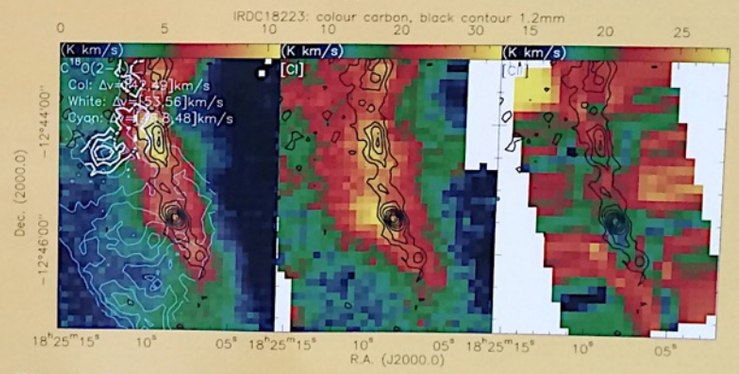


**Fig. 4:** Integrated molecular, atomic and ionized carbon (Sofia) emission for IRDC 18223. The black contours show the MAMBO 1.2 mm emission. The white an cyan contours present different velocity regimes also observable in the [CI] line (see also Fig. 6).

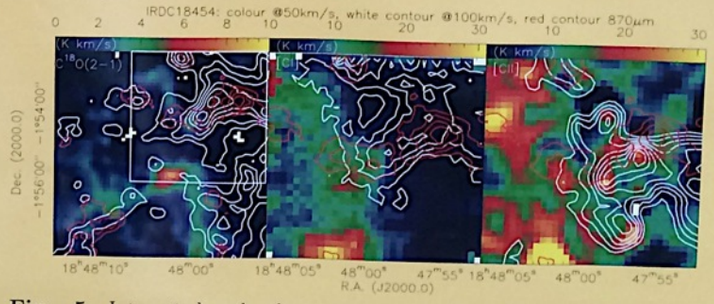


**Fig. 5:** Integrated molecular, atomic and ionized carbon (Herschel) for IRDC 18454. The color scale and white contours show the

Henrik Beuther

# Herschel view of massive star formation in NGC 6357

*Tigé J. (LAM), Schneider N. (CEA), Men'shchikov A. (CEA), Zavagno A. (LAM), Motte F. (CEA), Bontemps S. (LAB), Russeil D. (LAM), Molinari S. (INAF), White G. (RAL), Anderson L. (West Virginia University) et al.*

**Context:** The Herschel imaging survey of OB Young Stellar Objects (HOBYS) is the first systematic survey of a complete sample of nearby (within 3 kpc) high-mass star-forming regions (Motte et al. 2010).
The HOBYS program targets 10 molecular complexes forming OB-type stars at five wavelengths from 70 to 500 µm, one of which is NGC 6357, a giant molecular cloud located at 1.75 kpc which arbours many OB stars mainly located in the stellar cluster Pismis-24 (Persi and Tapia 2008).

**Method:** We use the source extraction algorithm '*getsources*' (Men'shchikov et al., 2012) to extract cores and measure their fluxes at all *Herschel* wavelengths. We also use MIPSGAL, ATLASGAL and SIMBA 1.2mm maps. We apply criteria on S/N ratio, size and ellipticity to select only the cores that represent circular-shaped "dense" cores with size around 0.1-0.2 pc. The spectral energy distribution is then fitted to determine physical parameters for the dense cores (temperature, envelope mass, luminosity).

**Goal - Massive Dense Cores (MDCs):** We want to make a census of the MDCs in NGC 6357, the cores that are potentially dense and massive enough to form one/several massive stars, and analyse their properties and locations regarding the current HII regions and stellar clusters of NGC 6357.
But what is the minimum amount of gas needed to form a massive star ?

For this we cross-correlated our dense cores catalog with known radio compact sources (<0.1pc) and 6.7-GHz methanol masers catalogs

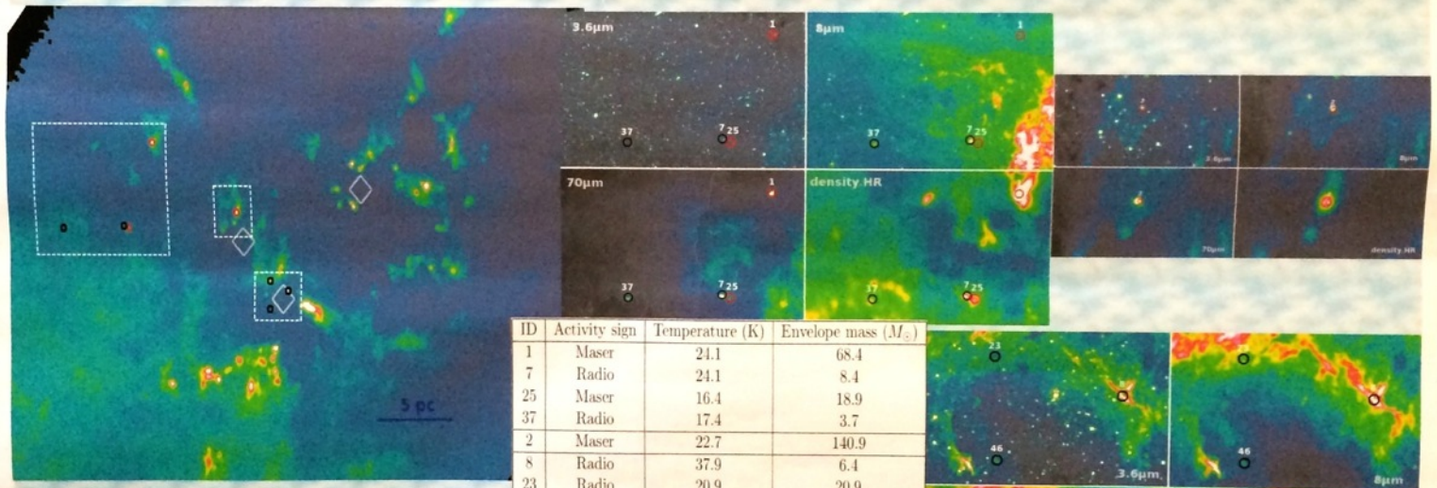


| ID | Activity sign | Temperature (K) | Envelope mass ($M_\odot$) |
|---|---|---|---|
| 1 | Maser | 24.1 | 68.4 |
| 7 | Radio | 24.1 | 8.4 |
| 25 | Maser | 16.4 | 18.9 |
| 37 | Radio | 17.4 | 3.7 |
| 2 | Maser | 22.7 | 140.9 |
| 8 | Radio | 37.9 | 6.4 |
| 23 | Radio | 20.9 | 20.9 |
| 46 | Radio | 26.6 | 6.1 |

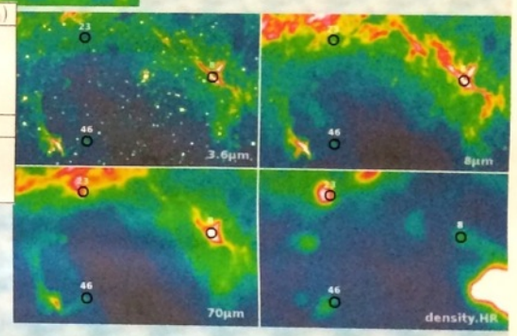


**Left** : Column density map with stellar clusters (grey diamond), ClassII methanol masers (red circles) and compact radio sources (black circles)
**Right** : Multi-wavelength view of the three white sub-zones
**Table**: SED fitting results

Inside the region, dense cores with 6.7Ghz maser activity are found more massive (140.9 M⊙) than dense cores with compact radio sources (6.1-20.9 M⊙)

Compact radio sources may represent an evolutionary stage when the cold envelope is already dissipated as they are seen at the edge of cold clumps

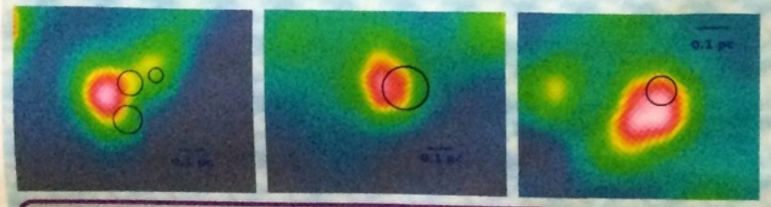


Column density map of selected clumps in NGC 6357 with radio compact sources at their edge

This results suggest to use the 6.7GHz masers associated mass as the minimum amount of gas for dense cores to be considered 'massive' and able to potentially form massive stars

References :
Men'shchikov et al. 2012 A&A 542


Jeremy Tigé

# W51

## Adam Ginsburg
## Fellow

Most luminous star-forming complex (Urquhart et al 2014)
$10^6$ $M_\odot$ (Carpenter & Sanders 1998)

Forming 1-2 massive clusters, M>$10^4$ $M_\odot$ & R<2 pc:
W51 IRS 2 & W51 Main (Ginsburg et al 2012)

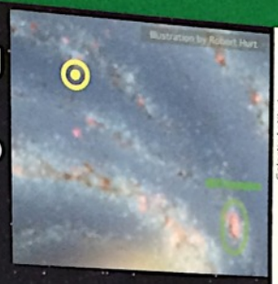

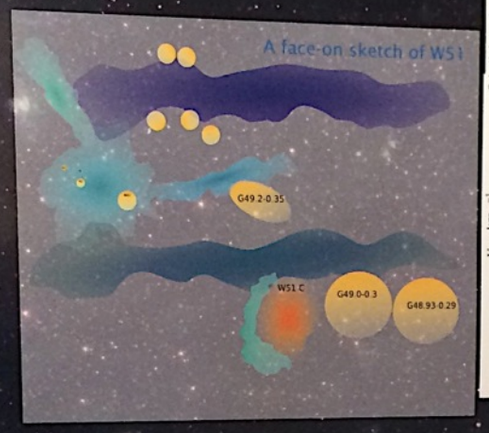


The top half of this poster shows large-scale figures, illustrating the geometry of the region.

The lower portion shows zoomed-in views with the VLA

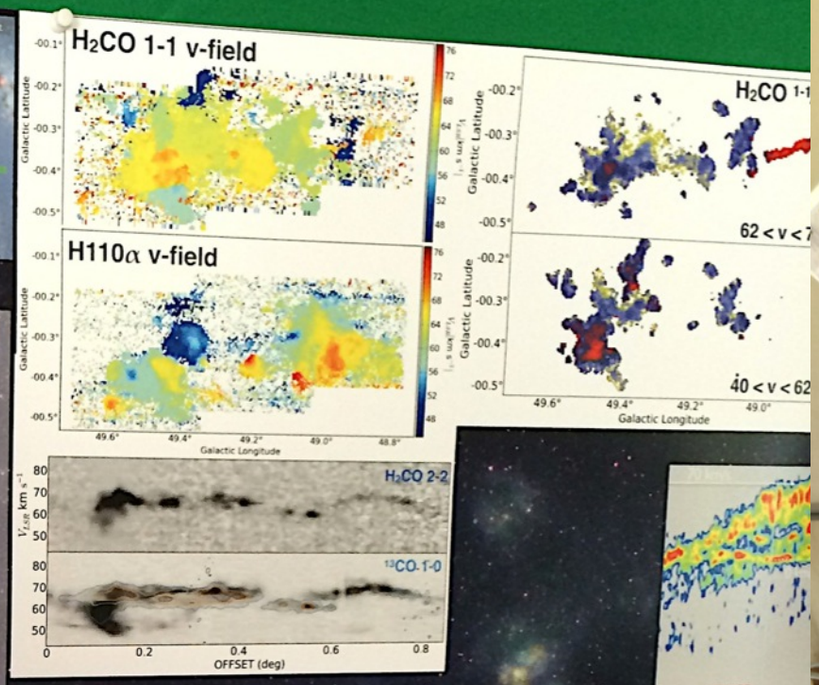





There is a long history of star formation in the cloud:
-W51 C supernova remnant (Brogan et al 2013)
-P Cygni supergiant [OMN2000] LS1 (Clark et al 2009)

Today, dense gas is absent from W51 B region: it has been blown apart or crushed by W51 C.
The high-density gas is focused in W51 A.

W51 A is at the intersection of two clouds, a 68 km/s foreground cloud and at least one cloud in the 45-55 km/s range.

The central cluster of W51 Main is linked to the large-scale filaments crossing the field.

Both clouds have been forming massive stars for Myrs.
A collision between them, perhaps related to their interaction with a spiral arm, is a plausible trigger for the cluster pair.

WISE 12um
WISE 22um
BGPS 1.1mm
Full image is 360x360 pc

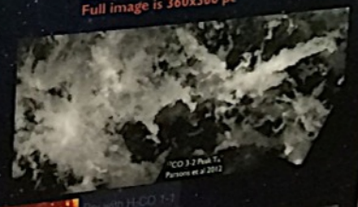


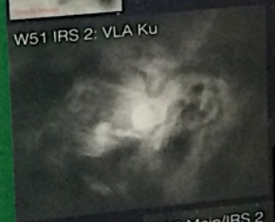




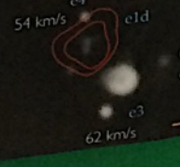


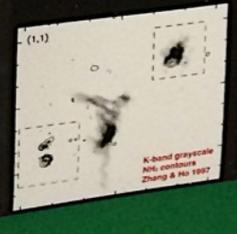


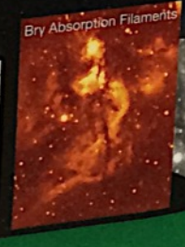




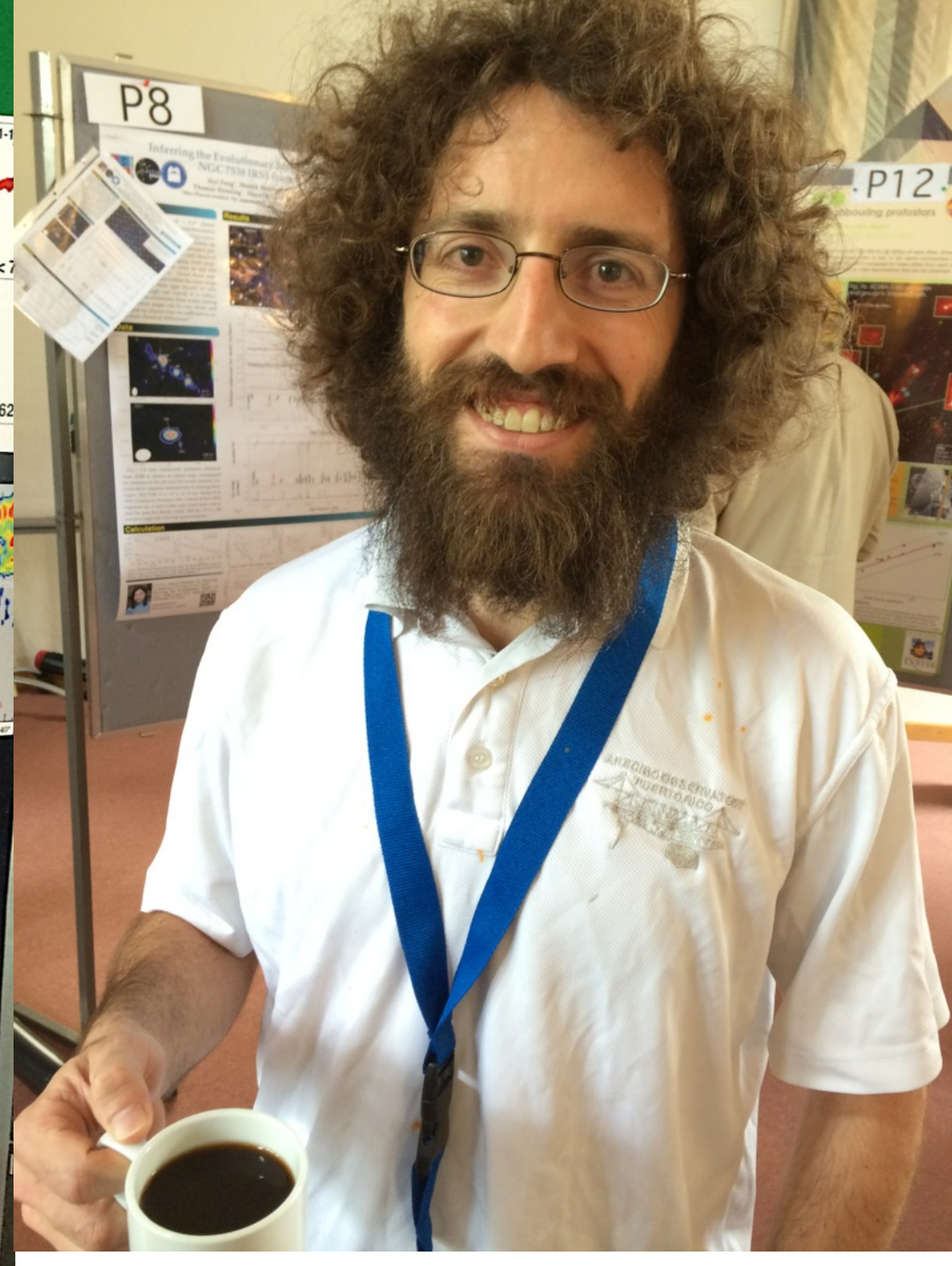


Adam Ginsburg

# Chemical variations in IRDCs: from starless cores to hot core candidates

T. Vasyunina[1], H. Linz[2], D. Semenov[2], U. Hincelin[3], E. Herbst[3], K. Furuya[4], Y. Aikawa[5], H. Beuther[2], B. Commercon[6], K. Oberg[7], F. Wyrowski[1], K. Menten[1]

[1]MPIfR, Germany, [2]MPIA, Germany, [3]UVa, USA, [4]Leiden observatory, the Netherlands, [5]KOBE U, Japan, [6]CRAL/ENS, France, [7]CfA, USA

Utilizing the high sensitivity and broad frequency coverage of the IRAM 30-m telescope, we targeted several high-mass star-forming regions from quiescent (IRDC-Q) and active (IRDC-A) Infrared Dark Clouds to High-Mass Protostellar Objects (HMPOs). We detected more than 20 species of different chemical families. This unique dataset enables us to perform a detailed analysis and chemical modeling at different evolutionary stages. Here, we present observational data and our first modeling results for two regions within IRDC028.34+0.06, the hot core candidate IRDC028.34-6 and the starless core candidate IRDC028-C1S.

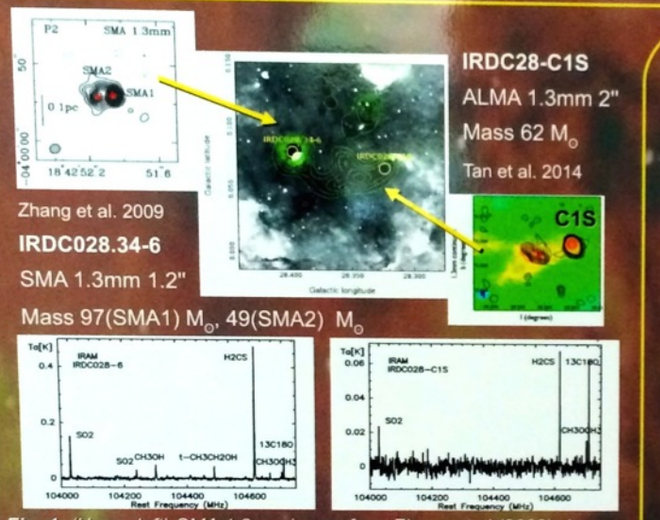


Zhang et al. 2009

**IRDC028.34-6**

SMA 1.3mm 1.2"

Mass 97(SMA1) $M_\odot$, 49(SMA2) $M_\odot$

**IRDC28-C1S**

ALMA 1.3mm 2"

Mass 62 $M_\odot$

Tan et al. 2014

*Fig. 1. (Upper left) SMA 1.3mm image from Zhang et al.(2009); (upper middle) 8micron Spitzer image overlayed with APEX 870 micron contour for IRDC028.34+0.06; (upper right) ALMA 1.3mm image from Tan et al. (2014). (Bottom left) IRAM spectra for hot core candidate IRDC028-6; (bottom right) IRAM spectra for starless core candidate IRDC028-C1S.*

## High sensitivity IRAM data

**Frequency**: 99–107 GHz (6 mK); 218–225 GHz (14 mK)
**Objects**: 7 IRDC-Q, 2 IRDC-A, 6 HMPO
**Detected species:**

| Sulphur | Carbon chain | Complex organics | Others |
|---|---|---|---|
| SO, SO2 | HC3N, HC5N | CH2CO, CH3OCHO, | CF+, HCNH+ |
| OCS, H2CS | CH3CCH l-C3H2 | CH3OH, CH3OCH3, | c-C3H2, HNCO |
| C2S | DC3N C4H | NH3CHO, t-C2H5OH | c-C3HD |

**Observational results:**

- 8 species detected in quiescent IRDCs for the first time.
- In each evolutionary stage the lines of the following species are particularly bright:

Carbon chain molecules in quiescent IRDC;

Complex organic molecules in active IRDCs;

High-energy transitions of methanol in HMPOs.

- CH3CCH and CH3CN analysis reveals warm 30-50K and hot 100-200K temperature components in active IRDCs and HMPOs.

## Model for Hot core candidate IRDC028.34-6

Chemical code „Nautilus“ (Hersant et al. 2009)
0-D model, T(t), n(t), and Av(t) not constant

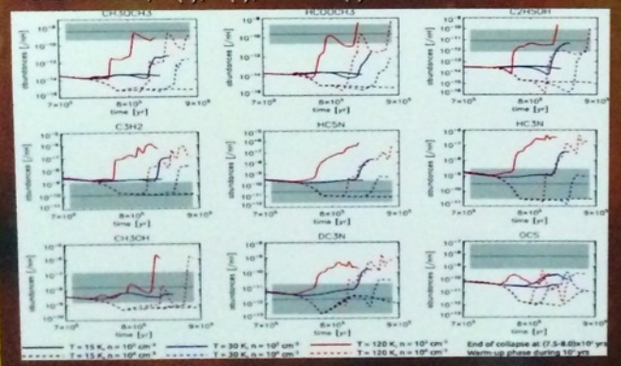


*Fig. 2. An example of abundance profiles for hot core candidate IRDC028.34-6. On all panels the grey area corresponds to observed value +/- error margin.*

**Modeling results:**

To reproduce 31 detected molecules, a warm-up model is required. The molecules can be subdivided in several groups according to the temperature that reproduces their abundances: low (15K), medium (30K) and high (120K). They might trace different regions within the cloud.

## Model for Starless core candidate IRDC028-C1S

Chemical code „ALCHEMIC” (Semenov et al. 2010)
1-D model, T(t), n(t), and Av(t)=constant

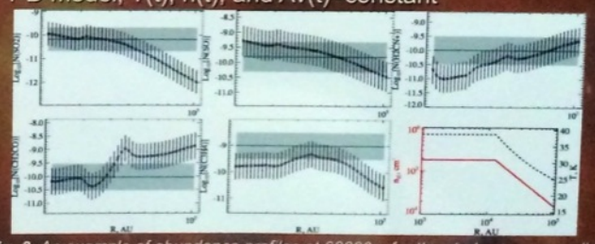


*Fig. 3. An example of abundance profiles at 60000yr for the starless core candidate IRDC028-C1S. On all panels the grey area corresponds to observed value +/- error margin. Bottom right panel presents temperature and density profiles.*

**Parameters of the best fit model:**

Out of 21 species, 2 are not reproduced: CCS,H2CS
**Agreement:** 83% **Age** 60,000 yr **r_in** = 12,680 AU,

**Modeling results:**

- With 21 molecules, a 0-D model is not sufficient anymore even for the quiescent IRDC.
- Elevated temperature at the inner radius might indicate beginning of star formation, corroborated by the previous detection of SiO and an H2O maser (Wang et al. 2008, Linz et al. in prep.). Hence, IRDC028-C1S might be in a more evolved phase than a starless core.

Tatiana Vasyunina

# New topic

# Q=1

- SFR reflects cosmic flow rate
- Disk gas mass = SFR x depletion timescale (SFE) <-- FB
- Feedback tells us about the gas mass in a galaxy
- Connects all scales. All is one.

# New topic

# Fibers

Hacar & Tafalla 2011, 2013

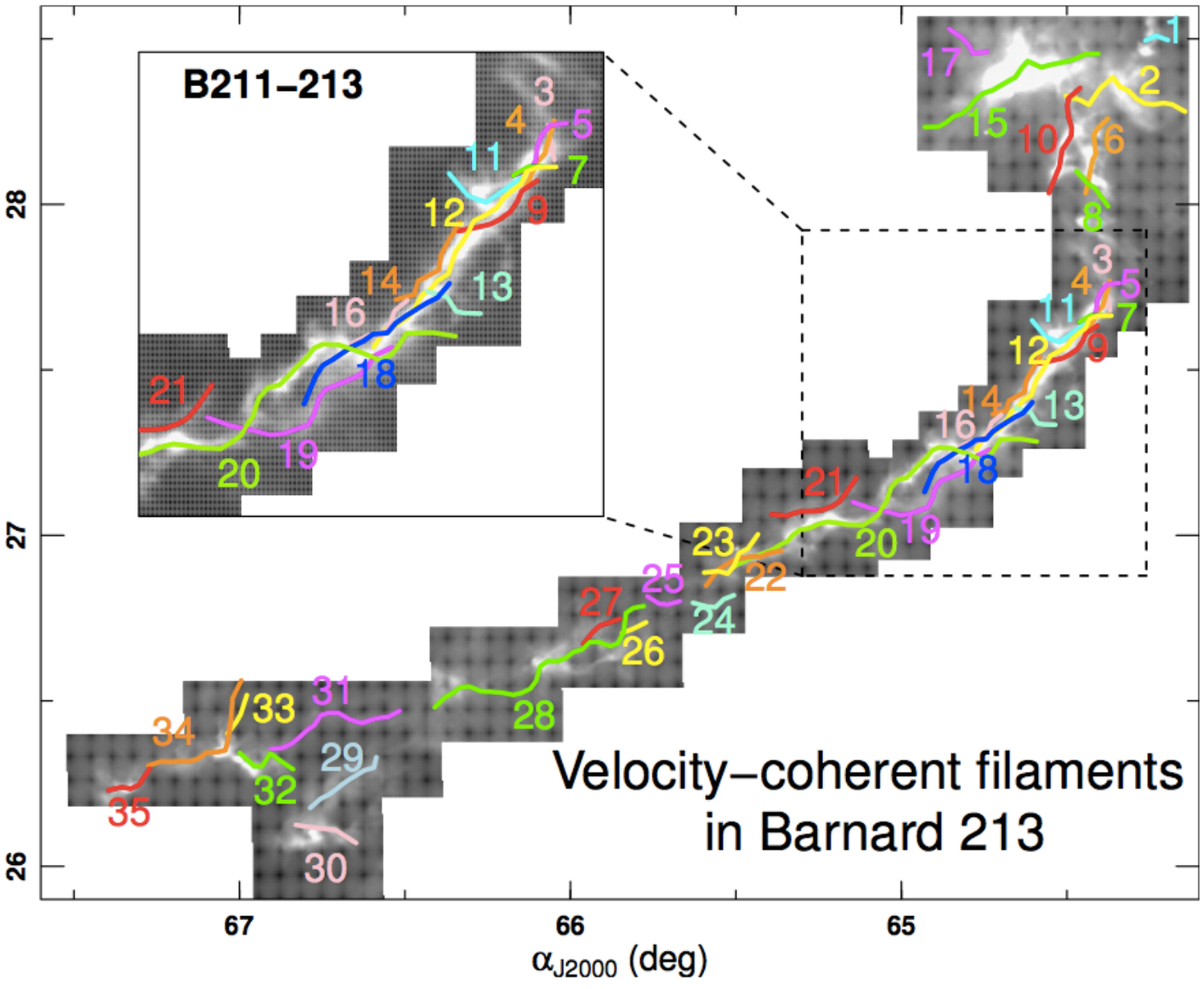


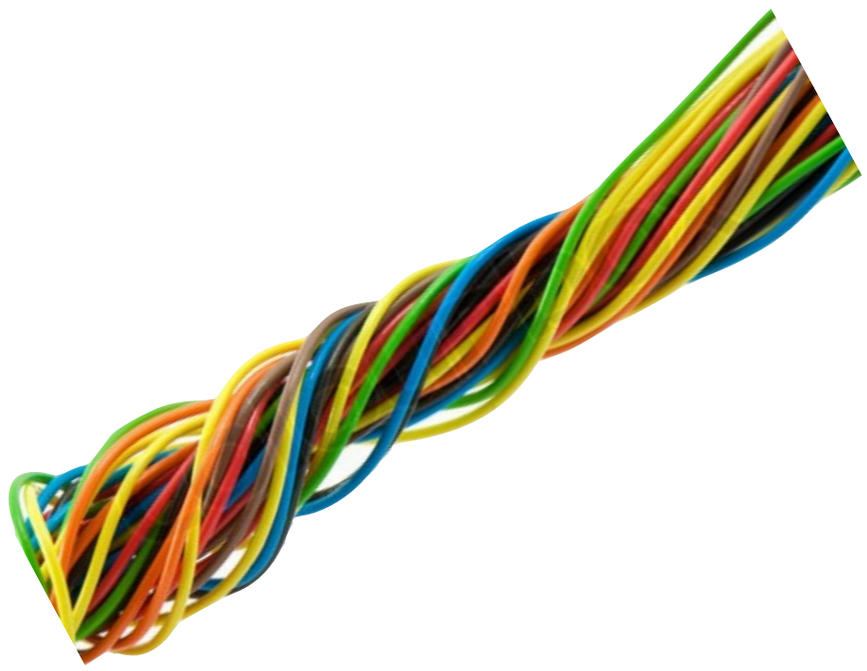

Bundles!

- Lengths ~ 0.5 pc
- Internal velocity dispersions ~ Cs
- Mass-per-unit-length ~ fragmentation threshold of isothermal cylinder at 10 K
- Few filaments “fertile” (w/ most cores) most “sterile” (SFR implications)

# the **velocity structure** of **filaments** in **turbulent molecular clouds**

Nickolas Moeckel
nickolas1@gmail.com
@nickolas1
nickolas1.com
and Andreas Burkert

## imulation

### initial conditions

hydrodynamic
no gravity
turbulent
Mach 8

This is a fairly 'vanilla' turbulent setup. We simulated an initially uniform density, isothermal, periodic box using ATHENA on a $1024^3$ grid. Random forcing for $1<|k| L/2\pi<3$; small scales develop from cascade. The turbulent forcing is solenoidal, and we drive until the Mach number saturates at Mach 8.

### further evolution

hydrodynamic
gravity
no driving
sink particles

We scale the box to a length of 10pc and mean density 100 $cm^{-3}$ at 10K. For the self-gravitating non-driven evolution we use Ramses, using adaptive mesh refinement up to an effective resolution of $16k^3$. Refinement is such that the local Jeans length is resolved by 32 cells. Sink particles are 755au and thus do not represent individual stars, but rather sites of collapse.

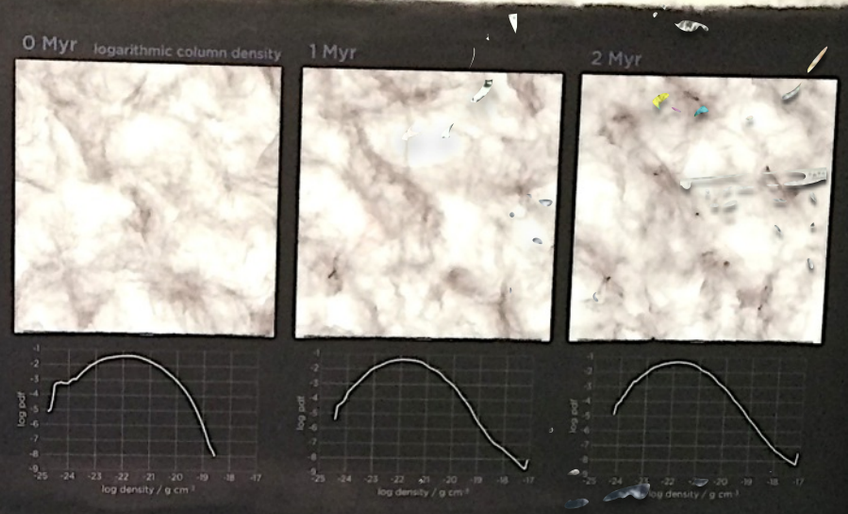


## real observation

### 10 pc in Taurus

$C^{18}O$
$N_2H^+$
PPV cubes

Hacar et al. (2013) observed the L1495/B213 complex in Taurus, including optically thin moderate and high density tracers. Among their results: in PPV space, the ~10pc filament breaks down into separate and mutually supersonic subfilaments.

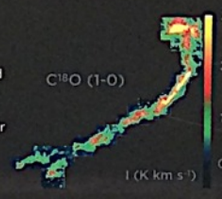



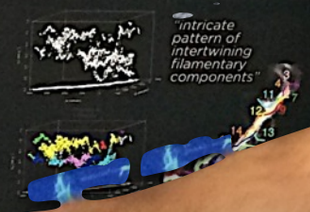


## fake observation

### 10 pc in a computer

"$C^{18}O$"
"$N_2H^+$"
PPV cubes

In order to compare to these observations, we construct (very) approximate $C^{18}O$ and $N_2H^+$ observations, (assuming optical thinness) using the mass-weighted velocity of different density ranges. Each point in the simulation contributes a Gaussian line with a thermal (10K) width to the spectrum, which is binned at 0.05 km $s^{-1}$ resolution.

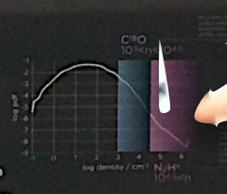


## some comparison

Our main question: do velocity structures similar to those in the observations of Hacar et al. show up in simulations? With the simulated data cubes we look at two times, roughly 1.25 and 2 Myr after the self-gravity is turned on and the turbulent driving is turned off. We identified (by eye) several features in the $C^{18}O$ maps that an observer might deem to be a filamentary structure.

This figure shows the four filaments we identified at 1.27 Myr, rotated into their 'native' frame with the long axis along the L direction. These are the bottom panels of each pair. The top panels show the density-weighted line-of-sight velocity for each filament, summed along the native short axis W. (This is effectively collapsing the PPV cube to a PV plane). Note that we plot the full summed spectra rather than detected line centroids as Hacar et al. do.

### 2. Inspect velocity structure

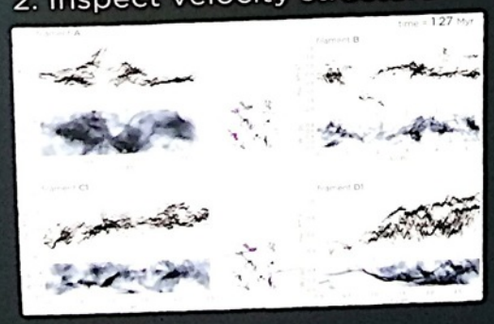


*Notable features*
**filament A**: this is a site of collapse and sink particle formation. There is a clear global infall signature in the velocity structure
**filament B**: in projection this appears to be a single

### 1. Identify filamentary features

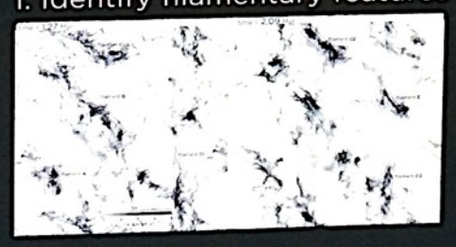

### 3. Third dimension

Filament B is actually a collection of unassociated regions of denser gas. It's not surprising that chance projections like this masquerade as filaments in column density. The fact that there's apparent overall coherence in velocity as well, despite spatial independence, is

### 4. Later time

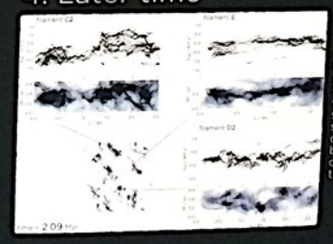


At later times, when self gravity is more dominant than the initial turbulent structure, we still see similar velocity structures; mildly supersonic dispersion between distinct components in the same filament.

### the future in collaboration with A. Hacar, J. Alves

This initial work is a qualitative comparison with observations. These velocity signals probably can be found in many simulations of star formation. Our next steps include:

- apples-to-apples comparison with observations

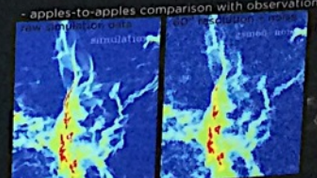


Nick Moeckel

# The Formation of Braided Filaments by Reconnection in Magnetized Sheets

Eric Keto (CfA)

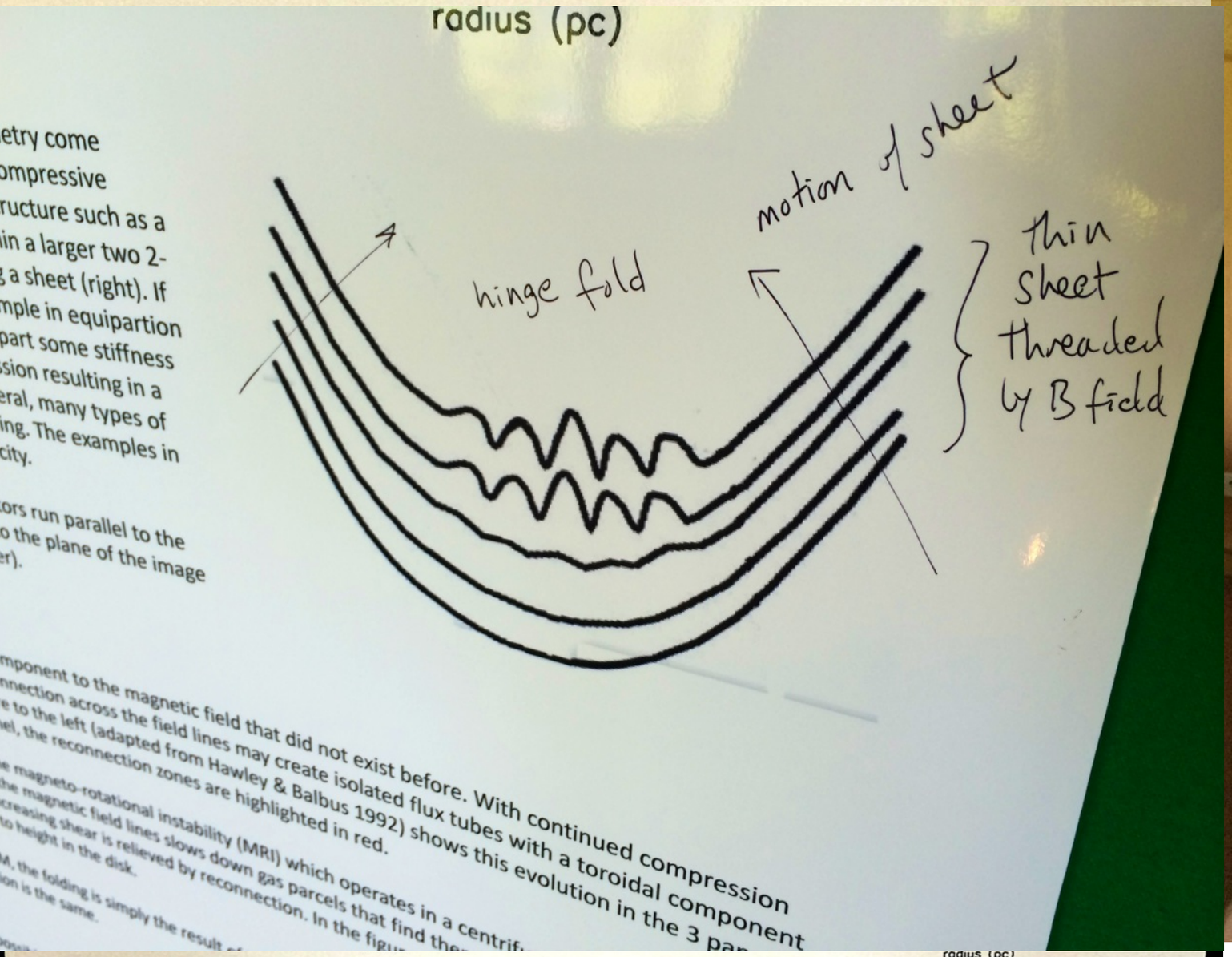


etry come
ompressive
ructure such as a
in a larger two 2-
g a sheet (right). If
mple in equipartion
part some stiffness
sion resulting in a
eral, many types of
ing. The examples in
city.

ors run parallel to the
o the plane of the image
er).

mponent to the magnetic field that did not exist before. With continued compression
nnection across the field lines may create isolated flux tubes with a toroidal component
e to the left (adapted from Hawley & Balbus 1992) shows this evolution in the 3 pa
el, the reconnection zones are highlighted in red.

e magneto-rotational instability (MRI) which operates in a centrif
he magnetic field lines slows down gas parcels that find ther
creasing shear is relieved by reconnection. In the figu
o height in the disk.

M, the folding is simply the result o
on is the same.

Eric Keto




**Folding:** How might such a magnetic field geometry come about? Suppose the filaments are formed by compressive flows in the turbulent ISM. A 1-dimensional structure such as a filament may be formed by compression within a larger two 2-dimensional sheet (left) or formed by folding a sheet (right). If the magnetic field is not too strong, for example in equipartion with the turbulent kinetic energy, it will impart some stiffness to the gas, but not fully resist the compression resulting in a folding of the magnetic field lines. In general, many types of compression and shear will result in folding. The examples in the 2 drawings are symmetric for simplicity.

In this geometry, the electric field vectors run parallel to the sheet in the direction perpendicular to the plane of the image (into and out of the page of this paper).

**Reconnection:** The folding creates a toroidal component to the magnetic field that did not exist before. With continued compression the magnetic field may fold back on itself. Reconnection across the field lines may create isolated flux tubes with a toroidal component stronger than in the surrounding gas. The figure to the left (adapted from Hawley & Balbus 1992) shows this evolution in the 3 panels from the top to the bottom. In the middle panel, the reconnection zones are highlighted in red.

This reconnection geometry is inspired by the magneto-rotational instability (MRI) which operates in a centrifugally supported (Keplerian) disk. In the MRI, the tension of the magnetic field lines slows down gas parcels that find themselves displaced inward and speeds up those displaced outward. The increasing shear is relieved by reconnection. In the figure to the left, the horizontal axis would correspond to radius and the vertical axis to height in the disk.

In the case of braided filaments in the ISM, the folding is simply the result of larger scale flows. There is no instability and

# New topic

# 3D from 2D PDFs

Kainulainen+14

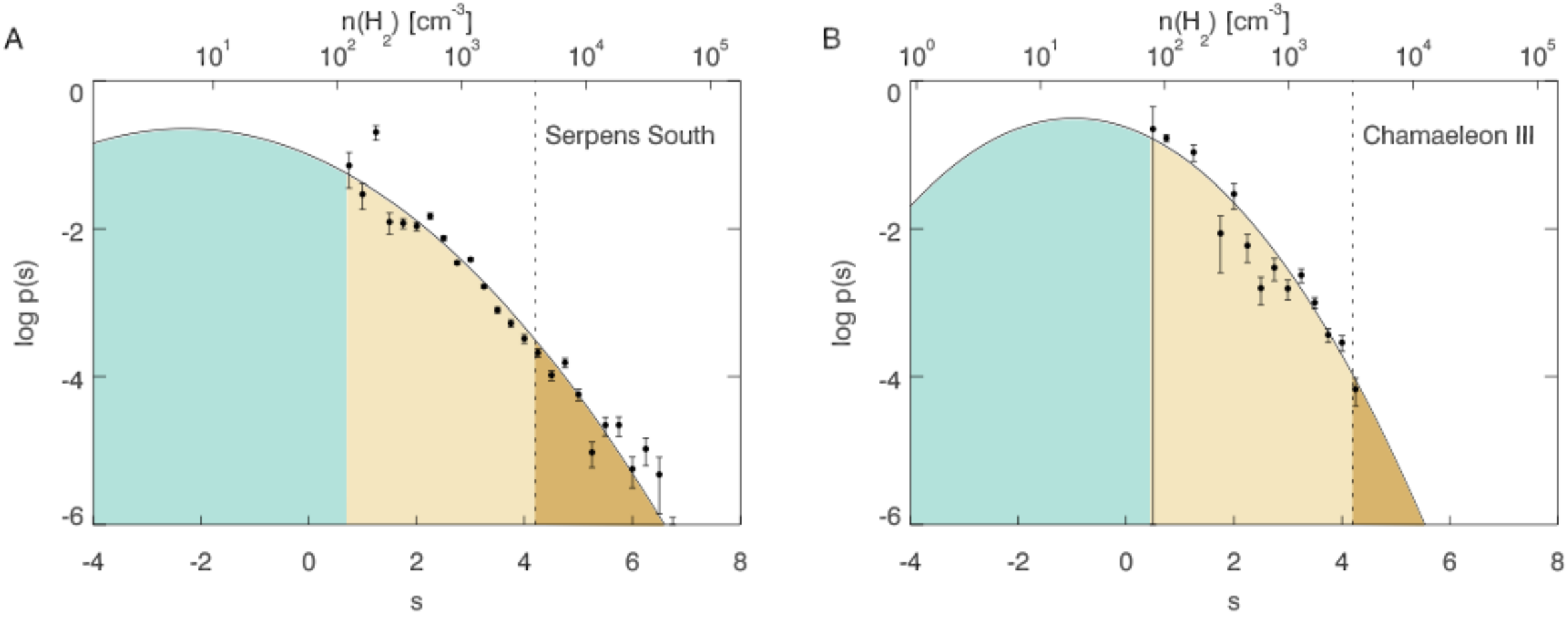


Threshold for SF ~ 5e3 cm^-3

**Sadavoy**: individual regions have different PDFs tails, Class 0 density correlates with slope of tail

# Warning

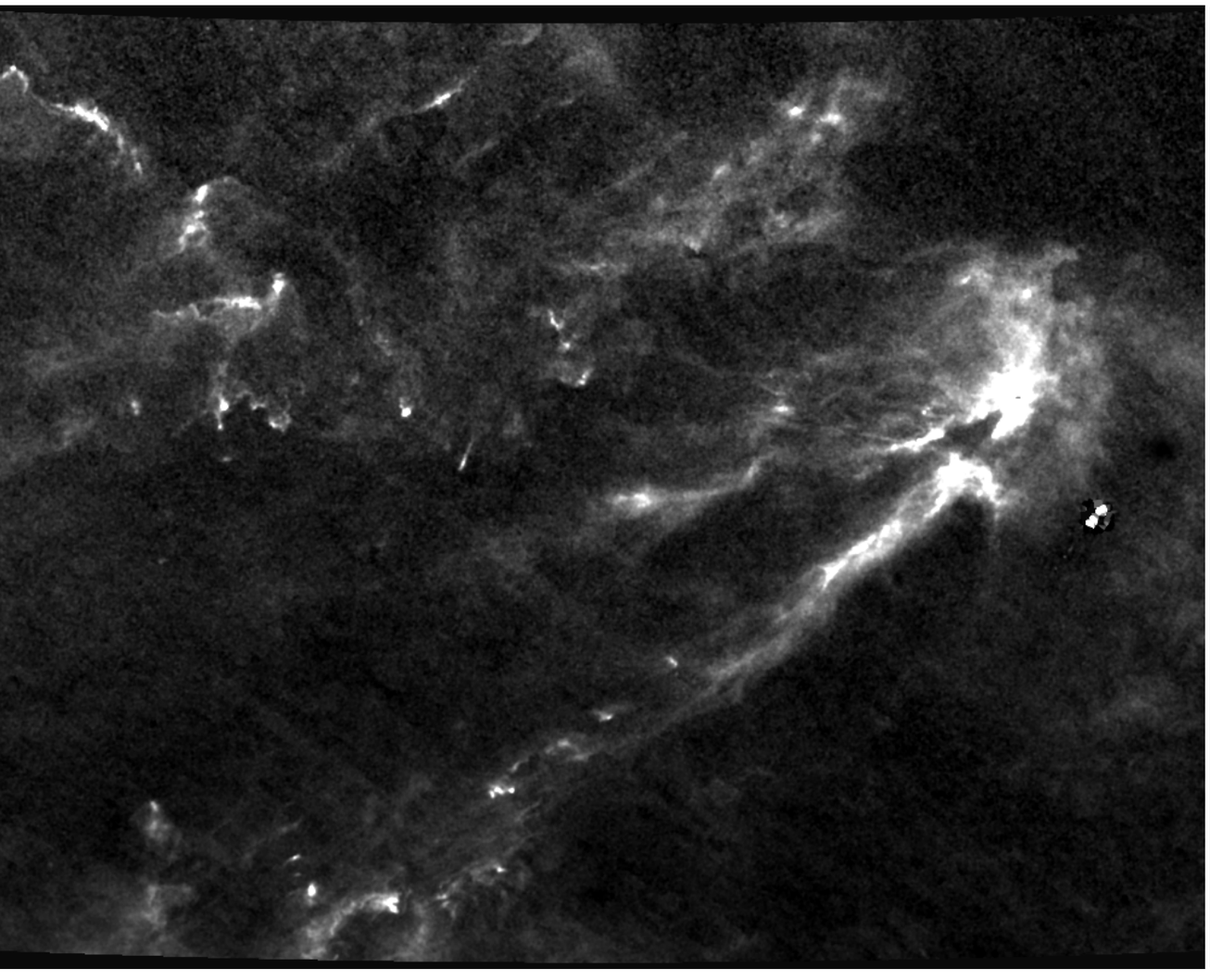

Same PDF

Chris Beaumont

# New facilities

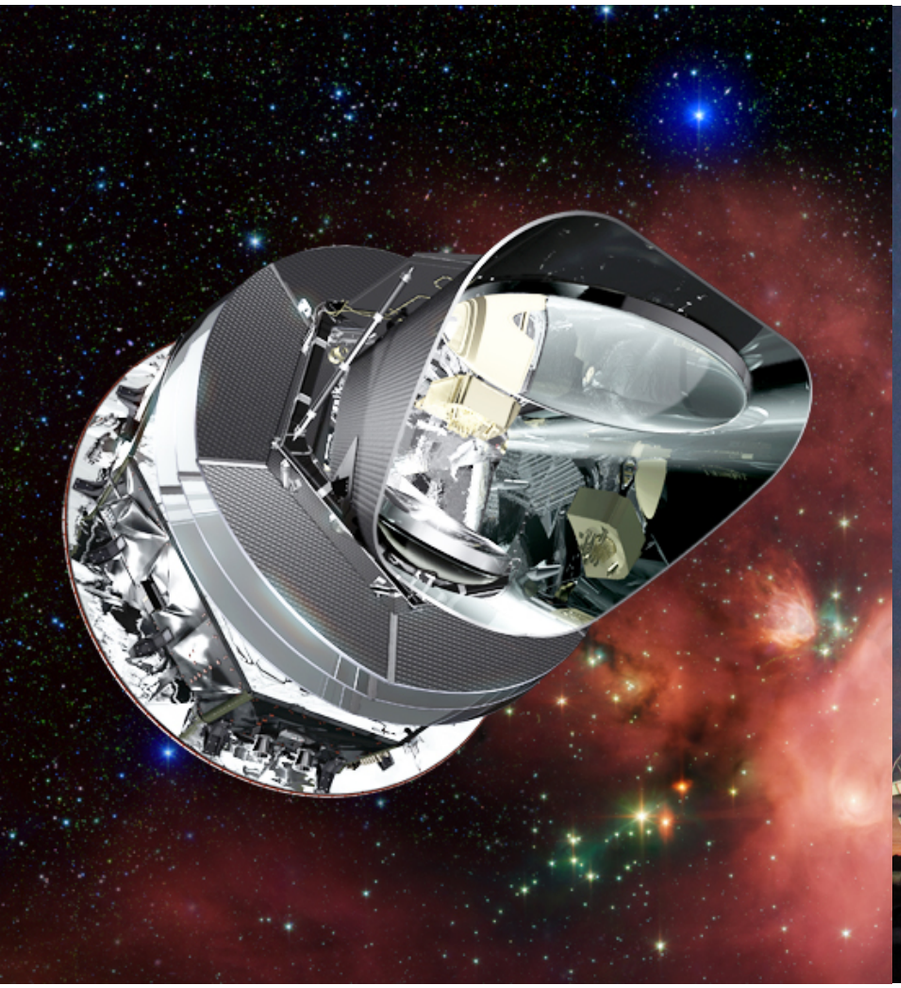

Planck

ALMA

SOFIA

# The conflicting

# (commercial break)


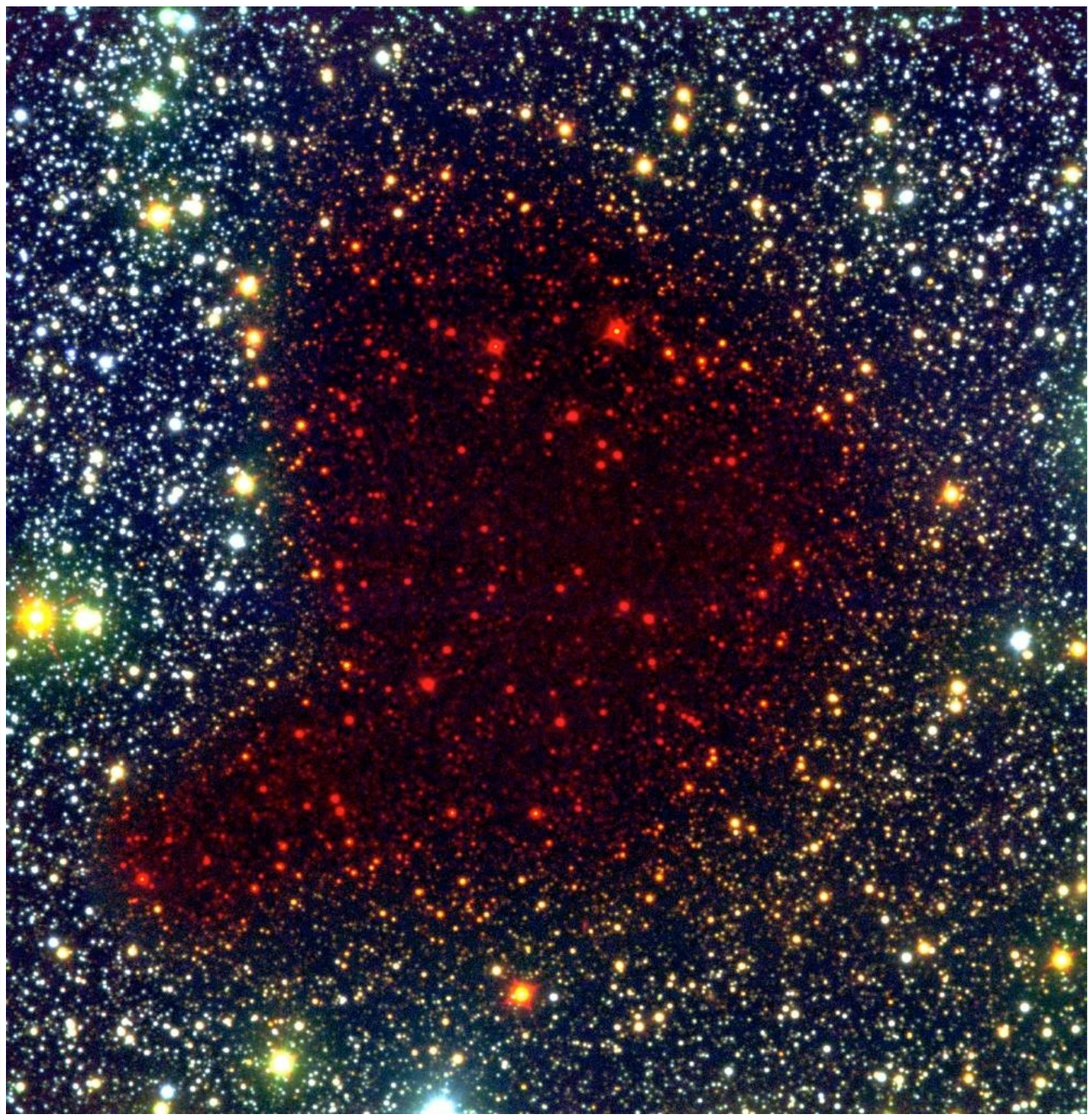

… now **50% rounder than any other core**
or your money back!

# The conflicting

***Padoan**: Who is the meat, who is the salt and pepper? Compressible supersonic turbulence? SN or disk instabilities?*
***Klein**: Weak B inconsistent with observ., not good for flows*
***Peretto, Smith, Basu, Tafalla**: Super-Jeans cores? Are there even cores in High-Mass SFR?*
***Smith**: 0.1pc is fit by only a few point in the filament center (r<0.04pc), hydro filaments also have p~2*
***Steinacker, Hacar**: turbulence "has" to be there*
***Friesen**: ALMA blobs not Jeans fragmentation*
***Maury**: PdBI disks are 50 AU, not 200 AU*
***Dunham**: You cannot just count blobs (proto-binaries)*
***Robitaille**: The CMF-IMF thing*

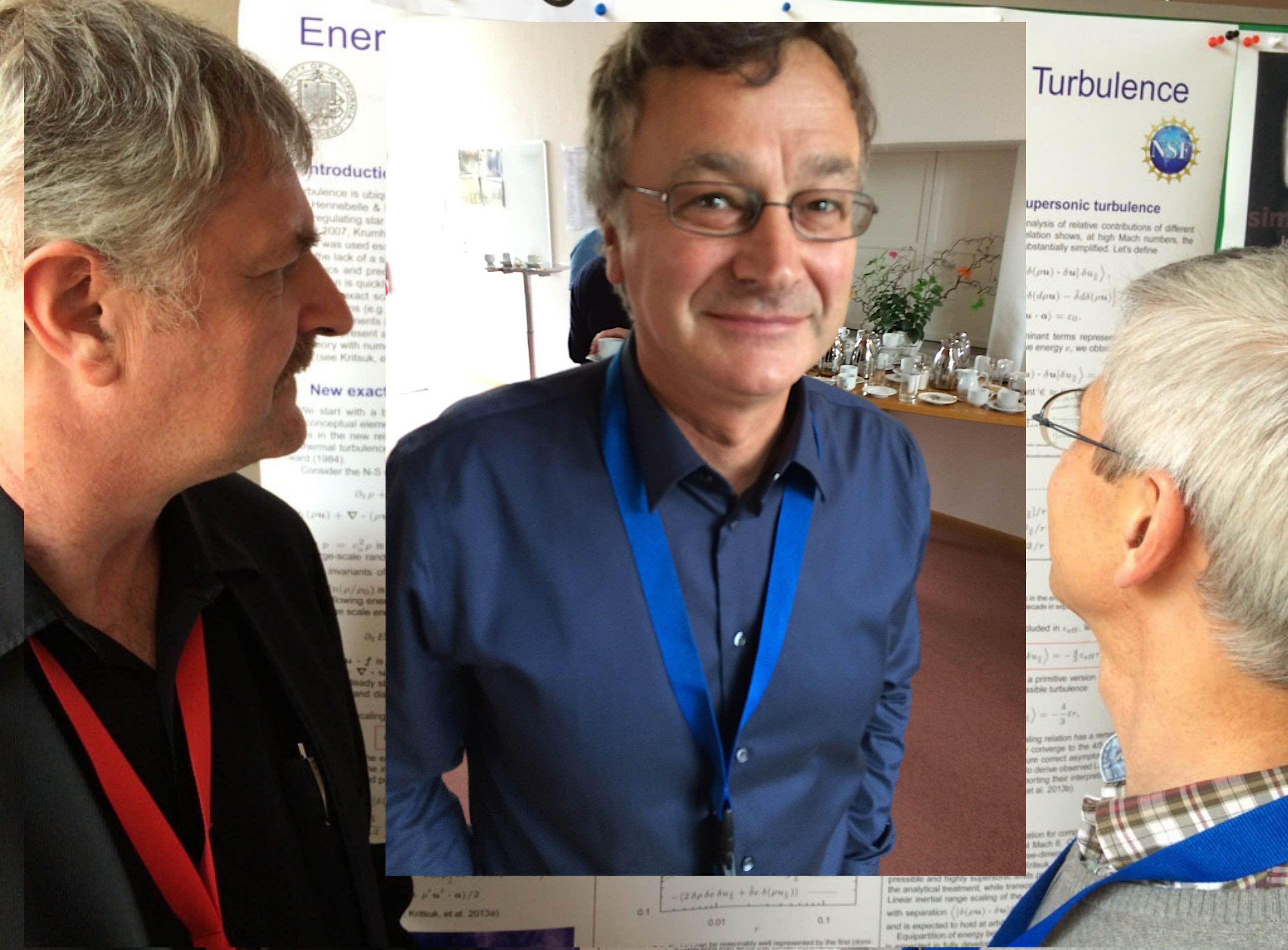
Turbulence
NSF
upersonic turbulence

# Turbulence-induced Collision Velocity of Dust Particles

Liubin Pan[1], Paolo Padaon[2] & John Scalo[3]
[1]Harvard –Smithsonian Center for Astrophysics; [2]ICREA & ICC, University of Barcelona
[3]Department of Astronomy, The University of Texas

## lotivation

e dynamics of particles of finite inertia suspended in turbulent flows is of rticular interest for understanding dust particle collisions in protoplanetary sks and star-forming molecular clouds. The evolution of the size distribution of ust particles is controlled by their collisions. Small particles tend to stick when lliding, and the size grows by coagulation. With increasing size, the particles ecome less sticky and, depending on the collision velocity and the particle ternal structure, collisions may result in bouncing or fragmentation. The icking, bouncing and fragmentation processes may lead to a quasi-equilibrium ze distribution. Due to the dependence of the collision outcome on the collision elocity, an accurate evaluation of the turbulence-induced relative velocity is nportant for modeling the dust size distribution.

urbulence-induced collision velocity is stochastic, and, assuming a Gaussian istribution, recent studies have shown that accounting for the probability listribution of the collision velocity leads to significant changes in the predicted particle size evolution. Using both numerical simulations and analytical models, we show that turbulence-induced collision velocity is highly non-Gaussian.

## Simulation

Our simulation was conducted in a periodic $512^3$ box using the Pencil code. We simulated a statistically isotropic and weakly compressible flow with a Mach number of ~0.1. In the simulated flow, we evolved 14 species of inertial particles of different sizes. Each species contains 33.6 million particles. The friction timescale of the particles spans about four decades from 0.1 Kolmogorov time to 40 large-eddy turnover time, covering the entire scale range of the flow. Using 4096 cores on the NASA/Ames Pleiades supercomputer, the simulation lasted 14 days, costing a total of 1.4 million CPU hours. We searched the simulation box for all particle pairs at given small distances, and analyzed the statistics of their relative velocity.

## Theoretical model

The analytical model of Pan and Padoan (2010) shows that the root-mean-square (rms) of the particle relative velocity induced by turbulent motions consists of two contributions, named the generalized shear term and generalized acceleration term, respectively. As illustrated in Figure 1, the generalized shear term physically represents the particles' memory of the *spatial* flow velocity difference the two particles saw on their trajectories within a friction timescale or so in the past, while the generalized acceleration term is associated with the *temporal* flow velocity difference along individual particle trajectories. We modeled the rms relative velocity using the spatial and temporal flow velocity statistics and assumed separation behavior of particle pairs backward in time. For equal-size particles, the acceleration term vanishes, and only the shear term contributes.

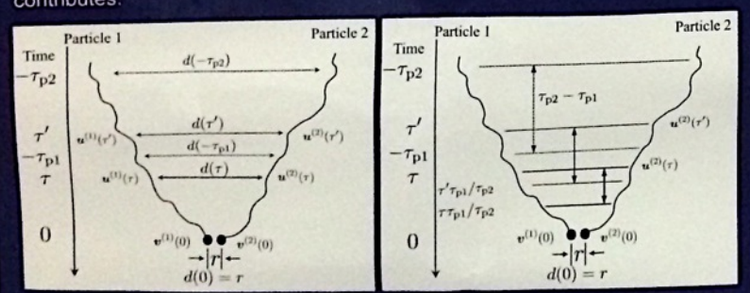


Fig 1. Schematic figures illustrating the physical pictures of the generalized shear (left panel) and acceleration (right panel) terms for two particles with friction times of $\tau_{p1}$ and $\tau_{p2}$, respectively. The generalized shear term depends on the spatial separation, $d(\tau)$, of the two particles backward in time.

## Results

In Figure 2, we show simulation results (data points) for the rms relative velocity as a function of the Stokes number pairs ($St_1$, $St_2$). Our model prediction (lines) in good agreement with data. In the left panel, $St_1$ is fixed, and the dips in the li at $St_1 \sim St_2$ indicate tighter velocity correlations between similar particles. The rig panel fixes the Stokes number ratio and plots the rms vs. the larger Stokes number, $St_h$. In a turbulent flow with a high Reynolds number, our model predict $St_h^{1/2}$ scaling for particles in the inertial range at any Stokes ratio. The generaliz shear term dominates for particles of similar sizes. The acceleration contribution increases with the Stokes number differences, and starts to dominate if the Sto numbers differ by more than a factor of 4.

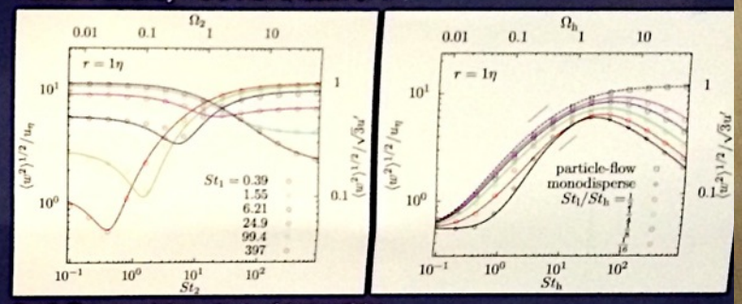


Fig. 2. The rms relative velocity of dust particles.

Figure 3 shows the probability distribution function (PDF) of the relative velocity of equal-size particles. Left and right panels correspond to particles with $St<1$ and $St>$ respectively. The PDF is highly non-Gaussian, exhibiting very fat tails. The non-Gaussianity peaks at $St \sim 1$. We identified two sources of non-Gaussianity: the imprin of intermittency of spatial turbulent structures and an intrinsic contribution from the particle dynamics. The PDF for particles of different sizes is also non-Gaussian. The contribution of the acceleration term samples the temporal flow velocity structures along individual particle trajectories. The acceleration term is less fat than the shear term, and, as the acceleration contribution increases with increasing Stokes number difference, the PDF for different particles becomes less non-Gaussian.

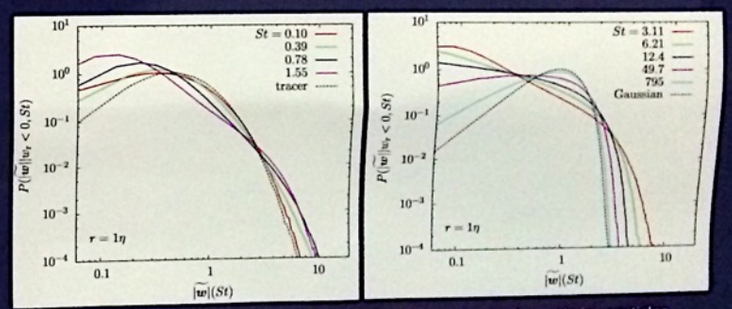


Fig. 3. The probability distribution function of the relative velocity of equal-size particles.

## Discussion and Conclusion

We studied turbulence-induced collision velocity of dust particles using both numerical simulation and theoretical modeling. We found that the commonly-used model for the rms relative velocity overestimates simulation results by a factor of 2, while our model is in good agreement with the data. The probability distribution of the collision velocity is found to be highly non-Gaussian. Applying the non-Gaussian distribution to dust particle collisions, we found that the transitions from sticking to bouncing and to fragmentation become more gradual. In particular, the sticking probability remains significant after the particle size exceeds the bouncing barrier, and, in comparison to the prediction with a Gaussian distribution, accounting for non-Gaussianity further alleviates the bouncing barrier for dust particle growth.

Liubin Pan

# Inferring the Evolutionary Stages of NGC 7538 S and NGC 7538 IRS1 from Chemistry

Siyi Feng[1], Henrik Beuther[1], Dmitry Semenov[1], Thomas Henning[1], Hendrik Linz[1] & Elisabeth A.C. Mills[2]

[1]Max-Planck-Institut für Astronomie, [2] National Radio Astronomy Observatory

## Summary

At a spatial resolution of $\sim 0.4''$ (linear resolution $\sim$ 800 AU), our interferometric study on the high-mass star-forming region NGC7538 ($\sim$ 2.65 kpc) with the Plateau de Bure Interferometer (PdBI) has revealed spatial complexity (Fig.1 & Fig.2) and chemical differentiations (Fig.3), ranging from properties known for starless cores to real hot molecular cores (Fig.5). Given these subsources are embedded within the same large scale gas clump, their ages should be very similar. Although not coeval, it is indicative that the evolutionary time-scales among these different stages can be very short, and short heat-up phases may be sufficient to explain such chemical differences[1].

## Data

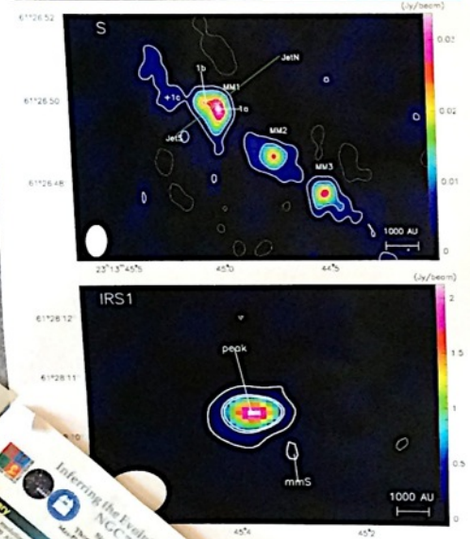


ontinuum emission obtained
s colour map, overlapped
15σ levels (dashed con-
due to missing flux).
6 μm, Werner et al.
ane & Kuno 2005)
2, mm3, with al-
51 ($8 \times 10^4$ L$_\odot$) still
dal resolution.

## Results

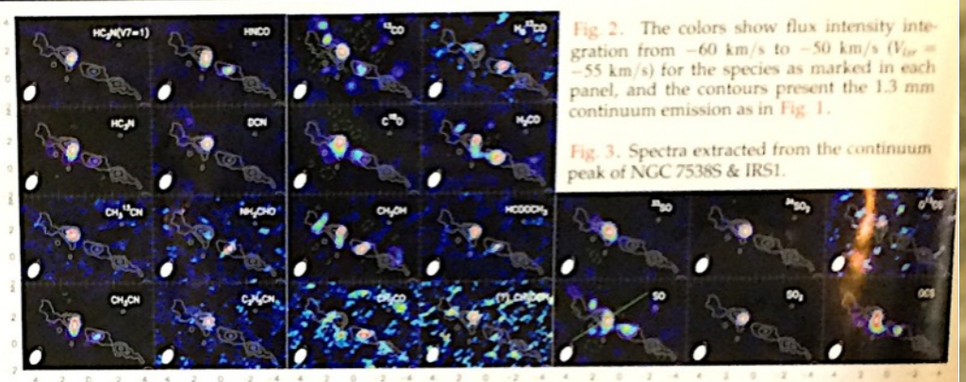


Fig. 2. The colors show flux intensity integration from −60 km/s to −50 km/s ($V_{lsr}$ = −55 km/s) for the species as marked in each panel, and the contours present the 1.3 mm continuum emission as in Fig. 1.

Fig. 3. Spectra extracted from the continuum peak of NGC 7538S & IRS1.

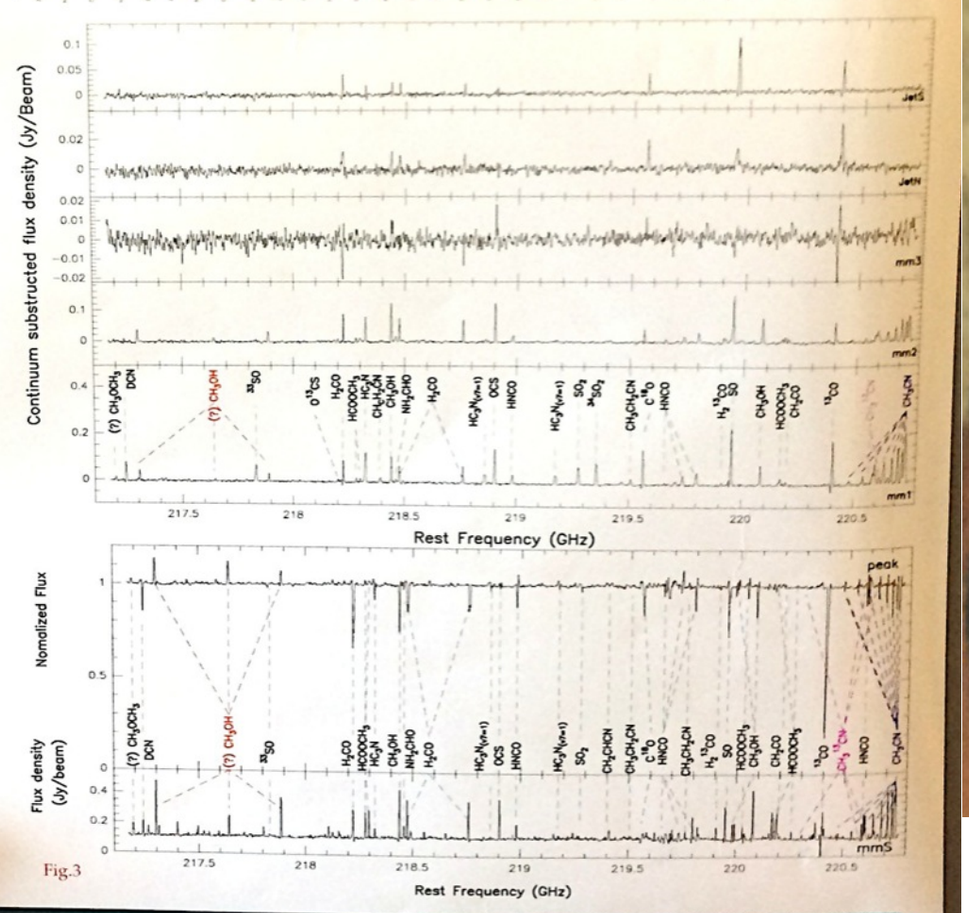


Fig.3

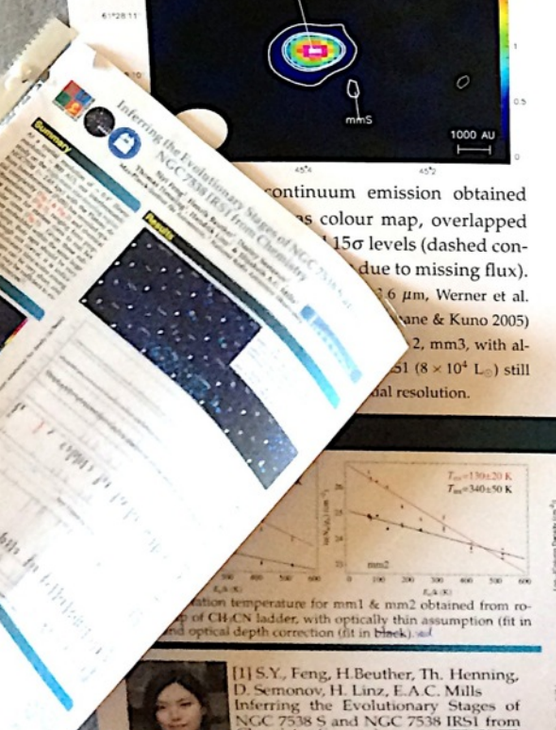





ation temperature for mm1 & mm2 obtained from ro-
p of $CH_3CN$ ladder, with optically thin assumption (fit in
nd optical depth correction (fit in black).

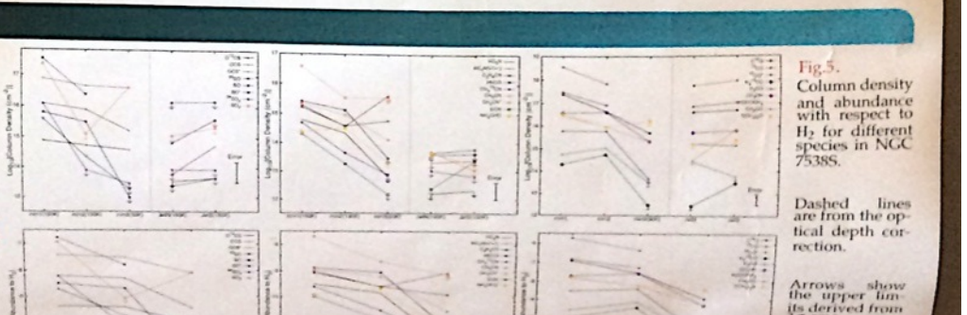

Fig.5. Column density and abundance with respect to $H_2$ for different species in NGC 7538S.

Dashed lines are from the optical depth correction.

Arrows show the upper limits derived from

[1] S.Y., Feng, H.Beuther, Th. Henning, D. Semonov, H. Linz, E.A.C. Mills Inferring the Evolutionary Stages of NGC 7538 S and NGC 7538 IRS1 from

Siyi Feng

# Fragmentation at the Earliest Phase of Massive Star Formation

**Ke Wang (ESO Fellow)**

kwang@eso.org www.eso.org/~kwang

(PDF poster and references are available on my homepage.)

## Overview

➢How a parsec-scale dense clump would collapse and fragment to give rise to a cluster that contains high-mass stars, when the thermal Jeans mass of the patient clump is 10 times lower than the stellar mass?

➢Our observations show that turbulence and/or magnetic fields play an important role during the early fragmentation in supporting super Jeans mass cores needed to form massive stars.

## Observations

➢We carried out a mini survey of massive (~$10^3$ $M_\odot$), low-luminosity (<$10^3$ $L_\odot$) infrared-dark cloud (IRDC) clumps using SMA and VLA.

➢Observations designed to resolve initial fragmentation (using SMA dust continuum) and at the same time to measure gas temperature and turbulence (using VLA $NH_3$). This coordinated effort allows us to infer the nature of the fragmentation and to constrain theoretical models.

## IRDC G11.11-0.12 (the "Snake") Wang et al. 2014

➢G11 sketches over 30 pc over at a distance of 3.6 kpc. The Spitzer mid-IR absorption and Herschel far-IR emission indicate that the dust is cold (~15 K).
➢We zoom-in the two most massive clumps P1 and P6.

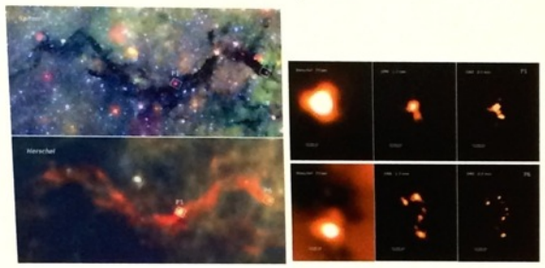


➢SMA dust continuum emission revealed structures sized ~0.1 and ~0.01 pc; probed much deeper than Herschel.

➢[ortho/para] $NH_3$ abundance ratios: 1.1 (A), 2.0 (B), 3.0 (C) → increase along outflow! Ortho-$NH_3$ is preferentially desorbed compared to para-$NH_3$.

➢$NH_3$ gas is shocked by the protostellar outflows.

➢Temperature map is highly structured at scales <1 pc.

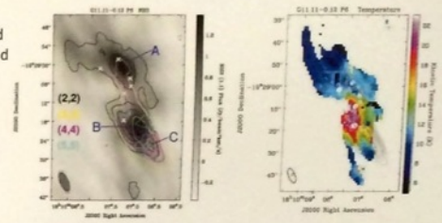


## IRDC G28.34+0.06 (the "Dragon") Wang et al. 2011, 2012

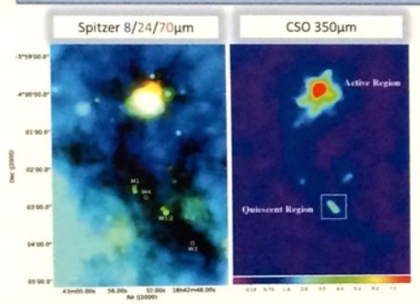


➢Zoom-in the southern "quiescent" 1-pc filament P1 in G28.

➢SMA dust emission revealed five group of compact cores along the filament, with size ~0.1 and ~0.01 pc.

➢Collimated CO(3-2) outflows from all of the five groups, orientation across the filament.

➢Sensitive VLA $NH_3$ revealed a faint filament joining the main filament, orientation coincident with global B-field lines → dynamically important B-fields.

➢Again, highly structured $T_{gas}$ map due to outflow heating.

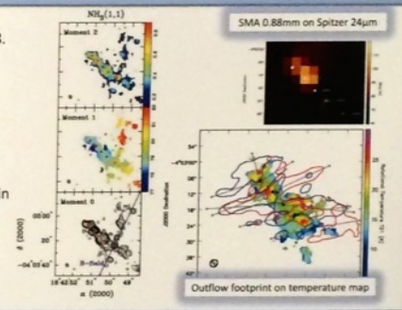


## IRDC G30.88+0.03 (the "Rabbit") Zhang & Wang 2011

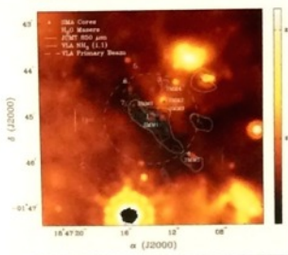

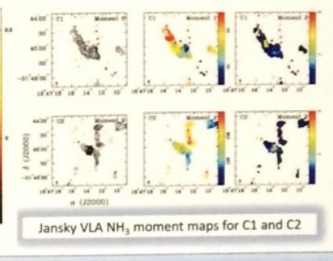

Jansky VLA $NH_3$ moment maps for C1 and C2

➢Two clumps along line-of-sight, with different velocities.

➢C1 @ 97 km/s, d = 6.5 kpc, T = 20 K, Mass = 1.8×$10^3$ $M_\odot$, associated with core SMM5 → pre-cluster?

➢C2 @ 107 km/s, d = 7.3 kpc, T = 19-45 K, Mass = 1.2×$10^3$ $M_\odot$, associated with all other dust cores → proto-sluster?

➢Simulated observation using the same (u,v) sampling as in real observations: Jeans mass cores can be reliably detected should they exist. No detection in real observations → no 0.1 pc cores of ≥8$M_\odot$ at this early stage!

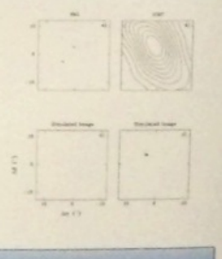

## Summary and more Questions

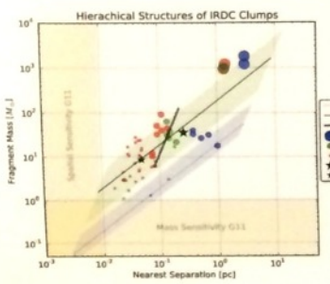


➢Observed fragment mass is almost always >10 times larger than thermal Jeans mass.
➢Turbulence appear to be sufficient in supporting these super Jean mass cores. B-fields may be as important as turbulence.
➢We suggest a general picture for the early phase (prior to hot core): multi-scale fragmentation results hierarchical structures down to ~0.01 pc. Star formation is launched at the smallest scale; feedback up to the 1 pc clump scale; SF may be fed continuously through filamentary structures.

**Further questions:**
➢How are clumps related with GMCs?
➢How the cores grow physically and chemically?
→ Proposal submitted to DFG priority program "Physics of ISM"

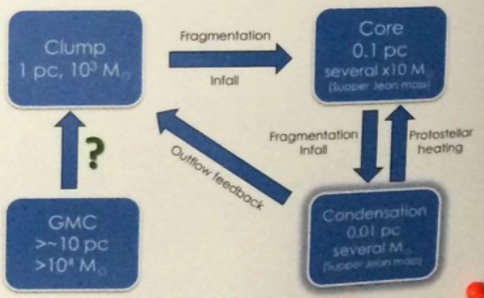


Ke Wang

# From Atoms to Stars

## — Tracing the Formation of Molecular Clouds, Supercritical Cores, and Super-Jeans Cores


Di Li[1], Pei Zuo[1], Zhiyuan Ren[1], Joshua E. G Peek[2], Nicholas Chapman[3]

[1]National Astronomical Observatories, Chinese Academy of Sciences

[2]Columbia University Department of Astronomy;

[3]Northwestern University


radio973.bao.ac.cn


**ABSTRACT**

We present three projects aiming to trace key stages of dense core formation and evolution. First, we combine the HI Narrow Self Absorption (HINSA: Li & Goldsmith 2003) technique with Herschel imaging and 2MASS extinctions to discover on-going molecular cloud formation in isolated dark clouds. Second, high resolution combined VLA+GBT ammonia maps of Orion molecular clouds are analyzed together with dust continuum to reveal likely super-critical core candidates. Third, CARMA $N_2H^+$, $HCO^+$, and 3mm continuum images show that extremely dense cores ($n\sim10^9$ cm$^{-3}$) which are in super-Jeans state and likely accreting mass.


### Isolated dark clouds exhibit the transition from HI to $H_2$

-Zuo et al. 2014, in prep.

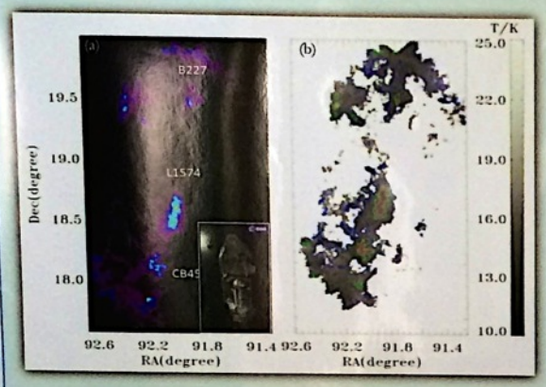


(a) The RGB image of Herschel comprised of three SPIRE band at 250 μm (blue), 350 μm (green), and 500 μm (red).
(b) Temperature distribution (10 to 25 K) of the three dark clouds overlaid with dust emission at 350 micron (blue: 0.03 Jy, green: 0.15 Jy, red: 0.27 Jy). (c) The HI absorption correlated with $^{13}$CO emission for three clouds. The circled regions of dust emission image corresponded with the spectrum of the clouds respectively.

◇**Projects**

- Herschel OT1 Program – Isolated Dark Clouds with Signs of On Going $H_2$ Formation (PI: Di Li)
- Arecibo Project – Reveal the Transition from Atomic to Molecular ISM (PI: Di Li Student PI: Pei Zuo)
- FCRAO Project – CO Emission of Dark Clouds

◇**HI Narrow Self Absorption (HINSA)**

HINSA traces cold atomic hydrogen which are cooled through collisions with molecular hydrogen and can be used for measuring the evolutionary state of clouds in terms of $H_2$ formation (Li & Goldsmith 2003, Goldsmith & Li 2005). The measured abundance of [HI]/[$H_2$] can be modeled in terms of the $H_2$ formation timescale based on

$$R_{H_2} = \frac{1}{2} S_{HI} \varepsilon_{H_2} n_{HI} \langle v_{HI} \rangle \sigma_{gr} n_{gr}$$

and

$$\frac{N(HINSA)}{cm^{-2}} = 1.95\times10^{18} \tau_0 \frac{\Delta V}{km\cdot s^{-1}} \frac{T_s}{K}$$

We selected three isolated dark clouds based on the intriguing morphology of displacement between CO, 2MASS extinction, and cold atomic gas. We obtained dust temperatures and column density based on SED fitting of Herschel data normalized by 2MASS extinction, HI abundance based on HINSA, CO column density based on $^{13}$CO.

◇**Results**

Three isolated dark clouds B227, L1574, and CB45 are at different stages of evolution.

- B227: Strong HINSA, no $^{13}$CO emission, weak dust indicating early core formation stage with ongoing $H_2$ formation.
- CB45: The dust emission is stronger, the strongest $^{13}$CO emission indicating middle stage with abundant CO.
- L1574: The strongest dust emission, the weaker $^{13}$CO emission, and lower HINSA abundance suggesting further evolution with possibly the onset of CO depletion.

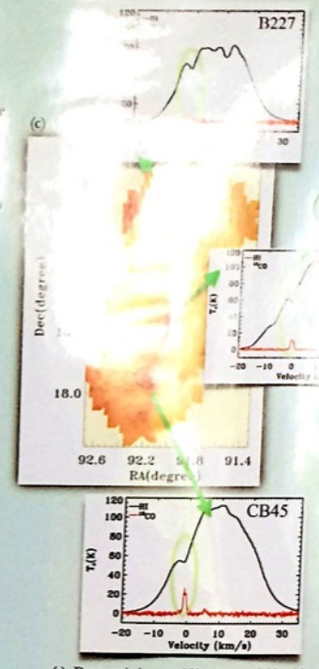


(c) Dust emission at 250 μm overlaid with corresponding HINSA and $^{13}$CO emission at three typical positions which is amplified for 10 times.

### The Super-Critical Starless Core Candidates -VLA + GBT $NH_3$ Maps

- Li et al. 2013, ApJL, 768, L5

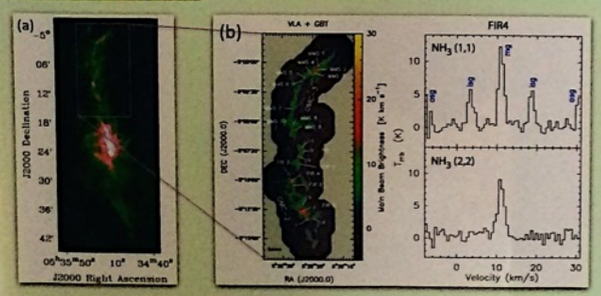


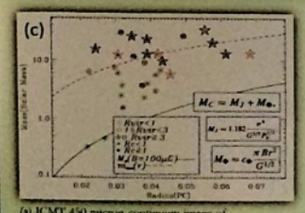


(a) JCMT 450 micron continuum image of the OMC (John stone et al. 1999);
(b) Integrated $NH_3$ (1,1) image of the OMC-2, 3 region; $NH_3$ (1,1) (2,2) spectra towards FIR4.
(c) The core mass–size relationship for the identified Orion cores. Solid line: mass supported by a steady magnetic field of 0.1 mG. Dashed line: upper limit of total pressure support from thermal and turbulent motions.

**Observation:**

We mapped the quiescent regions in the Orion Molecular Cloud (OMC) in VLA $NH_3$ (1,1) (2,2)
→ accurate $T_{kin}$ and ΔV measurements.

**Results:**

- 30 cores identified in OMC-2, 3
  ⟨M⟩=11 $M_{solar}$, ⟨r⟩=0.039 pc, ⟨$T_{kin}$⟩=17 K,
  ⟨$R_{vir}$⟩=$M_{gas}/M_{vir}$=3.9 (virial parameter)
  ⟨$R_c$⟩=1.5 (critical mass ratio)
- 14 cores have $R_c$>1. Some cores supercritical for $E_p/E_k$ energy ratios, with uncertainties considered.

**Conclusion:**

- Thermal and non-thermal gas motions alone cannot prevent collapse. Strong B-field of B>0.5 mG needed to render them subcritical (if exists).
- Orion dense cores are much more tightly bound

### Extremely Dense and Likely Super-Jeans Cores - CARMA Maps

- Ren, Li, & Chapman 2014, ApJ in Press, astro-ph:1404.7413

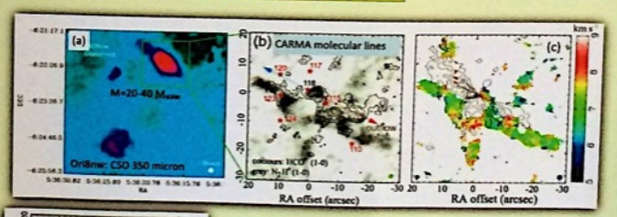


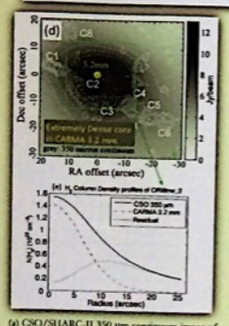


(a) CSO/SHARC-II 350 μm continuum image of ORI8nw_2. (Li et al. 2007);
(b) Integrated $N_2H^+$ and $HCO^+$ images which reveal the internal gas distribution of the 350 μm core;
(c) The velocity field of the $N_2H^+$ and its coherence with the CO outflow (contours);
(d) The location 3.2 mm continuum core within the 350 μm core;

**Source Selection:**

Ori8nw_2: the largest $R_c$ among the sample of Li et al. (2007, 2013)

**CARMA Observation:**

3.2 mm continuum, $N_2H^+$ and $HCO^+$ (1-0) at 1.5" resolution.

**Results:**

Plausible fragmentation in $N_2H^+$ clumps (Fig 3b,c)
The core is extremely centrally concentrated (Fig. 3d, e)
the gas density reaches n($H_2$)=1.6×10$^9$ cm$^{-3}$
Outflow shaping the gas structure (Fig. 3c).

**Implication:**

plausible fragmentation halted the high-mass star formation:
(T=30 K, n=10$^7$ cm$^{-3}$, B=1 mG) ⟹ $\lambda_{Jeans}$=5"
comparable to the N2H+ clump size.

To halt fragmentation:
[1] The B-field should be stronger (>5 mG) and closely coupled with the gas to resist the self-gravity, or
[2] The temperature increases so that the thermal pressure becomes more important.

The central dense core property:
[1] Absence of IR sources ⟹ likely pre-stellar stage.


Di Li

d on the respective intensity weighted velocity map (*colors*). All the *K* components show
ure. The emission regions trace closer to the center for higher *K* with larger *Eup*.
tes $H_2O$ masers (Tofani et al. 1995), and the cross is the 345 GHz continuum peak
le) Integrated intensity map (*contours*) overlaid on the respective intensity weighted vel
s) of the optimized synthetic image cube. (Lower) Integrated intensity map of the residual

# 3D LTE Spectral Line RT Models

e have constructed 3D LTE spectral line radiative transfer (RT) mod
erate synthetic image cubes for comparison with the observed data
model consists of a rotating infall envelope (Ulrich 1976) and a fl
retion disk (Pringle 1981) with additional heating from stellar irradia
nyon & Hartmann 1987). The Levenberg-Marquardt method was use
imize the model parameters by minimizing the chi-square value.
imized model gives a central stellar mass of ~12 $M_\odot$, which agrees with
ss derived by Johnston et al. (2011) through fits of the Spectral Ener
tribution (SED). The mass and size of the disk are about 2 $M_\odot$ and 850 A
nilar to those found in pervious studies (Keto & Zhang 2010; Cesaroni et a
05).

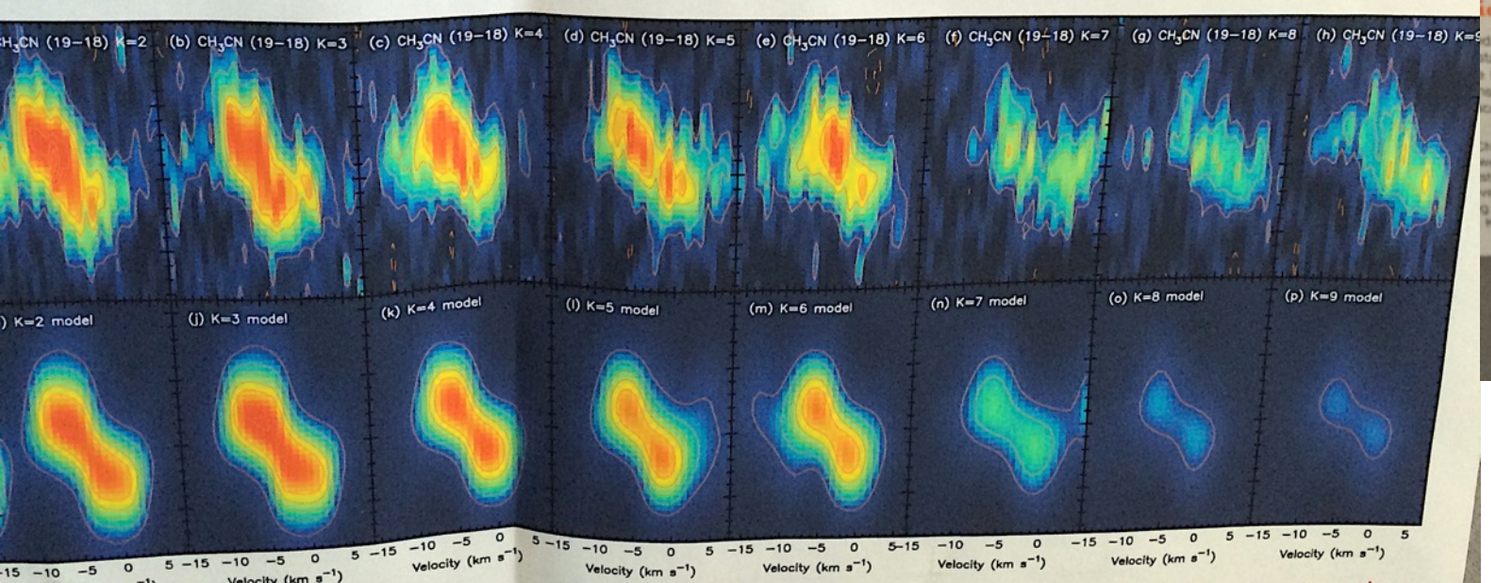


(Upper) Position-velocity diagram of the *K*=2,...,9 components of the $CH_3CN$ (19-18) transition along P.A.=67°. The velocity gradient is clearly detected in all the K components and gets progressively steeper with increasing *Eup*. (Lower) Position-velocity diagrams of the optimized synthetic image cube.

Our line and continuum observations with high angular resolution have successfully resolved the accretion disk around the massive protostar IRAS 20126+4104. The physical parameters derived from the optimized spectral line RT model suggest a hot disk with Toomre Q parameter mostly larger than unity, as previously suggested by Keto & Zhang (2010) and Johnston et al. (2011).

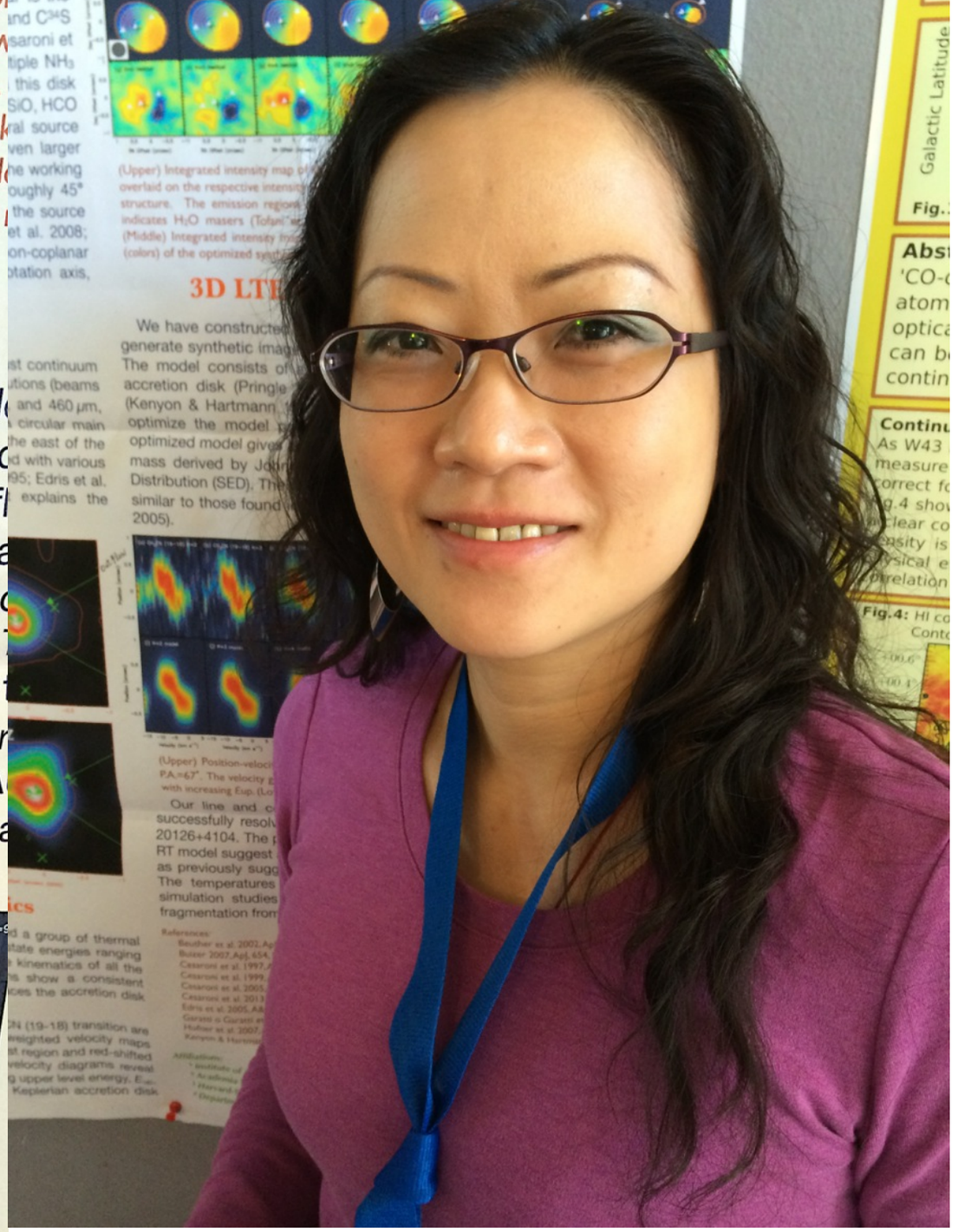

Vivien Chen

# The intriguing

***Arce**: 30% efficiency is not yet confirmed observationally*
***Steinacker**: Coreshine needs micron size grains, CONSTANT dust size distribution across a core.*
***Falgarone**: velocity shears up to 700 km/s/pc*
***Testi**: no grain grow over time? lots of optimism.*
***Bacmann**: COM around low-mass SFR, no model works.*
***Planck**: A lot of polarization, no clear insight yet.*
***Padoan**: how to reconcile the few micro-gauss galactic field with the higher field in molecular clouds?*
***Clark**: CI gives better coverage than CO both solar+lowZ*
***Crutcher**: line pol easier than dust continum pol, CN mapping*
***Jorgensen**: What if Chemistry doesn't matter?*
***Nordlund**: MRI not needed to solve the ang. momentum problem, turbulence is key*

# Magnetic fields

Holding the ocean, or going with the flow?

n) is caused by a time-evolution (the
the subsequent phases are resolved

epend on the spatial scale
e cloud scale

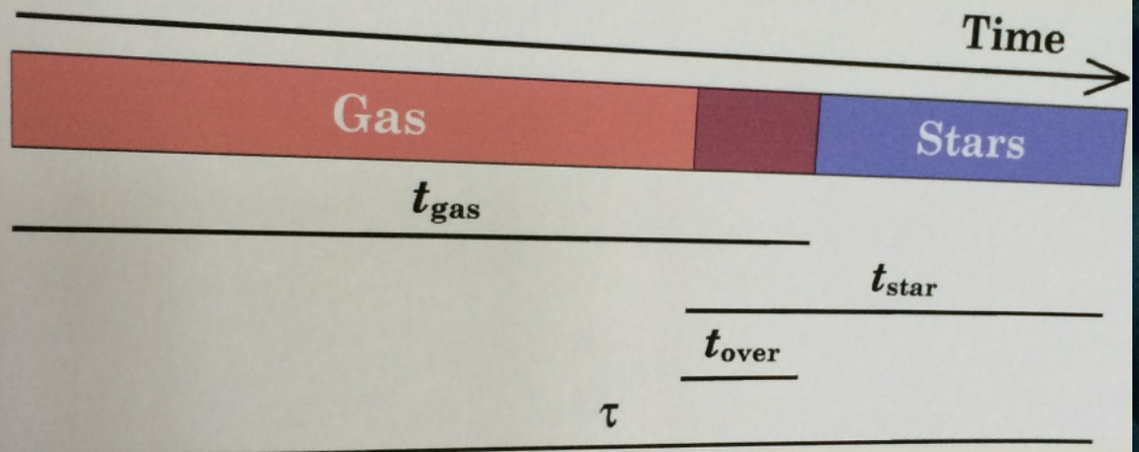


Time-sequence of star formation within a single star-forming region. Gas (red) turns into stars (blue) as time progresses. Both overlap during the purple phase, which is characterised by ongoing star formation and/or gas removal by feedback (depending on the tracers).

tic

les
ter

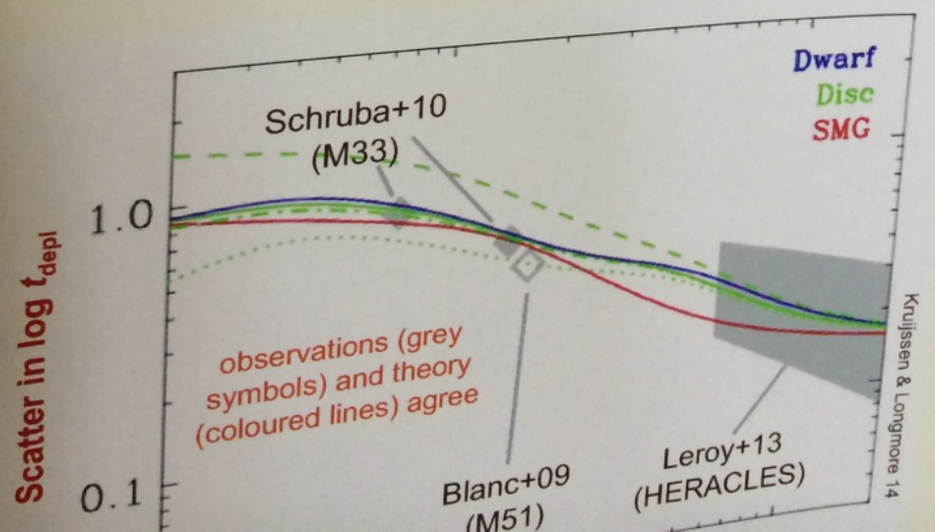


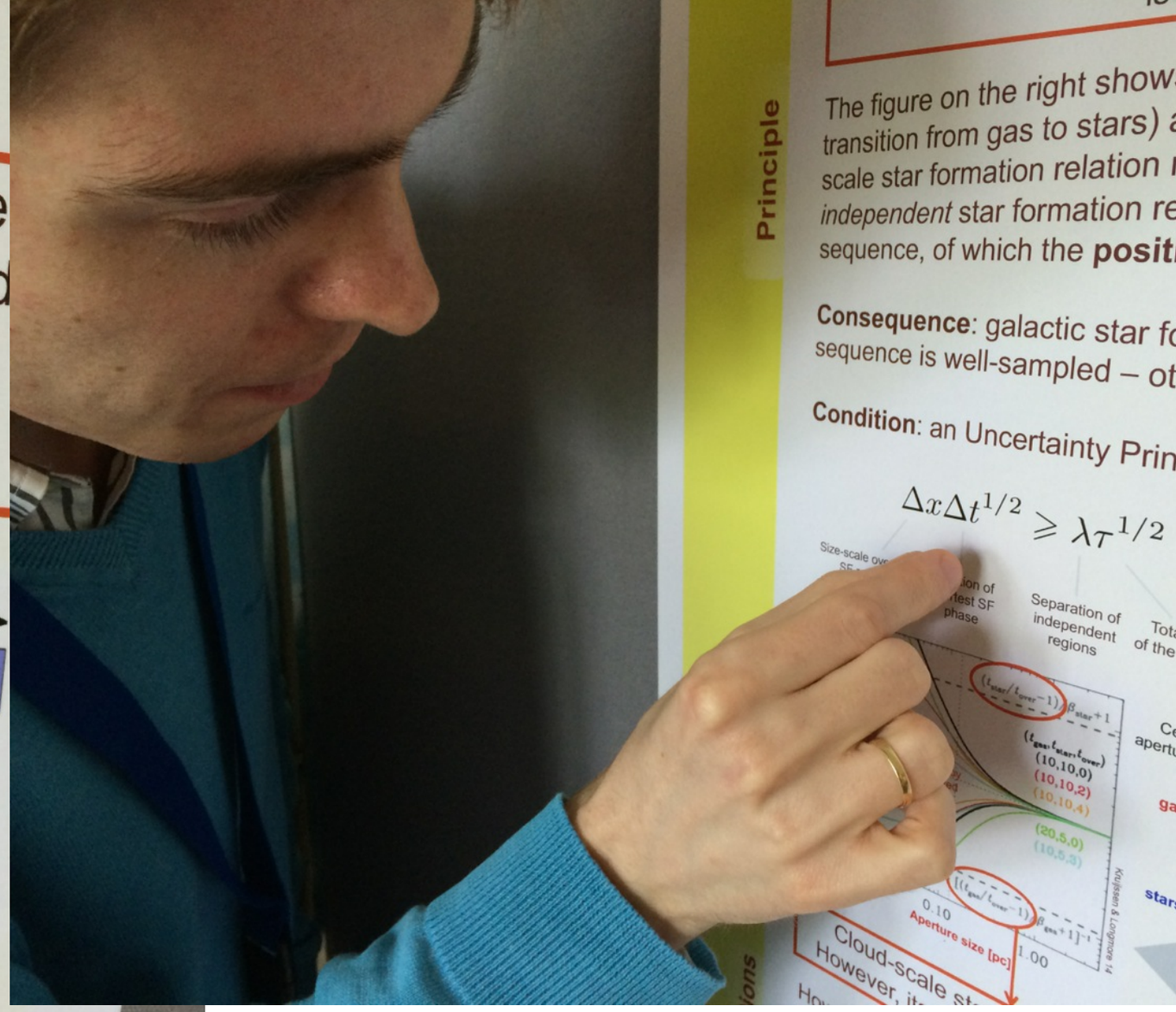


Diederik Kruijssen

# Similarities between neighbouring protostars

J. Hatchell and the JCMT Gould Belt survey team
http://www.jach.hawaii.edu/surveys/GBS_Abstract.html

**Abstract** Neighbouring SCUBA-2 450 micron cores, within 40" (10,000 AU @ 250pc) of each other, show similarity in their peak fluxes. This suggests that close pairs and small groups form in situ in the same environment through filament fragmentation. It also suggests that these neighbours have not (yet?) competed for mass either from each other or from the wider environment (e.g. through filament flows) as this would lead to mass asymmetries that are not observed.

## 1. Introduction

Pairs and small groups of neighbouring sources are interesting because they test for dynamic interactions between protostars. If neighbouring sources compete for mass, either with each other or with the environment, then one of the pair will gain mass at the expense of its companion, leading to mass imbalances. On the other hand, if pair masses are similar, then environment rather than interactions determine their masses. I have been testing this in Serpens South and Serpens Main using submillimetre continuum maps from the JCMT Gould Belt survey.

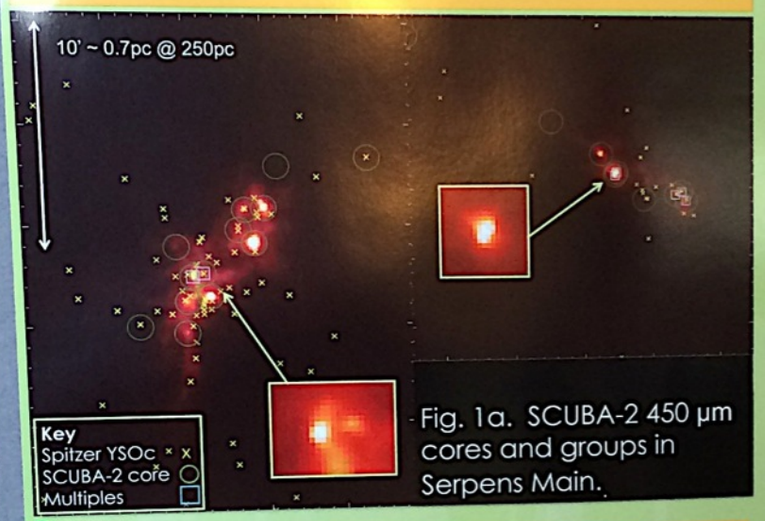


Fig. 1a. SCUBA-2 450 μm cores and groups in Serpens Main.

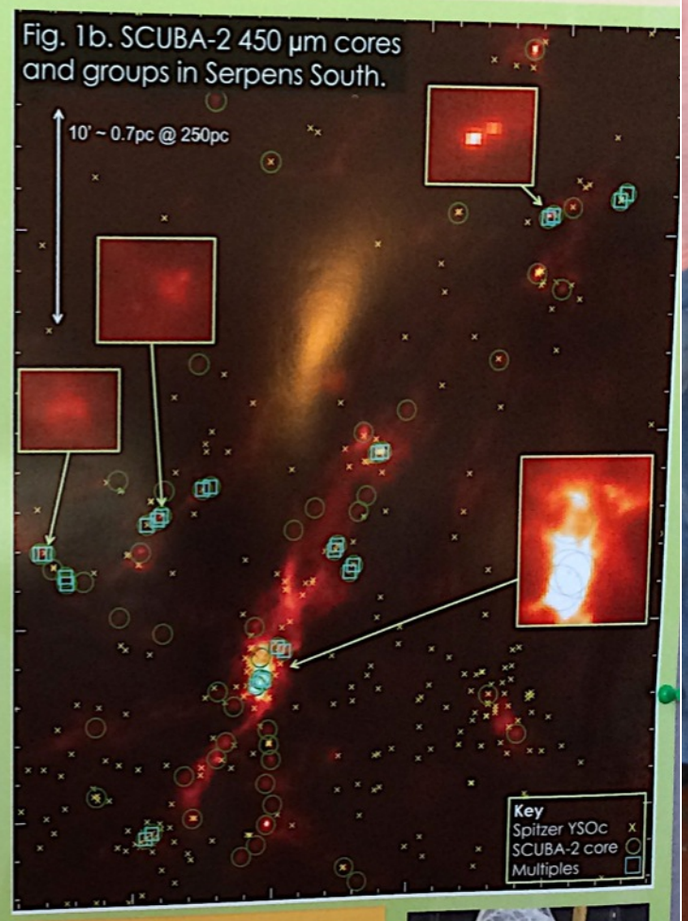


Fig. 1b. SCUBA-2 450 μm cores and groups in Serpens South.

## 2. Protostellar candidates

The Serpens/Aquila region was mapped using SCUBA-2 on JCMT simultaneously at 850 and 450 microns as part of the JCMT Gould Belt Legacy Survey (GBS). Reduced maps were processed by the GBS team using the Starlink mapmaker SMURF (Chapin et al. 2013). Peaks at 450 microns were identified using the Fellwalker algorithm (Berry et al. in prep.) and peak fluxes and 20" aperture fluxes extracted. Protostellar candidates (see Figs. 1a and 1b) were identified by cross-matching with the Spitzer Gould's Belt survey catalogues of YSO candidates (Harvey et al. 2007, Gutermuth et al. 2008) and/or by 450 micron concentration C (Enoch et al. 2007),

$$C = \frac{\text{peak flux/area} - \text{aperture flux/area}}{\text{peak flux/ area}}$$

## 3. Multiples

Pairs and groups of near neighbours were identified by position matching within 40" (10,000 AU @250pc). Sources can be separated down to the 8" 450 μm primary beam size (Dempsey et al. 2013). The groups are mainly pairs with some groups of three (see Figs. 1a and 1b).


## 4. Results and discussion

Multiples are not limited to crowded regions (Fig. 1). Also, the flux distribution for sources in multiples is similar to that of the protostellar population as a whole (Fig. 2). Both of these are consistent with a similar evolution for sources in multiples and single sources.

From Fig. 3, the fluxes of neighbouring sources are strongly correlated (correlation coefficient $r$=0.94) with the second (and third) sources roughly half the flux of the primary, on average.

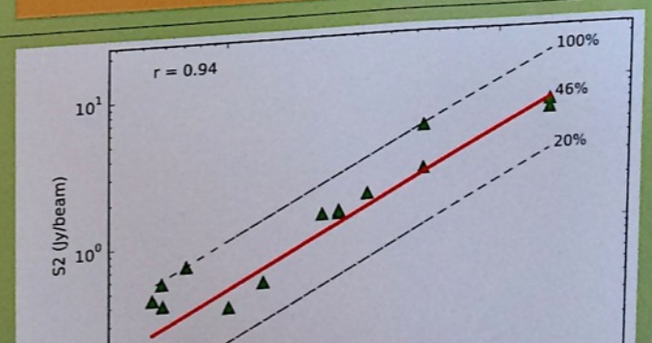


Jennifer Hatchell

# The dynamics and star-forming potential of the massive Galactic centre cloud Go.253+0.016

Katharine Johnston, Henrik Beuther, Hendrik Linz, Anika Schmiedeke, Sarah Ragan, and Thomas Henning

(Max Planck Institute for Astronomy and Cologne University)

## MOTIVATION

The massive infrared dark cloud Go.253+0.016, projected ~45 pc from the Galactic centre, contains ~$10^5$ $M_{sun}$ of dense gas whilst being mostly devoid of observed star-formation tracers.

We have carried out a concerted SMA and IRAM 30m study of this enigmatic cloud in dust continuum and molecular gas tracers to scrutinise the **physical properties, dynamics and structure** of this cloud with reference to its star-forming potential.

**Please see our paper on ArXiv!**
http://arxiv.org/abs/1404.1372

## Go.253+0.016: a massive cluster progenitor?

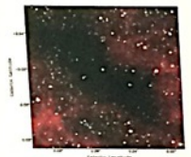

**Fig. 1 GLIMPSE Three-colour image** (3.6, 4.5, and 8 μm) of Go.253+0.016. From Figure 1 of Longmore+ 2012

**Projected 45pc** from the Galactic Centre

**Cold dust temperature:** ~18-30 K

**Dense:** 2 x $10^4$ - 6 x $10^5$ $cm^{-3}$

**High mass:** 0.8 - 7 x $10^5$ $M_{sun}$

Geometric mean **radius:** 2.8 pc

Peak **column density:** 4.4 x $10^{23}$ $cm^{-2}$ ($H_2$)

(Lis et al. 1994; Lis & Menten 1998; Lis et al. 2001; Longmore et al. 2012; Immer et al. 2012, this work)

**However... minimal evidence of ongoing SF!**

## SMA and IRAM 30m observations

### SMA Continuum and Line Observations

- SMA compact array configuration, 6 pointing mosaic
- Two 4 GHz sidebands at 218.9 & 230.9 GHz (1.37 & 1.3mm)
- Imaged spectral resolution: 2 $kms^{-1}$
- Angular resolution ~4″ x 3″ (~0.15 pc), largest scale ~21″
- rms ~70 mJy/beam for lines, 2.5 mJy/beam in continuum

**Fig 2. (right): SMA detected lines**
SiO, $CH_3OH$, HNCO, SO - shock tracers
$^{12}CO$, $^{13}CO$, $C^{18}O$, - Diffuse gas tracers
$H_2CO$ - Dense gas tracer, temperature probe

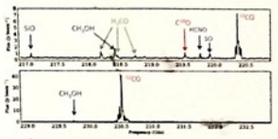


### IRAM 30m Line Observations

- Two 8 GHz sidebands placed at 217.3 and 233.0 GHz
- EMIR with FTS backend
- OTF mapping of 3′ x 4′ area (in RA/Dec)
- Angular resolution ~11 – 12″ (~0.5 pc)

## Dust emission: 36 cores detected at ~1.3mm

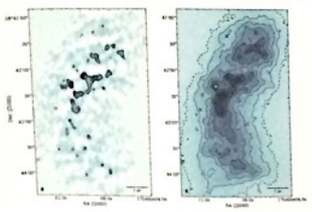

**Fig. 3 Left: 230.9 GHz or 1.3mm SMA dust continuum emission.**

**Right: Combined SMA 1.3mm and scaled SCUBA 450μm dust emission.**

The water maser observed by Lis+1994 is marked by a plus sign.

The three crosses mark the positions of the 1.3cm sources VLA 4 to 6 from Rodriguez & Zapata (2013).

## Temperatures from $H_2CO$

We used the ratio between the integrated flux of two $H_2CO$ transitions. $3(0,3) - 2(0,2)$ and $3(2,1) - 2(2,0)$

**Average line ratio : 1.4**

**Corresponding to:**

**$T_K$ > 370 K**
(>320 K for $10^{15}$ $cm^{-3}$)

**Conclusion:** gas is very hot on the size-scale traced by the SMA beam (~0.15 pc). Much hotter than found by single-dish observations of the CMZ using $H_2CO$ line ratios: $T_K$ ~60K (Ao+2013)

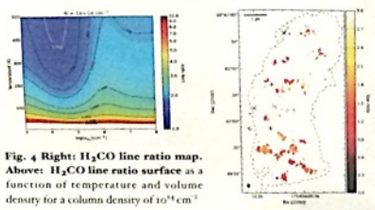

**Fig. 4 Right: $H_2CO$ line ratio map. Above: $H_2CO$ line ratio surface** as a function of temperature and volume density for a column density of $10^{14}$ $cm^{-2}$

## CONCLUSIONS

1. **We detect and characterise 36 dust cores in Go.253+0.016 at ~1.3mm**
2. **We find that the kinetic temperature of the gas traced by $H_2CO$ ratios is >320 K on size-scales of ~0.15 pc**
3. **Shock tracers and broad linewidths in the south of the cloud indicate Go.253+0.016 is colliding with another cloud at ~70 $kms^{-1}$**
4. **The CMZ is an elongated structure, orientated with Sgr B2 closer to the Sun, however its actual geometry may be more complex than an elliptical ring**
5. **The column density PDF of Go.253+0.016 is log-normal and is consistent with no SF. The Δ-variance spectrum is also consistent with no SF.**
6. **The absolute column density threshold modified for Galactic Centre turbulence is not sufficient to explain the lack of massive stars, indicating that further physical aspects may be important**

Please email any questions or comments to:
johnston@mpia.de

## Evidence for cloud collision

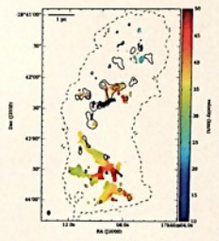

**Fig. 5 SMA $CH_3OH$ first moment map.** Black contours show 1.3mm continuum.

**Fig.6 3D rendering of Go.253+0.016.** Black: $CH_3OH$ Green: $^{13}CO$ (SMA)

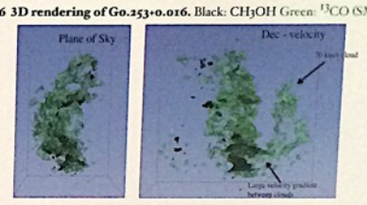


Shock tracers (such as $CH_3OH$, SO, SiO and HNCO), large velocity gradients in the south, and Go.253+0.016 overlapping in PPV space with another cloud at 70 $kms^{-1}$ suggest cloud collision (e.g. Lis+01, Higuchi +14).

## The Galactic Centre environment

**Fig. 7 HNC l-v diagram**, using the MOPRA 3mm survey of the CMZ (Jones+ 2012). Arm I and Arm II were originally shown in Sofue+ 1995. Excluding more positive longitudes than Sgr B2, these two arms could trace an elliptical orbit in l-v space or two distinct coherent velocity streams such as two spirals.

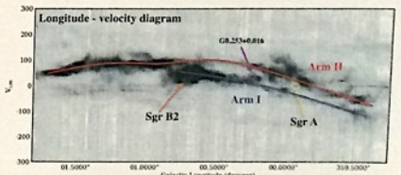



**Fig. 8 Left:** Schematic of the dynamical picture put forward by Molinari+ 2011, where the "twisted ring" observed in the far-IR with Herschel is interpreted as the stable X2 orbit of the barred Galactic potential.
**Right:** Interpretation which explains the observed l-v diagram, also determined by Sawada+ 2004.

## The star-forming potential of Go.253+0.016

PDF is log-normal! i.e. no indication of gravitational collapse

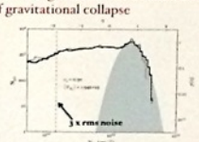


**Fig. 9 Column density probability distribution function (PDF).** Black line: combined SMA+SCUBA PDF. Grey line: SCUBA-only PDF. Grey filled area: by-eye fit to combined PDF.

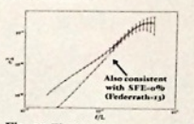


**Fig. 10 The Δ-variance spectrum of Go.253+0.016** as a function of the fractional length scale l/L. Grey line: SCUBA-only. Black line: SMA+SCUBA. Red line: best fit to the combined SMA +SCUBA Δ-variance.

**Density thresholds for star formation**

M ~ $10^5$ $M_{sun}$ lies above Lada+2010 column density threshold for SF (0.024 g $cm^{-2}$), and should produce 4 x $10^4$ YSOs, but these are not observed!

**Can turbulence explain zero observed massive stars?**

Virial mass: $M_{vir} = \frac{5R\sigma_v^2}{G\alpha_{vir}}$

For a bound cloud or core with radius R,
$N_{th} \propto M_{vir}/R^2 \propto \sigma_v^2$

**Scaled threshold column density by ratio of $\sigma_v^2$:**

$N_{th}' = N_{th}\left(\frac{\sigma_{100\,M_\odot,0.05\,pc}}{\sigma_{Giul.disk}}\right)^2$ (14 km/s / ~2.5 km/s)

$N_{th}' \sim 0.75$ g $cm^{-2}$

**Mass above new threshold and number of YSOs** (0.18 YSOs / $M_{sun}$):

$M_{th}' \sim 5.4 \times 10^4\ M_\odot \quad N_{YSO} \sim 9.7 \times 10^3$

**Number of YSOs > 15 Msun given Kroupa IMF:**

Still expect 10 YSOs > 15 Msun (not observed!)

***Possible Solutions:***

Evolution? Threshold over-density? IMF?

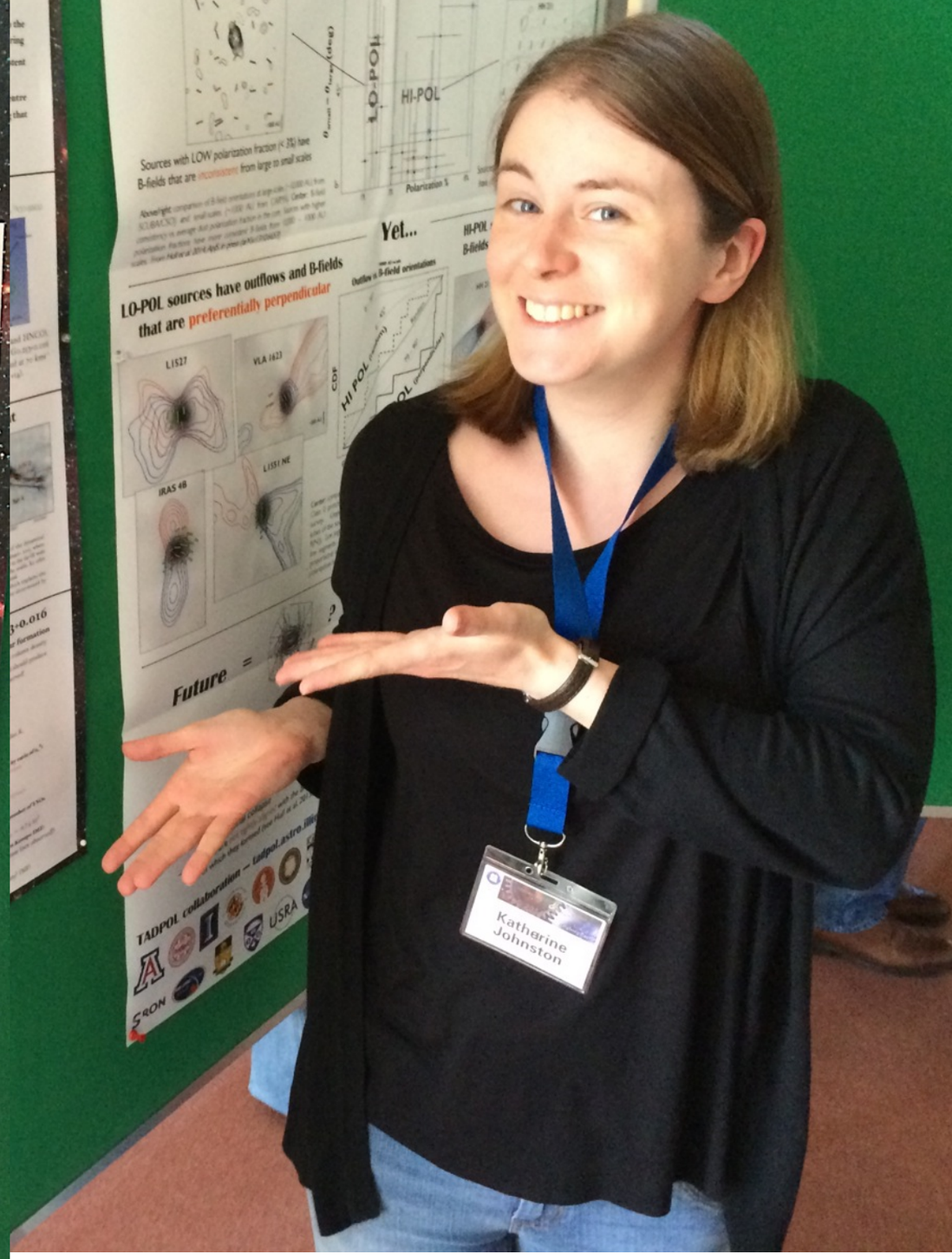


Katharine Johnston

# Outflows and clustered star formation on scales of cores to clouds

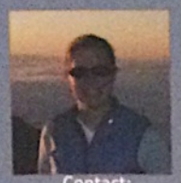

Contact:
adele.plunkett@yale.edu

Adele Plunkett[1], Héctor Arce[1], Michael Dunham[2]

Yale University[1], CfA-SAO[2]

## Overview

Protostellar clusters are the complex environments that host the majority of star formation. During the star formation process, molecular outflows are generally understood to be necessary and ubiquitous, but quantifying their impact on the nearby protostars and the surrounding cloud remains a challenge. Outflows inject momentum and energy into the cluster, feed turbulent motions, and may disperse surrounding gas. Distinguishing between these outcomes may constrain the timescales relevant to the cluster formation process, and observations will provide constraints for outflow parameters in models. Observations of clusters over a range of evolutionary stages provide evidence of the way protostellar sources evolve.

## Molecular line observations

Here we present maps of $^{12}$CO (J=1-0) to show outflow morphology. For mass, momentum, and energy calculations, $^{13}$CO is critical to correct for optical depth of the $^{12}$CO line, and the (J=3-2) transition is utilized to estimate excitation temperature. For details, please see Plunkett et al. (2013, 2014 in prep).

## Serpens South

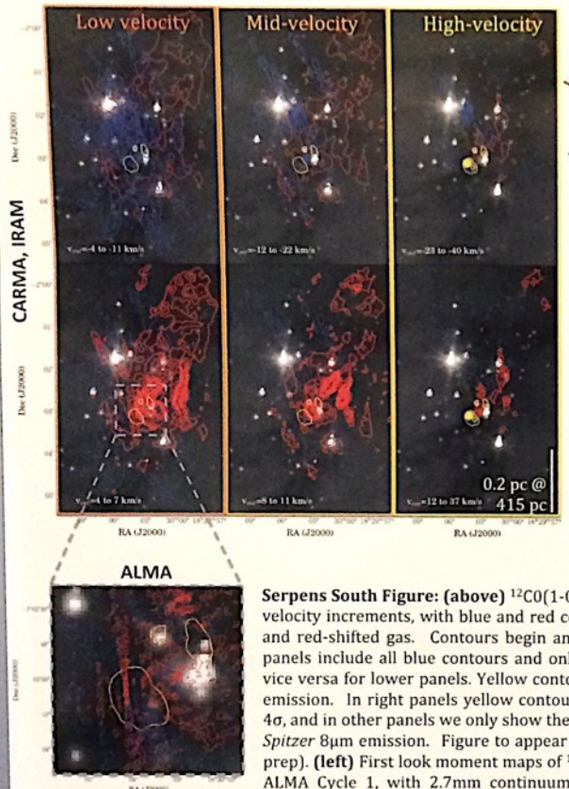


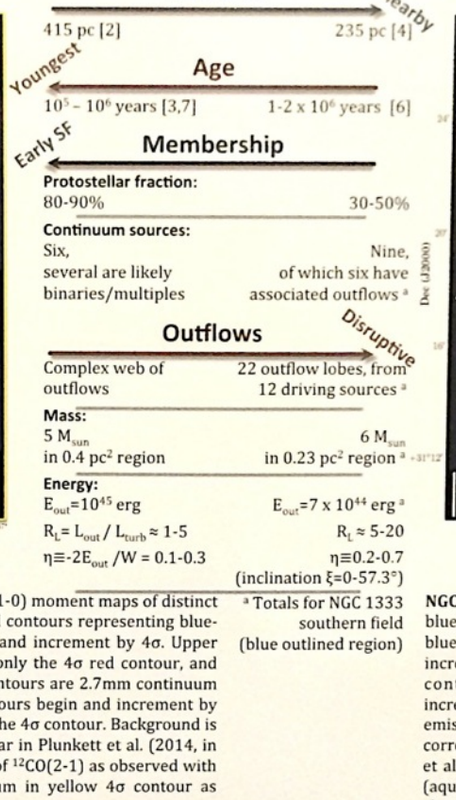


[a] Totals for NGC 1333 southern field (blue outlined region)

## NGC 1333

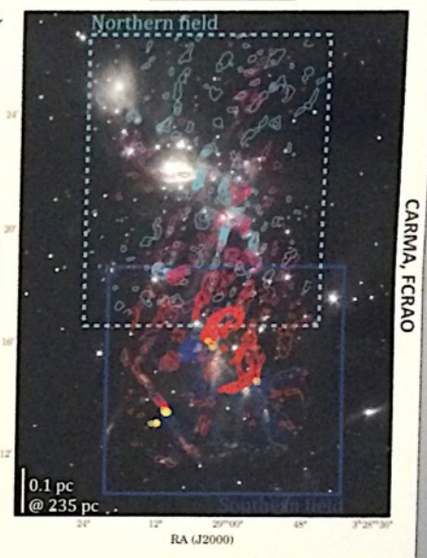


**Serpens South Figure: (above)** $^{12}$C0(1-0) moment maps of distinct velocity increments, with blue and red contours representing blue- and red-shifted gas. Contours begin and increment by 4σ. Upper panels include all blue contours and only the 4σ red contour, and vice versa for lower panels. Yellow contours are 2.7mm continuum emission. In right panels yellow contours begin and increment by 4σ, and in other panels we only show the 4σ contour. Background is *Spitzer* 8μm emission. Figure to appear in Plunkett et al. (2014, in prep). **(left)** First look moment maps of $^{12}$CO(2-1) as observed with ALMA Cycle 1, with 2.7mm continuum in yellow 4σ contour as above for reference.

**NGC 1333 Figure:** $^{12}$CO(1-0) moment maps, with blue/aqua and red/magenta contours representing blue- and red-shifted gas. Contours begin at 3σ and increment by 6σ. Yellow contours show 2.7mm continuum sources, beginning with 4σ and incrementing by 12σ. Background is *Spitzer* 4μm emission. Blue/red contours in lower (blue) box correspond to southern region presented by Plunkett et al. (2013), while aqua/magenta contours in upper (aqua, dashed) box correspond to northern region also observed with CARMA and currently in prep.

## Observational techniques

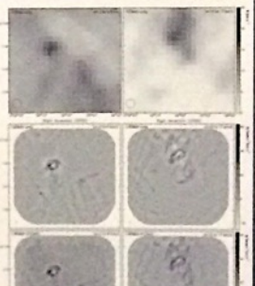

Single dish (e.g. FCRAO, IRAM 30m)
+ On-the-fly mapping technique
+ Scales up to map sizes of ~1 pc → cloud scales
- Lower resolution (~few x 10", or ~10,000 AU)

Interferometry (e.g. CARMA,)
+ Mosaic mapping technique
+ High resolution (~5", or ~1000 AU) pc → core scales
- Filter out cloud-scale emission (beyond ~90", ~.1 pc)

Combined map
+ Probe scales ~1000 AU to 1 pc in nearby regions
+ Necessary to accurately measure dynamics of outflows with small- and large-scale structure
+ To be done efficiently with ALMA

## Takeaway points

- We probe scales over two orders of magnitude, corresponding to sizes ranging from cores to clouds in nearby star-forming regions.
- It is necessary to combine interferometer mosaic (i.e. CARMA) and single dish OTF maps (e.g. FCRAO, IRAM 30m).
- In NGC 1333 we associate 22 outflow lobes with their driving sources.
- In Serpens South, higher resolution observations (i.e. ALMA Cycle 1, Plunkett et al. in prep) required to untangle a complex web of outflows.
- Outflows drive energy sufficient to sustain turbulence.
- In these regions, outflows *do not yet* contribute enough energy to cause total disruption.
- Outflows in Serpens South likely have less impact on the cloud so far, compared with NGC 1333 because Serpens South is less evolved.

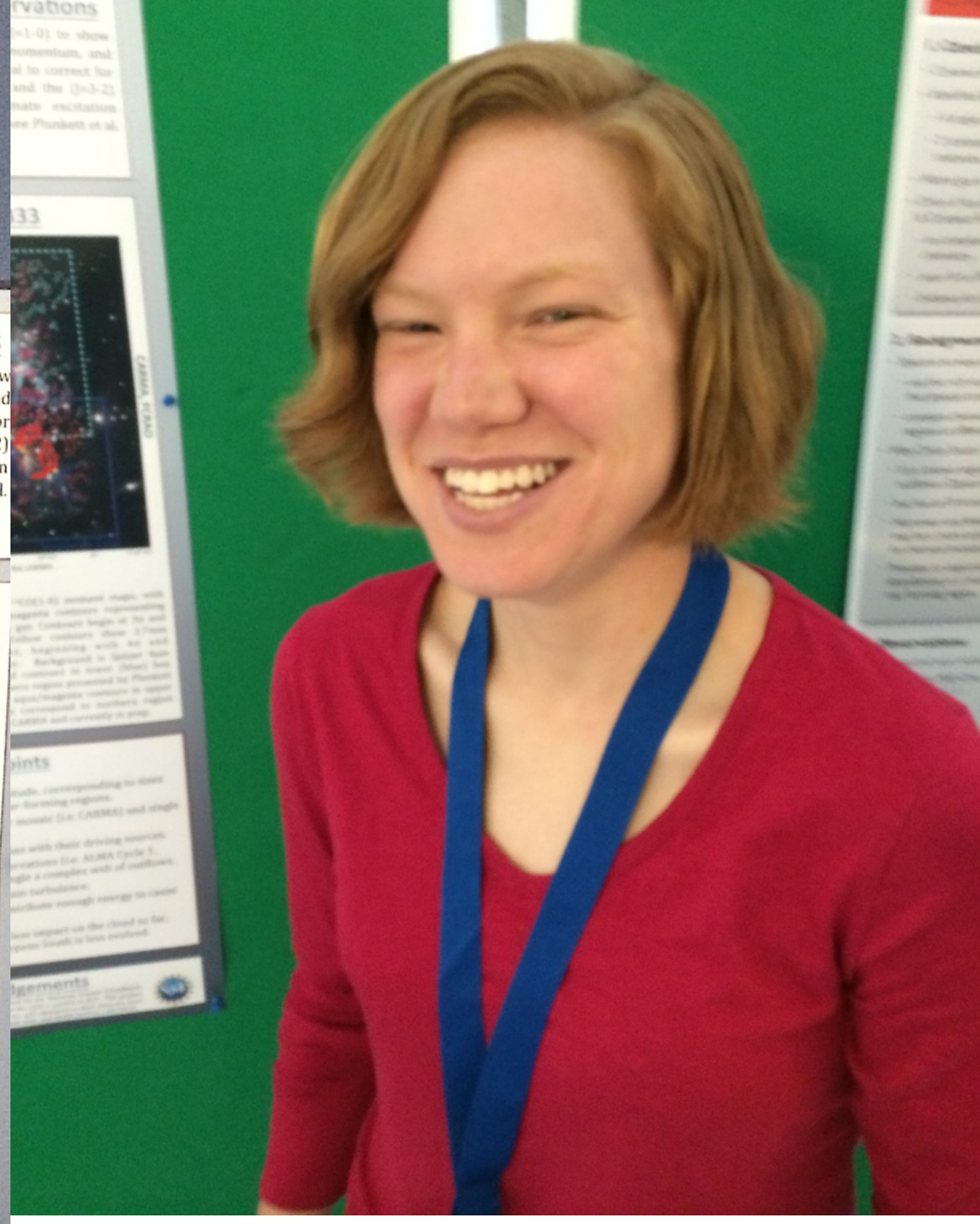

Adele Plunkett

# Investigating Outflow and Cloud Energetics in Ophiuchus and Other Gould Belt Clouds

Imperial College London

E. Drabek-Maunder[1,2], J. Hatchell[2], J. V. Buckle[3,4], E. Curtis[3], S. Graves[5], J. Richer[3,4], and G. White[6,7]

JCMT Gould Belt Legacy Survey

## Abstract

Molecular outflows are critical in understanding the early conditions of stellar formation, influencing both the final stellar mass and surrounding environment of the molecular cloud. We present $^{12}$CO, $^{13}$CO and C$^{18}$O J=3-2 data of the main Ophiuchus molecular cloud (L1688) from the Gould Belt Legacy Survey (GBS) using the JCMT. The physical characteristics of the cloud have been examined, including the excitation temperatures and optical depths. Using calculations of the mass and energetics, the Ophiuchus cloud appears to be gravitationally bound. An individual molecular outflow analysis on 30 Class 0/I protostars confirmed 8 sources with outflows. The mass, momentum, and energy of the outflows were also calculated and compared to the cloud mass and energetics, indicating outflows drive less than 10% of the turbulent kinetic energy and are not a driving agent of turbulence in Ophiuchus. This comparison of the outflow energy and cloud turbulence has been made for other nearby Gould Belt clouds (i.e. Ophiuchus Core, Serpens Main, Perseus and Orion B), investigating the significance of outflow energy driving turbulence in star forming regions.

## Calculating the mass and energetics of Ophiuchus (C$^{18}$O)

We use the C$^{18}$O isotopologue to investigate the bulk mass and energetics (i.e. turbulent and gravitational energies of the cloud because it is typically more accurate at tracing denser gas in molecular clouds since it is less abundant and less optically thick than $^{12}$CO and $^{13}$CO. The cloud mass is calculated by assuming LTE and correcting for C$^{18}$O optical depth:

$$M_{\mathrm{C^{18}O}} = 2.29\times10^{-5}\left(\frac{\text{Pixel length}}{3.49\times10^{-3}\mathrm{pc}}\right)^2\left(\frac{X_{\mathrm{C^{18}O}}}{10^{-7}}\right)^{-1} \times\sum_j\left(\frac{T_{\mathrm{ex},j}}{\exp\left(\frac{-31.6}{T_{\mathrm{ex},j}}\right)}\frac{\tau_{\mathrm{C^{18}O},j}}{1-\exp(-\tau_{\mathrm{C^{18}O},j})}\int T_{\mathrm{MB},j}\,\mathrm{d}v\right)\ \mathrm{M}_\odot,$$

where $X_{C^{18}O}$ is the relative abundance of C$^{18}$O to $H_2$, pixel length is the length of one pixel in parsecs assuming the distance of the cloud at 120 pc, $\tau_{C^{18}O}$ is the C$^{18}$O optical depth (calculated from the ratio of $^{13}$CO and C$^{18}$O; see Ladd et al. 1998), $T_{MB}$ is the main-beam temperature of C$^{18}$O and $j$ is an index over map pixels. The excitation temperature $T_{ex}$ is calculated from the 13CO peak temperature (e.g. Myers et al. 1983).

From the mass and assuming a uniform cloud density, the gravitational binding and turbulent kinetic energies are then calculated using the following:

$$E_{\mathrm{grav}} = -\frac{3}{5}\gamma\frac{GM^2}{R}$$

$$E_{\mathrm{kin}} = \frac{3}{2}M\sigma^2,$$

where $M$ is the mass of the cloud, $\gamma$ is typically 5/3 assuming a spherical cloud, $R$ is the radius of the cloud (0.50 pc at 120 pc distance) and $\sigma$ is the 1D velocity dispersion.

## High velocity blue- and red-shifted emission ($^{12}$CO)

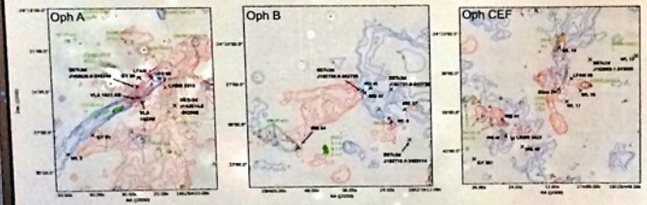


***Above:*** Images of $H_2$ 2.122 μm of the L1688 Ophiuchus cloud centred on the Oph A, B and CEF clumps. Blue and red contours denote blue- and red-shifted $^{12}$CO integrated intensities indicative of high-velocity emission from bipolar outflows. Contours: 3, 5, 10, 15, 30 and 45 K km s$^{-1}$. Protostellar sources are denoted by ×. $H_2$ knots are labelled as .

## Global outflow energetics in Ophiuchus ($^{12}$CO)

Unlike the cloud properties calculated with C$^{18}$O, the outflow energetics are only calculated from the high velocity ranges associated with the molecular outflows. The more abundant $^{12}$CO isotopologue is used to calculate the properties of the high velocity emission associated with molecular outflows. Assuming LTE, a constant $T_{ex}$ of 50 K (e.g. Curtis et al. 2010; Graves et al. 2010; Hatchell et al. 2007) and correcting for the $^{12}$CO optical depth, the kinetic energy from the high velocity emission is calculated from

$$E_{flow} = 3.77\times10^{-8}\left(\frac{X_{\mathrm{CO}}}{10^{-4}}\right)^{-1}\left(\frac{d}{120\ \mathrm{pc}}\right)^2\times\left(\frac{A_{\mathrm{pixel}}}{\mathrm{arcsec}^2}\right)\sum_j\left(\int T_{\mathrm{MB}}(v-v_s)^2\frac{\tau_{12}}{1-\exp(\tau_{12})}\mathrm{d}v\right)\ \mathrm{M}_\odot\frac{\mathrm{km}^2}{\mathrm{s}^2}$$

where $X_{CO}$ is the relative abundance of CO to $H_2$ (Blake et al. 1987), $A_{pixel}$ is the pixel area (36 arcsec$^2$), j is an index over map pixels, $\tau_{12}$ is the optical depth calculated from the ratio of $^{12}$CO and $^{13}$CO (see Hatchell et al. 1999; Curtis et al. 2010; Graves et al. 2010). The kinetic energy was only calculated for high velocities from -8.0 to 0.8 and 5.8 to 15.0 km/s. A correction for outflow inclination was also applied (see Bontemps et al. 1996), which increased the energy by a factor 3.

## Comparing the mass and energetics of Gould Belt clouds

| Cloud Name | Mass ($M_\odot$) | Turbulent kinetic energy (J) | Gravitational energy (J) | Outflow energy[1] (J) |
|---|---|---|---|---|
| Ophiuchus (L1688) | 515 | 6.3 x 10$^{38}$ | 4.5 x 10$^{38}$ | 1.3 x 10$^{38}$ |
| Perseus (NGC 1333)[2] | 439 | 1.7 x 10$^{38}$ | 3.5 x 10$^{38}$ | 1.5 x 10$^{39}$ |
| Perseus (IC 348)[2] | 196 | 2.6 x 10$^{37}$ | 1.2 x 10$^{38}$ | 1.0 x 10$^{37}$ |
| Perseus (L1448)[2] | 59 | 1.4 x 10$^{37}$ | 2.5 x 10$^{38}$ | 5.4 x 10$^{36}$ |
| Perseus (L1455)[2] | 19 | 3.6 x 10$^{36}$ | 5.5 x 10$^{37}$ | 1.5 x 10$^{37}$ |
| Serpens Main[3] | 203 | 4.4 x 10$^{38}$ | 4.9 x 10$^{38}$ | 3.0 x 10$^{38}$ |
| Orion B (NGC 2024)[4] | 600 | 1.6 x 10$^{40}$ | 0.2 x 10$^{40}$ | 3.0 x 10$^{40}$ ($^{13}$CO) |
| Orion B (NGC 2071)[4] | 400 | 0.4 x 10$^{40}$ | 0.1 x 10$^{40}$ | 11.2 x 10$^{40}$ ($^{13}$CO) |

[1]Outflow energies calculated from $^{12}$CO. NGC 2024 and NGC 2071 outflow energies calculated from $^{13}$CO
[2]Values taken from Curtis et al. (2010)
[3]Values taken from Graves et al. (2010)
[4]Values taken from Buckle et al. (2010)

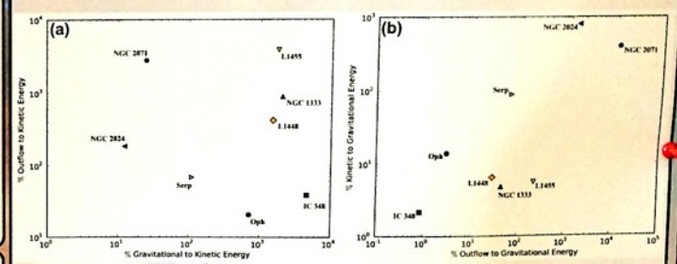


(a) Comparison of the outflow and gravitational energies (weighted by the cloud kinetic energy). There does not seem to be a correlation.

(b) Comparison of the outflow and turbulent kinetic energies (weighted by the cloud gravitational energy). There is a possible correlation between high outflow energy and high turbulence in the clouds.

(c) Comparison of the gravitational binding and turbulent kinetic energies (weighted by the outflow energy). There is a possible correlation between high turbulent kinetic and high gravitational binding energies in the clouds.

## Outflow injection ($L_{tot}$) and turbulent dissipation rates ($L_{turb}$)

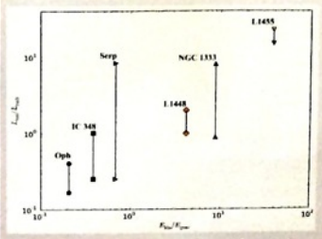


***Above:*** Plot comparing the ratio of the outflow injection rate and turbulent dissipation rate to the ratio of the turbulent kinetic and gravitational energies. The range of $L_{out}/L_{turb}$ is from the two turbulent dissipation rates calculated using outflow and cloud scales.

Outflow injection rate assuming $T_I$ is the lifetime of a Class I protostar (0.5 Myr; Evans et al. 2009) is $L_{tot} = E_{out}/T_I$. The turbulent dissipation rate (MacLow 1999) is

$$L_{\mathrm{turb}} = f\frac{\frac{1}{2}M{v_{\mathrm{FWHM}}}^2}{\lambda_d/v_{\mathrm{FWHM}}}$$

where $f$=0.33, $M$ is the cloud mass, $v_{FWHM}$ is the FWHM velocity and $\lambda_d$ is the driving scale of supersonic turbulence.

As the outflow injection rate increases with respect to the turbulent dissipation rate, the cloud kinetic energy increases with respect to the gravitational energy. This could indicate a correlation between outflows and turbulence in the cloud.

## References

Blake et al., 1987, ApJ, 315, 621
Bontemps et al., 1996, A&A, 311, 858
Buckle et al., 2010, MNRAS, 401, 204
Curtis et al., 2010, MNRAS, 408, 1516
Evans et al., 2009, ApJS, 181, 321
Graves et al., 2010, MNRAS, 409, 1412
Hatchell et al., 1999, A&A, 344, 687
Hatchell et al., 2007, A&A, 472, 187
Ladd et al., 1998, ApJ, 495, 871
MacLow, 1999, ApJ, 524, 169
Myers et al., 1983, ApJ, 264, 517
Background: Ophiuchus L1688, NASA

## Affiliations

[1]Imperial College London
[2]University of Exeter
[3]Cavendish Laboratory (Cambridge)
[4]Kavli Institute for Cosmology (Cambridge)
[5]Joint Astronomy Centre
[6]Rutherford Appleton Laboratory
[7]Open University

e.drabek-maunder@imperial.ac.uk
Twitter: @EDrabek

Emily Drabek-Maunder

# What Drives the Outflows in Star Forming Clusters?

## SiO (5-4) Outflows and the 1.3 mm Continuum Driving Sources in NGC2264-C

Nichol Cunningham[1], Stuart Lumsden[1], Claudia Cyganowski[2,3]
(1) University of Leeds . (2) University of St. Andrews . (3) Harvard-Smithsonian CFA
Email: pync@leeds.ac.uk
UNIVERSITY OF LEEDS

**Observations** – NGC2264-C, an active massive star forming region, was observed with the Submillimeter Array (SMA) at 1.3 mm in compact configuration (~3", ~2000au). The frequency range observed (216.8-220.8, 228.8-232.8 GHz) includes a myriad of molecular emission, in particular the **active outflow tracer SiO (5-4),** allowing us to present the **first interferometric observations of SiO (5-4) towards NGC2264-C.**

NGC2264-C was selected for higher resolution follow up with the SMA for a number of reasons;

- Our previous JCMT single dish observations reveal multiple outflows in both CO (3-2) (Maud et al in prep) and SiO (8-7) (Cunningham et al in prep)
- It harbours the closest RMS Survey [1] source (~740pc) with a Lbol > 1000Lsun (the infrared bright B2 9.5 solar mass star GL989-IRS1)
- Previous observations also reveal a plethora of mm peaks with masses in the range of 2~40Msun [2, 3] along with several CO outflows and H2 jets [4, 5].

*NGC2264-C therefore provides a unique environment to explore outflow emission from a multitude of cores of varying mass and evolutionary stage.*

### SiO (5-4) Outflows

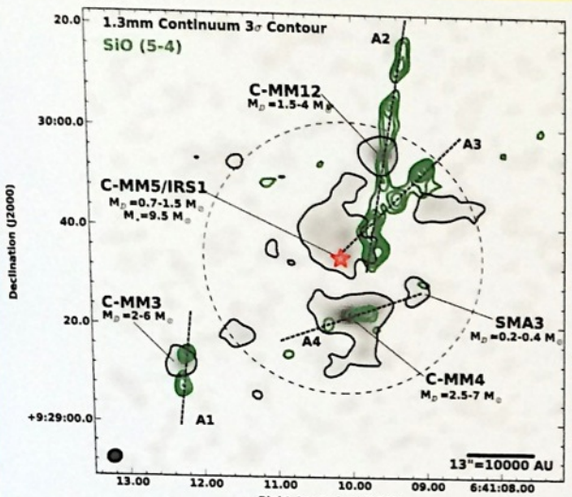


Fig 1 Integrated intensity map of SiO (5-4) (green contours) overlaid on the 1.3mm continuum (greyscale peak=0.16Jy/beam, rms=2mJy/beam) . The dashed black circle represents the FWHP of the primary beam and the filled circle the synthesised beam (~3").

- SiO (5-4) emission is detected along 4 potential outflow axis (Fig.1). ***Collimated, knotty, bipolar SiO(5-4)*** *emission is observed towards C-MM3 and C-MM12, along axis A1 and A2.*
- The moment 1 map (Fig 4) shows highly red- and blue-shifted SiO (5-4) emission towards ***C-MM3*** and ***C-MM12*** (up to **30km/s** w.r.t the vlsr of ~8km/s)(Fig.4).
- Along A3, while we do not identify a driving source, SiO (5-4) emission with velocities (>10 km/s) is detected.
- Towards C-MM4, along axis A4, only weak SiO (5-4) emission with no high velocity component (<9 km/s) is observed.

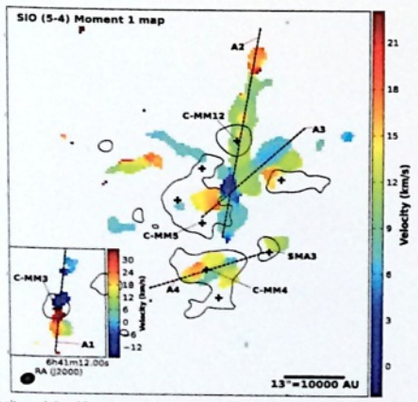


Fig 4 Velocity weighted integrated SiO (5-4) map, black contour is 1.3 mm 3sigma contour.

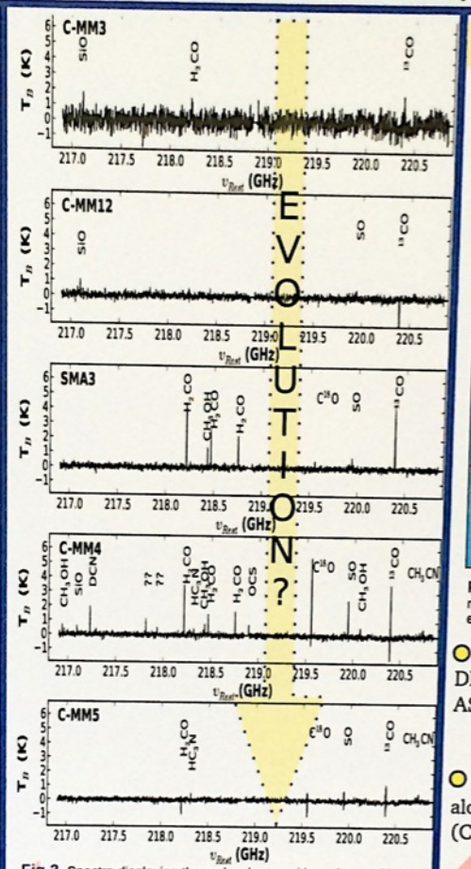


Fig 3 Spectra displaying the molecular transitions detected in the frequency range (216.8-220.8 GHz) towards each of the the respective 1.3mm continuum peaks (label top left corner).

### Nature of the Outflow Driving Sources

- Of the 10 1.3 mm continuum peaks identified in NGC2264-C, SiO (5-4) emission is unambiguously observed towards the three brightest C-MM3, C-MM12 and C-MM4.
- And of these three brightest peaks, the **highly red- and blue-shifted, collimated, bipolar SiO (5-4) outflow emission** is found towards two of the infrared darkest, molecular poorest and potentially **coldest/youngest** most centrally compact mm continuum sources, **C-MM3 and C-MM12.**

### Nature of the Continuum Peaks

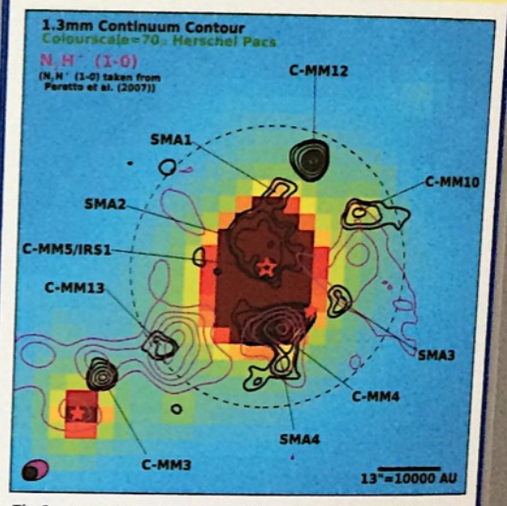


Fig 2 1.3mm continuum contours overlaid on the 70micron Herschel PACS map. Magenta contours are N2H+(1-0) taken from Peretto et al. (2007) [3] the edge of the N2H+ mosaic does not cover C-MM12.

- **10** 1.3 mm continuum peaks are identified from DENDROGRAM [6] fits to the data using ASTRODENDRO [7].
- **4 new 1.3mm** peaks (SMA- Fig.2) are identified along with 6 of the previously detected peaks (C-MM- Fig.2) [2, 3].
- Inspection of the spectra at the mm peaks (Fig 3) reveals a possible evolutionary trend going from ***molecular poor*** towards ***C-MM3 and C-MM12*** to a ***molecular rich/ hot core type spectra towards C-MM4 and SMA3.***
- C-MM5 (GL989-IRS1), which has associated CH3CN emission, is considerably brighter in the Herschel 70micron map (Fig.2) and shows no associated strong N2H+(1-0) emission. Whereas the ***darker*** 70 micron sources, ***C-MM3 and C-MM13, have associated N2H+(1-0).***
- Assuming dust temperatures of ***17-38K*** we estimate masses from ***~0.1 -7 Msun*** with a limiting 5 sigma sensitivity of ~0.1 Msun. The three most massive cores are C-MM3, C-MM4 and C-MM12.

Nichol Cunningham

# Turbulence dissipation and fragmentation in an isothermal filament: initial conditions for star formation

**Jaime E Pineda**[1], A.A. Goodman[2], H. Arce[3], P. Caselli[4], G. Fuller[5], S. Corder[6], T. Bourke[7]
1: ETH Zurich, 2: CfA, 3: U. Yale, 4: MPE, 4: U. of Manchester, 6: ALMA JAO/NRAO, 7: SKA

## The Barnard 5 Dense Core

Barnard 5 is a dense core in the Perseus cloud (~250 pc, ~40$M_{sun}$). The velocity dispersion from a high-density tracer ($NH_3$) shows subsonic turbulence within the dense core (Pineda et al., 2010).

Filaments are revealed with high-resolution JVLA + GBT $NH_3$ data (Pineda et al.. 2011).

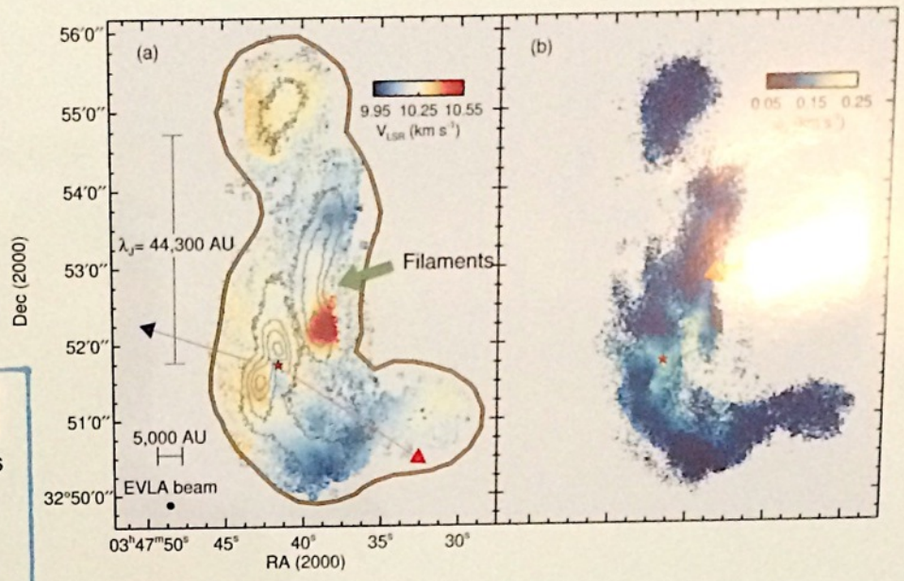


## Filament fragmentation

New SMA observations shows a starless condensation (~0.15$M_{sun}$). Excellent laboratory to study initial conditions for low-mass star formation. Is angular momentum conserved at these scales (e.g. Belloche et al., 2013)?

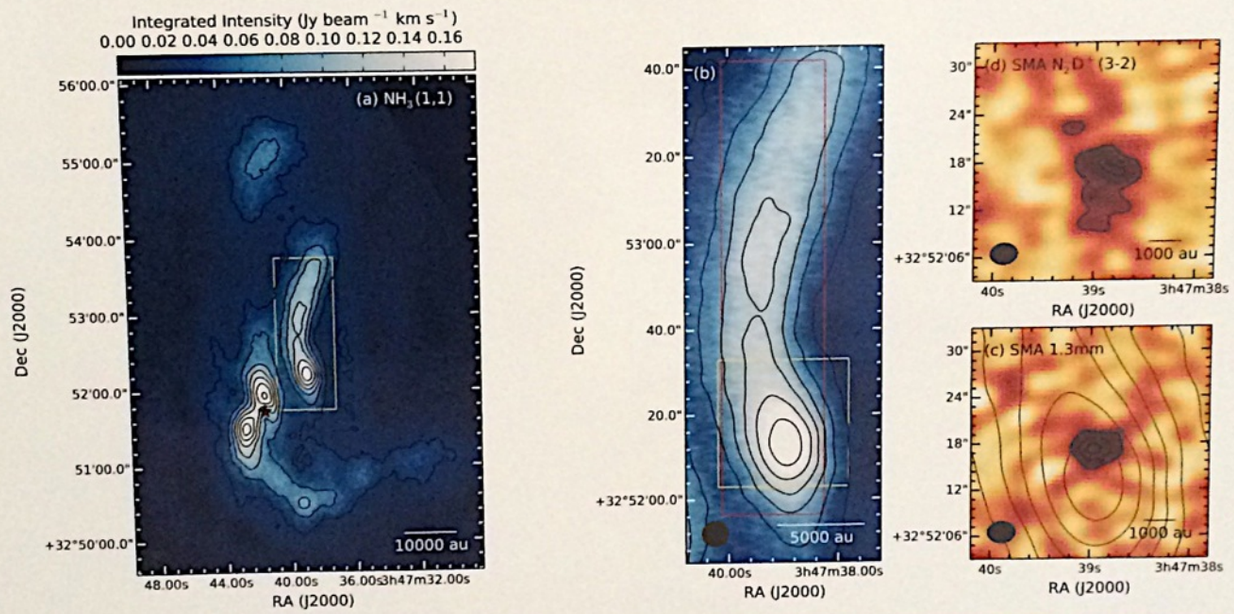


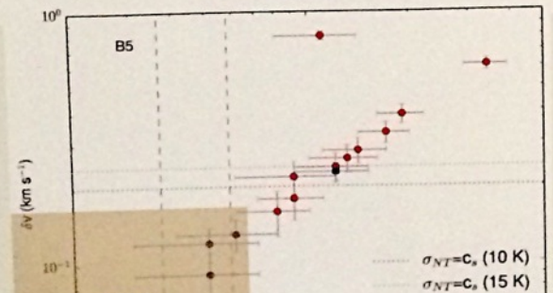


## Turbulence in the sonic regime

The turbulence in molecular clouds has been described using different techniques (PCA, SCF, VCA, VCS, power-spectrum) in the supersonic regime. However, since dense cores are located in regions of subsonic turbulence, the scaling relation will have a strong impact on the fragmentation scales and angular momentum transport. In addition, it can be used to directly test how turbulence is

Jaime Pineda

# The lovely

***Kuiper**: Bloated massive object (4000K)*
***Haugbolle**: BE + turbulent pressure gives the right IMF peak*
***Rosero**: jets seem to be common among high mass stars*
***Fendt**: disk magnetization changes substantially with disk evolution*
***Sakai**: Identification of centrifugal barrier*
***Bergin**: lovely chemistry from Orion to the Solar System*
***Li**: lovely complex talk, prediction: puffed-up disks*
***Tomisaka**: lovely complex talk, B reduces lambda in special cases, but mostly provides support*

Thomas P. Robitaille, Christine Köpferl, Francesco Biscani, and Rolf Kuiper
*Max Planck Institute for Astronomy*

# Hyperion

*3-d Monte-Carlo Radiative Transfer*

**Hyperion:**

- is an open-source 3-d Monte-Carlo radiative transfer code that is designed to be as generic as possible.

- can compute radiative transfer through a variety of three-dimensional grids, including cartesian, spherical or cylindrical polar, adaptive cartesian grids, and now unstructured Voronoi meshes.

- supports radiative transfer through dust, and we are working on implementing support for molecular lines and photoionization.

- is problem-independent, and only requires an arbitrary 3-d density structure, dust properties, and the position and properties of the illuminating sources.

- can compute temperatures, SEDs, images, and polarization maps.

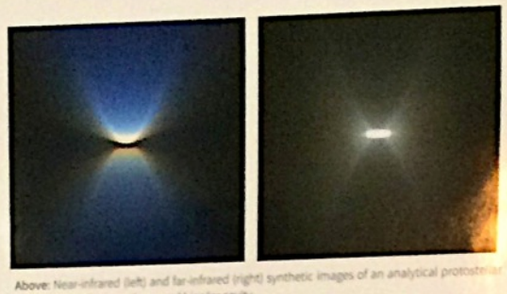

**Above:** Near-infrared (left) and far-infrared (right) synthetic images of an analytical protostellar model with a disk, envelope, and bipolar cavity.

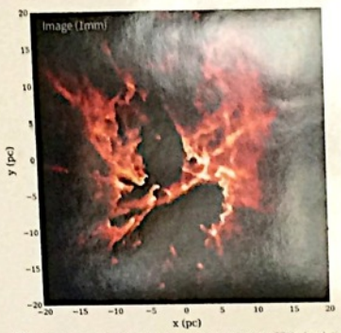


**Above:** mm image produced by Hyperion using an SPH simulation that shows the effect of feedback from massive stars (simulation from Jim Dale).

## Star formation from local to global scales

One of the fundamental aspects of Hyperion is the ability to compute radiative transfer on arbitrary density grids, which makes it suitable for computing models relevant to star formation, from individual young stellar objects (YSOs) to whole star formation regions or galaxies.

For example, Hyperion is currently being used to compute a new generation of model YSO SEDs that will supersede the Robitaille et al. (2006) models, and has also been used to self-consistently compute the diffuse emission from the Milky-Way (Robitaille et al. 2012).

## New features

Support for **SPH simulations**, with an easy way to grid the SPH particles onto an octree grid (see figure above).

Support for computing **vertical hydrostatic equilibrium** in disks:

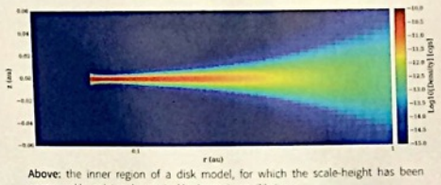


**Above:** the inner region of a disk model, for which the scale-height has been computed by solving the vertical hydrostatic equilibrium.

Support for **unstructured Voronoi meshes**, following the algorithm by Camps et al (2013). This kind of mesh only requires a set of (x, y, z) points to define the sites around which cells are placed, and points can be added anywhere resolution is required:

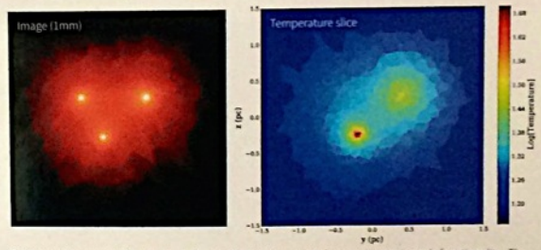


**Above:** simple model of a cloud containing three stars, using the new Voronoi mesh functionality. The number of cells is low to highlight the mesh structure.


**Above:** volume rendering visualization of the density and temperature for a dynamical simulation of a forming star with a bipolar outflow (simulation from S. Offner).

## Interfacing with simulation tools

Hyperion is able to compute radiative transfer on adaptive mesh refinement (AMR) grids, octrees, and Voronoi meshes, making it suitable to do (post-processing) radiative transfer on dynamical simulations.

In addition, the output from Hyperion can be easily exported to the yt package (http://yt-project.org), which can produce high quality volume rendering visualizations.

The plot on the left shows a simulation of a forming star by Offner et al. (in preparation). The density grid is taken from the simulation, the temperature was computed from Hyperion, and the visualization was produced by yt.

## Planned features

We are actively working on adding support for molecular line radiative transfer, as well as photoionization. If you are interested in helping develop and/or test these features, let us know!

http://www.hyperion-rt.org

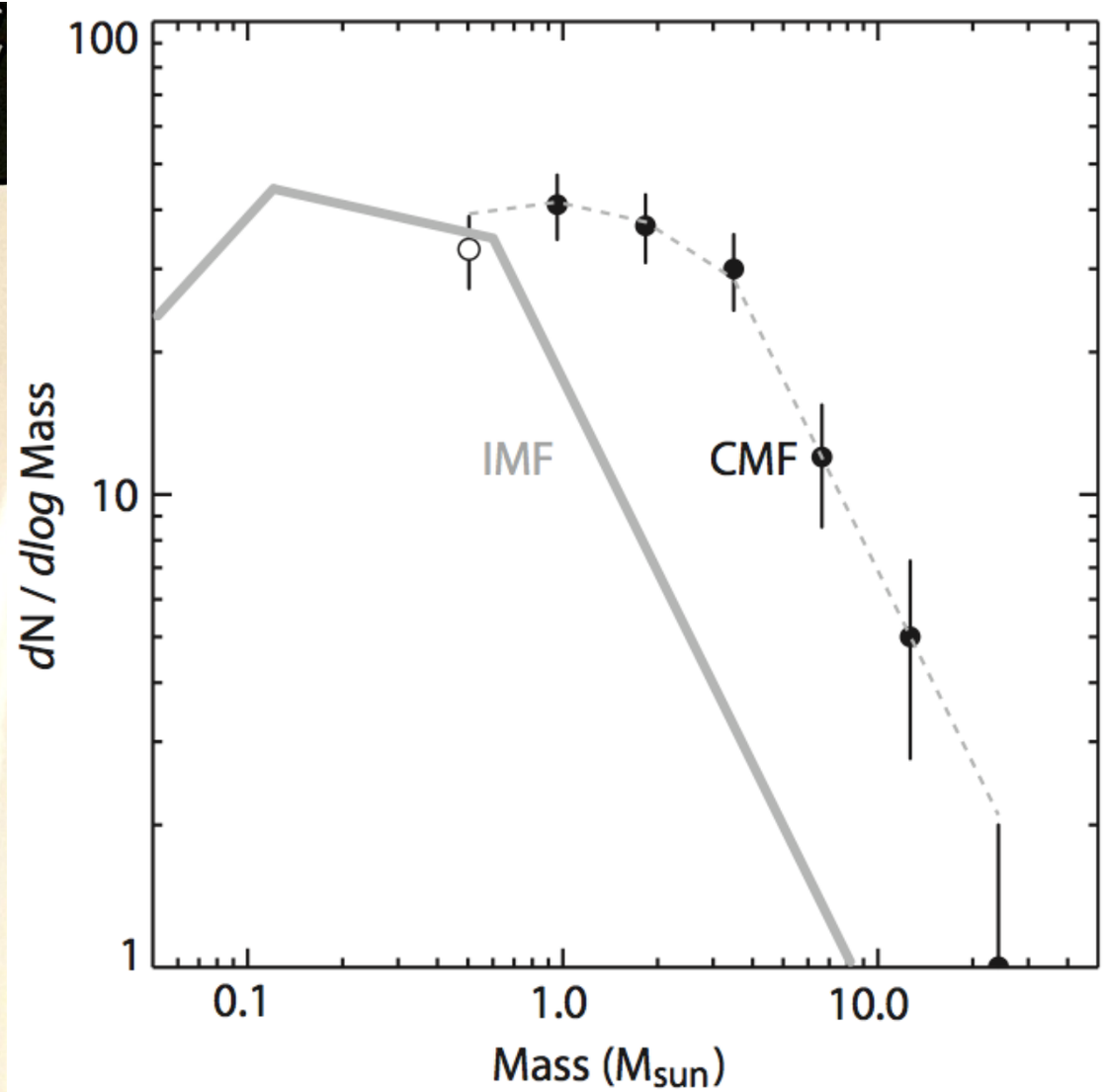


Thomas Robitaille

# FuSIOn
# Feedback in massive star forming regions: from SImulations to Observations

A. F. Mc Leod[1], L. Testi[1], J. E. Dale[2], A. Ginsburg[1], S. Ramsay[1]

[1]European Southern Observatory, Karl-Schwarzschild-Str. 2, 85748 Garching b. München, Germany
[2]Universitäts-Sternwarte München, Scheinerstr. 1, 81679 München, Germany

## Abstract

*Massive stars and star clusters have great impact on their immediate surroundings: via their strong stellar winds and radiation they are able to shape and deplete the surrounding molecular clouds they originally formed from, and are thought to be the cause of new star formation at the rim of these clouds. The feedback mechanisms have been modelled with powerful smoothed particle hydrodynamic simulations, showing that radiation from massive clusters clears bubble-shaped gas voids exposing pillar-like structures, reduces the overall star formation rate and efficiency and affects the geometrical distribution of stars. While many of the features observed in numerical simulations are in qualitative agreement with the observed morphology of massive star forming complexes, a detailed quantitative comparison is lacking. We are using the extensive library of numerical simulations of high-mass star formation with feedback assembled by Dale et al. to extract time dependent observable parameters to be compared with the observational data.*

## Computing stellar feedback

- hybrid 2-body/SPH code by Dale et al.
- types of feedback: stellar winds, photoionization
- here: $M_{i,cloud} = 10^4\ M_\odot$, $R_i = 2.5$ pc, $n(H_2) = 9096$ cm$^{-3}$

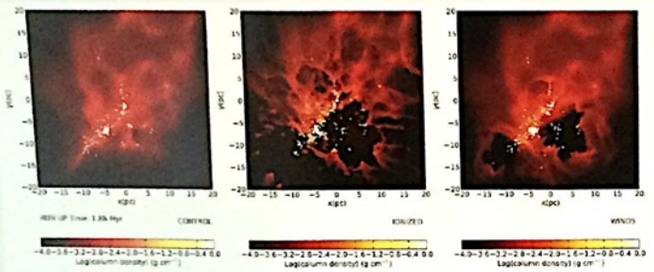

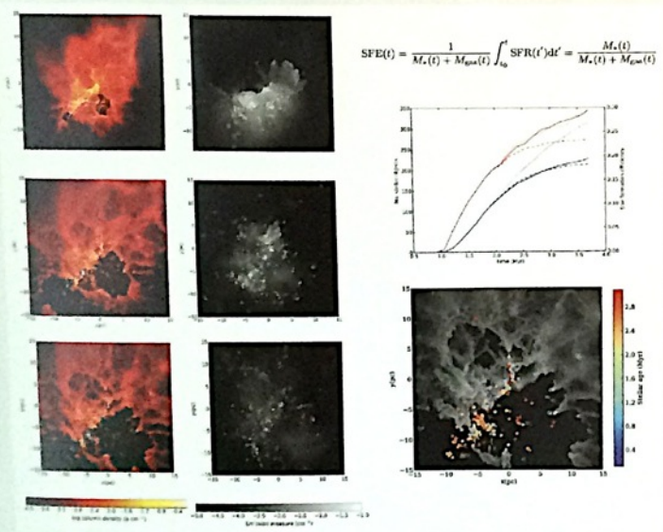


## SED fit: temperature, column density and cloud mass

- data: Herschel Hi-GAL 70, 160, 350 and 500 $\mu$m
- initial source sample: 23 cloud clumps[a], $10^4 M_\odot < M < 10^6 M_\odot$

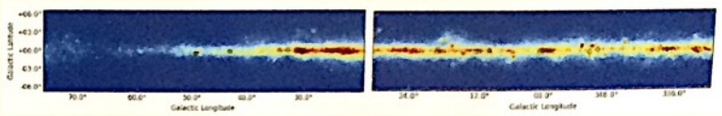

IRAS17220-3609:

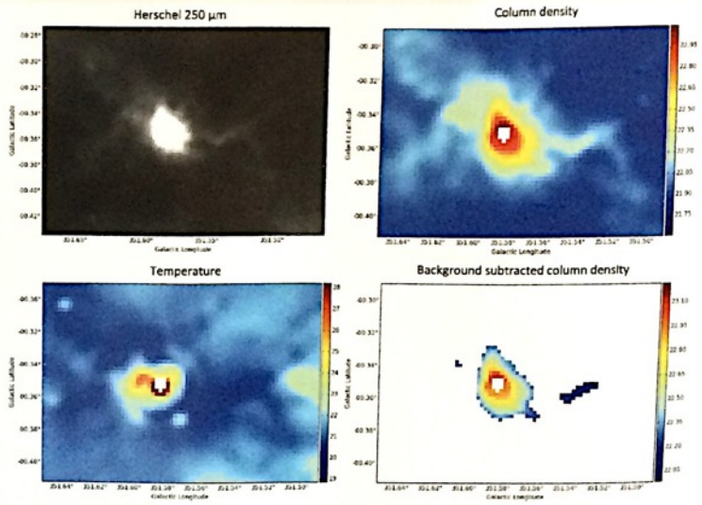


- Faùndez et al., 2004: M = 24000 $M_\odot$ with D = 10 kpc
- this work: M $\simeq$ 23990 $M_\odot$

[a]from SIMBA survey of high-mass star forming regions (Faùndez et al., 2004) and Bolocam Galactic Plane Survey (Ginsburg et al., 2012)

## Observable extraction

*Aim* Extraction of observable parameters from simulations,

## References

Anna Mc Leod

# Molecular cloud evolution: Cloud destruction by stellar feedback.

Manuel Zamora-Avilés[1], Robi Banerjee[2] & Enrique Vázquez-Semadeni[1]

[1]Centro de Radioastronomía y Astrofísica, UNAM, Campus Morelia, México [2]Hamburger Sternwarte; Hamburg; Germany

Abstract: We present MHD simulations including radiative transfer and magnetic field (using the FLASH code) of the evolution of molecular clouds formed by two colliding warm neutral medium flows. These clouds eventually begin to form stars/clusters and also to collapse globally. We found that the massive stars formed, effectively stop the global collapse evaporating and dispersing a large fraction of dense gas, thus regulating the rate and efficiency of star formation.

## Sink formation

Jeans criterion (Truelove,1997) ⟹ $\lambda_J/\Delta x \geq 4$, $\lambda_J = \left(\frac{\pi c_s^2}{G\rho}\right)^{1/2}$, $\rho \sim (\Delta x)^{-2}$ → • Refinement • Sink formation

At low ρ and high T

→ Sink mass spectrum is resolution-dependent!!!

Solution:

Constant mass Criterion ⟹ • Regular Grid $(\Delta x, \rho_0)$ • Cell mass $m_0 = \rho_0 (\Delta x_0)3$, $m > f\, m_0$, $\rho = f\, \rho_0 (\Delta x_0/\Delta x)^3$ → • Refinement • Sink formation

At high ρ and low T

## Star formation prescription

•Jeans criterion

•Constant mass Criterion

→ • Refinement • Sink formation

• mass accretion → massive sinks

Each sink is a group of stars!

Kroupa IMF

Calculate the mass of the most massive star that should exist in a sink of mass $M_{sink}$

UV flux from ZAMS models

## FLASH setup...

Velocity field ("x" direction)

The FLASH (AMR) code includes:

•Magnetic Field
•Self gravity
•Radiative cooling and heating
•Stellar feedback (UV)

| | |
|---|---|
| Box size | 256 x 128³ pc³ |
| Levels | 10 |
| Resolution | 0.03 pc |

256 pc

Simulation parameters

| | |
|---|---|
| Initial uniform number density/ temp | 2 cm⁻³ / 1450 K |
| Inflow Mach number | 2.44 |
| Inflow radius | 32 pc |
| Inflow length | 112 pc |
| Initial rms Mach number | 0.7 |
| Sink formation threshold | $4 \times 10^4$ cm⁻³ |
| Magnetic Field (x direction) | 3 μG |

## Numerical Model

## Ionization Feedback

$I(r) = I(0)\exp(-\tau(r))$

$\tau(r) = a_0 N(r)$

$\Delta N = \sum_{i=0} n(H)_i a(H)_i \Delta s_i$

-Includes a detailed treatment of ionization (Frank & Mellema, 1994)
-Neglects the effects of scattering and diffuse radiation.

## Results

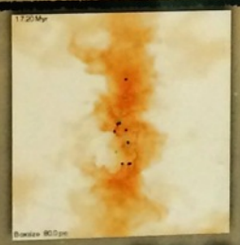

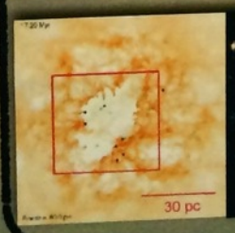



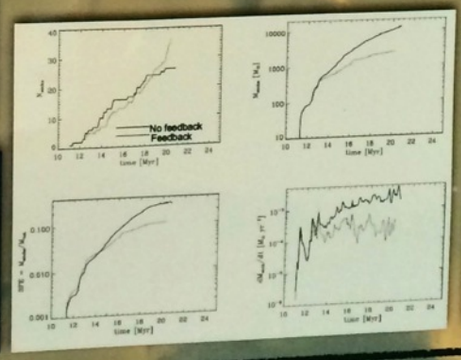


The feedback from massive-stars:
-Regulates the star formation process and therefore the fate of the Clouds, and
-Promotes low-mass star formation and inhibits the formation of massive stars.

Simulated cores reproduce the observational properties; as mass, size, density and velocity profiles, etc...

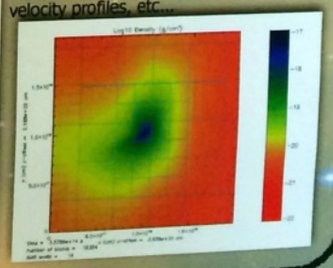

## Conclusions:

1.-The feedback regulates the SFR and the sink distribution by disrupting the cloud and terminating the local SF burst.
2.- Early collapses produce enough massive stars to eventually disrupt the cloud before all of its mass is consumed
3.- The scenario of global cloud collapse, with the SFR and SFE regulated by massive star-feedback is plausible.

References

- Truelove, J. K., Klein, R. I., McKee, C. F., Holliman, J. H., II, Howell, L. H., Greenough, J. A. 1997, ApJ, 489, L179
- Frank, A., & Mellema, G. 1994, A&A, 289, 937
- Zamora-Avilés, M., Banerjee, R., Vázquez-Semadeni, E. In preparation

M. Zamora-Avilés

# HERSCHEL ORION PROTOSTAR SURVEY

# Connecting Environment with Protostars with the Herschel Orion Protostar Survey HOPS

Thomas Stanke (ESO), Amy Stutz (MPIA Heidelberg), Tom Megeath (U. Toledo), & the HOPS team

HOPS:
~400 protostars in Orion
at same distance – in varied environments
Multiwavelength observations –> SEDs
Spitzer, NIR (e.g., HST):
inner envelope/outflow cavity; geometry!
APEX: optically thin, total envelope mass and size
Wide field FIR/submm maps:
APEX: Laboca 870mum
–> wide field temperature and column density maps @ ~20" res

L1622
NGC 2071
NGC 2068
Ori B9
NGC 2024
Horsehead

Comparing Star Formation in two Filaments in the Orion A cloud
L1641–S
OMC 2–3
– Size of plot symbols scales with log(Lbol)
– maps are shown with same spatial and intensity scaling
– L1641–S filament: lower protostellar luminosities, greater spacing between protostars
– OMC2–3 filament: higher protostellar luminosities, lower spacing between protostars
How do the Luminosity Functions change? What controls Spacing between protostars?

OMC 2–3
OMC 4
L1641–N
L1641–S
colour scale: Dust Temperature; contours: column density

Comparing Luminosities by Region: L1641 vs. ONC
Compare luminosity functions of subregions in Orion
– Orion Nebula Cluster (ONC) region:
includes OMC–2, OMC–3, and OMC–4;
Orion Nebula exluded due to bright nebulosity
– L1641 region: loose groups, lower gas column densities
– Plots show 70mum flux as proxy for Lbol
– luminosity functions (from SEDs); completeness...
– KS test: luminosity functions ARE different:
**shifted to higher luminosities in ONC/OMC2–3**
(i.e., not just better sampling a high luminosity tail due to larger number of objects)

N(H2) > 3E21 cm-2 distribution
Preliminary column density map

OMC3
OMC2
Orion Nebula
OMC4
L1641–N
L1641–C
HH1/2
L1641–S

Protostar luminosities
$$L_p = L_{\rm phot} + f_{\rm acc}\frac{Gm\dot{m}}{r}$$
photosphere accretion luminosity
For protostars, the bolometric luminosity is dominated by the accretion luminosity

Luminosity and Density of Protostars vs. Gas Column Density
– all Orion protostars in HOPS survey
– **higher gas column densities –> higher protostellar luminosities**
– **high gas column densities –> smaller protostellar spacing**

**Summary:**
– Higher gas column densities –> clustering
– Higher gas column densities –> higher luminosities
– in high column density areas, luminosity functions **are shifted to higher luminosities!**
–> as Lbol is dominated by accretion for protostars, **accretion rates are higher in high column density areas;**
and if the IMF is independent of environment:
**Protostars evolve faster in high column density areas!**
**... but what does the Temperature do?**
**...future (imminent...) work!**

Thomas Stanke

# Magnetic Fields and Massive Star Formation

Josep Miquel Girart[1], Qizhou Zhang[2], Keping Qiu[3], Pau Frau[4], Hauyu (Baobab) Liu[5], Ya-Wen Tang[5], Patrick M. Koch[5], and the SMA Legacy "*Filaments, Star Formation & Magnetic fields*" team*

[1] Institut de Ciències de l'Espai (CSIC – IEEC); [2] Harvard-Smithsonian Center for Astrophysics; [3] Nanjing University; [4] OAN / CAB-CSIC; [5] Academia Sinica Institute of Astronomy and Astrophysics


## NGC 1333 IRAS 4A: A textbook case for low mass stars

Observed magnetic field configuration with the SMA toward IRAS 4A (blue segments: $B_{pos}$ ; color image: polarized intensity; contours 880μm dust)

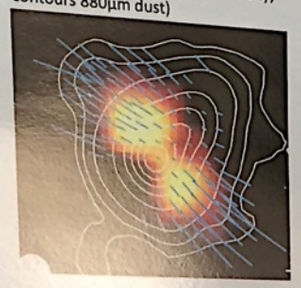

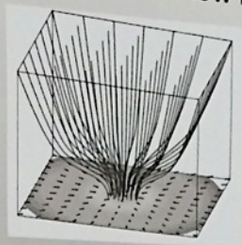

Magnetic field lines from a bird's-eye view for the case of a weakly magnetized and slow rotating core (Machida et al. 2005)

Comparison of the SMA Stokes I, Q and U images with models of magnetized molecular dense cores show that the magnetic fields threading IRAS 4A play an important role in the dynamical evolution of the core.

**Does this scenario holds in more massive regions?**

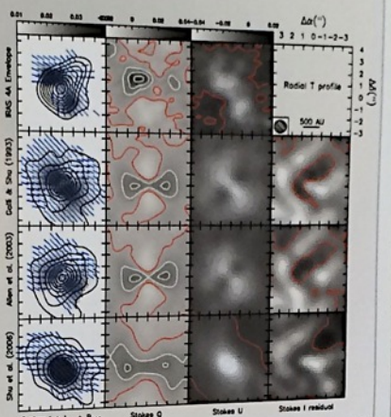


**Bibliography:**
Allen, Shu, Li 2003, ApJ, 599, 351; Frau, Galli, & Girart 2011, A&A, 535, A44; Girart, Crutcher & Rao 1999, ApJ, 525, L109; [illegible] 2006, Sci., 313, 812; Gonçalves, Galli, & [illegible] 09; Machida et al. 2005, MNRAS, 362, [illegible] 12, A&A, 543, A16

## SMA Legacy Project (2011A-S031): Filaments, Star Formation & Magnetic Fields



**Context:** Previous limited BIMA and SMA polarimetric observations reveal a range for magnetic field morphologies from well ordered to chaotic distributions (e.g., Lai et al. 2001, Girart et al. 2006, Cortes et al. 2008, Tang et al. 2009).

**Goal:** To investigate the role of magnetic fields in filament and massive star formation, and to make significant progress in understanding the role of magnetic fields in the formation of filaments, dense cores and massive stars.

**Method:** Image polarization at 880 μm with the SMA in the subcompact, compact and extended configurations, providing an angular resolution of typically 1" and 1σ rms noise of 2 mJy beam$^{-1}$. Carried out in two steps: First to conduct a shallow survey to find strong polarized sources, and second to follow them up in deeper, multi configuration observations. Simultaneous line observations of dense molecular tracers ($H^{13}CO^+$ 4-3, SiO 8-7, CO 3-2, hot core lines)

**Sample:** We selected a sample of filamentary molecular clumps from mm surveys of IRDCs, the Cygnus-X region and the Galactic Plane (Rathborne et al. 2006, Motte et al. 2007, Aguirre et al. 2011), and polarization with SCUBA (Matthews et al. 2009). To ensure polarization detection, a continuum flux lower limit of 0.5 Jy/beam at 880 μm .

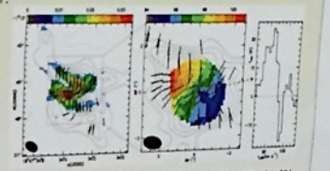


**Bibliography:**
Aguirre et al. 2011, ApJS, 192, 4; Cortes et al. 2008, ApJ, 676, 464; Frau et al. 2104, A&A, arXiv:1405.6742; Girart et al. 2009, Sci., 324, 1408; Lai et al. 2001, ApJ, 561, 864; Matthews et al. 2009, ApJS, 182, 143; Motte et al. 2007, A&A, 476, 1243; Rathborne et al. 2006, ApJ, 641, 389; Tang et al. 2009, ApJ, 695, 1399

## Molecular dense core diversity

The spatially resolved polarization images show that **magnetic fields at the core scale of 0.01 to 0.1 pc tend to be more organized rather than chaotic**. Observations show a variety of magnetic field configurations, as well of different dust continuum morphologies. Some regions exhibits clear bipolar molecular outflows, but other have a rather complex high velocity emission.

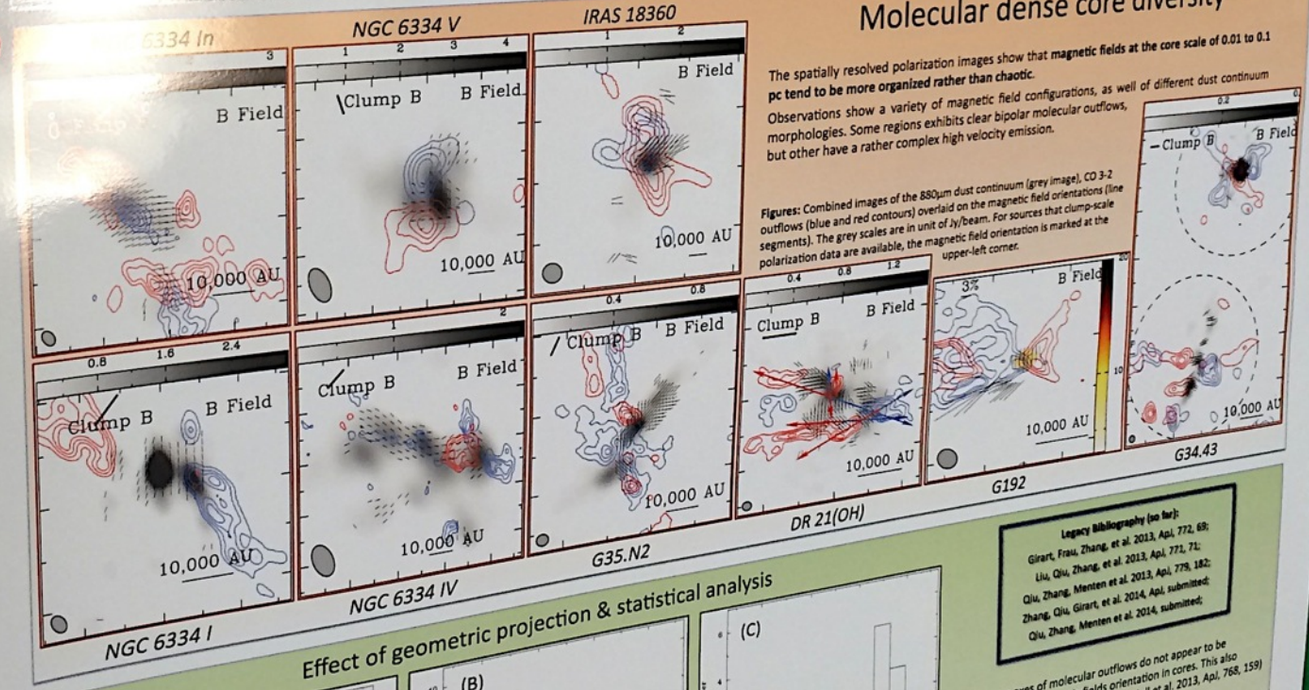


**Figures:** Combined images of the 880μm dust continuum (grey image), CO 3-2 outflows (blue and red contours) overlaid on the magnetic field orientations (line segments). The grey scales are in unit of Jy/beam. For sources that clump-scale polarization data are available, the magnetic field orientation is marked at the upper-left corner.

## Effect of geometric projection & statistical analysis

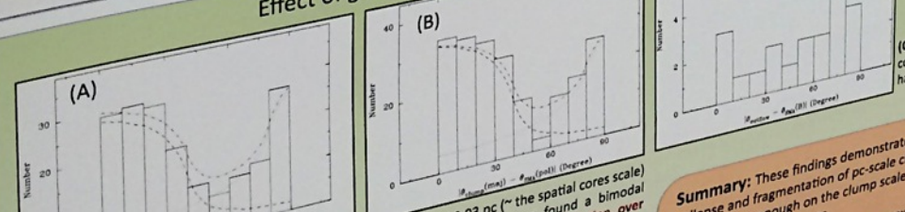


(C) The major axes of molecular outflows do not appear to be correlated with the magnetic fields orientation in cores. This also happens in low mass star forming cores (Hull et al. 2013, ApJ, 768, 159)

**Summary:** These findings demonstrate that magnetic fields play an important role during the [illegible] and fragmentation of pc-scale clumps, and the formation of dense cores. The magnetic [illegible] ough on the clump scale to guide the concentration of clump material along the [illegible] ris indicates either that the field on the disk formation [illegible] endicular to the field, or that the disk [illegible] h as gravitational interactions in

**Legacy Bibliography (so far):**
Girart, Frau, Zhang, et al. 2013, ApJ, 772, 69;
Liu, Qiu, Zhang, et al. 2013, ApJ, 771, 71;
Qiu, Zhang, Menten et al. 2013, ApJ, 779, 182;
Zhang, Qiu, Girart, et al. 2014, ApJ, submitted;
Qiu, Zhang, Menten et al. 2014, submitted;

Josep M. Girart

# Far- and sub-mm Lines from Herschel Cores

H. Linz, H. Beuther, S. Ragan, O. Krause, Th. Henning, A. Stutz,
R. Launhardt, M. Nielbock (all MPIA Heidelberg), T. Vasyunina (MPIfR Bonn)

Our group has conceived a Herschel key programme (whimsically termed EPoS), in order to map selected IRDCs and other cold higher-mass star-forming clumps as well as isolated low-mass cores in the FIR and sub-mm continuum from 70 - 500 micron. As a spin-off to EPoS towards the end of the Herschel mission, we employed the two versatile Herschel spectrographs SPIRE-FTS and PACS-Spec to scrutinise 10 very young protostars from the EPoS sample. These comprise a large range of masses and luminosities and feature low-mass Class-0 protostars as well as higher-mass cores embedded in IRDCs. Here, we show very first results of this programme. We recover CO emission from the rotational transitions 4-3 up to 13-12 with SPIRE-FTS, as well as the well-known fine structure lines of [CI] and [NII]. In some objects, the data reveal activity and higher-temperature gas that escaped our attention when solely relying on continuum data and on lower molecular line transitions. With the PACS spectroscopy for a sub-sample of objects we trace the most important cooling lines of oxygen, carbon, and water.

## SPIRE 250 micron continuum maps of the target regions

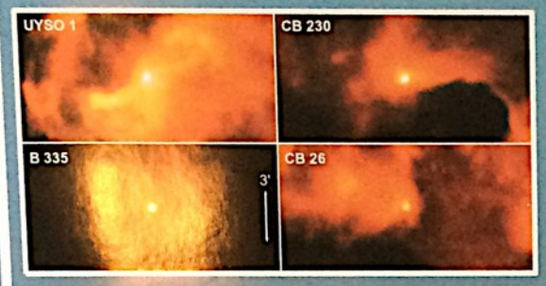


The low-mass targets: these are embedded protostars (CB230, B335) and Class I-II sources (CB26) within Bok globules, as well as a sub-millimeter core with intermediate luminosity without 24 µm counterpart (UYSO 1). All are plotted on the same *angular* scale.

This circle indicates the unvignetted field-of-view of the SPIRE FTS observations (2'), to scale with the images to the left and right.


The high-mass targets: most of them are embedded within filamentary IRDC structures. The targets are always the bright compact emission sources in the center of the images. All are plotted on the same *angular* scale.

## Examples for fitted $^{12}$CO ladders in the SPIRE FTS spectra

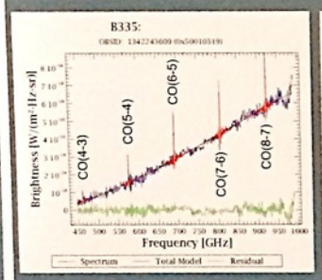


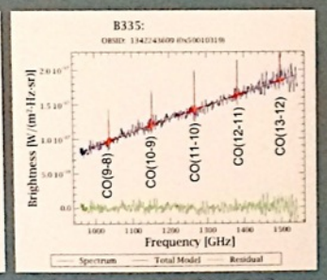


The active low-mass protostar B 335: Blue lines are the data, Red gives the fits to the $^{12}$CO line series. Green denotes the fit residuals. Here, all CO lines within the FTS range are well detected. Hence, warm gas seems to be present. The details of the excitation (purely thermal, or with additional shock and uv-excitation components) have to be studied further.

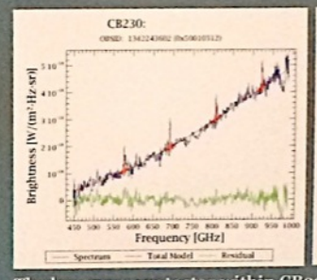


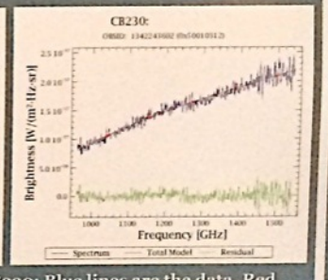


The low-mass protostar within CB230: Blue lines are the data, Red gives the fits to the $^{12}$CO line series. Green denotes the fit residuals. Only the lower CO transitions are detected. This is interesting, since also CB230 has an outflow, and has a higher $T_{bol}$ (189 K) compared to B 335 ($T_{bol}$ = 37 K, both values from Launhardt et al. 2013).

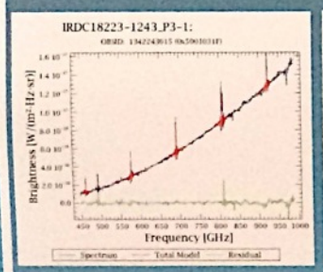


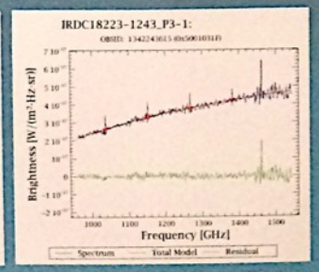


The active intermediate-mass protostar P3 within IRDC18223: Blue lines are the data, Red gives the fits to the $^{12}$CO line series. Green denotes the fit residuals. CO is well detected. This completes the picture of previous findings: this protostar drives a bipolar outflow and is associated with shocked gas ("green fuzzies"), as reported by Beuther & Steinacker 2007, and Fallscheer et al. 2009.

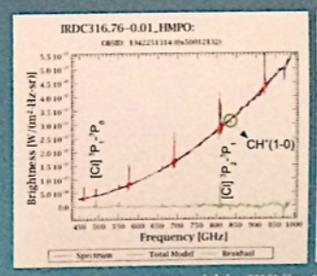


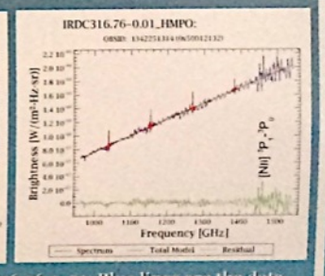


The active protostar within IRDC316.76-0.01: Blue lines are the data, Red gives the fits to the $^{12}$CO line series. Green denotes the fit residuals. Also here, the CO is detected also in the higher transitions. Some more lines are marked. As in other IRDCs, the [CI] and [NII] lines are ubiquitous and not just concentrated towards the embedded protostars. $CH^+$ is in absorption and indicates its presence in the cold foreground ISM (see Naylor et al. 2010).

## A first glimpse on PACS-S spectra towards IRDC18223-P3

Hendrik Linz

# Results from the Herschel/HEXOS Full Band Spectral Survey of Orion South

UNIVERSITY OF CALGARY

René Plume, Kianoosh Tahahi (U. Calgary), Ted Bergin (U. Michigan), & the Herschel/HEXOS Team

## 1. Conclusions:

- Covered 460-1900 GHz with resolution of 1.1 MHz.
- Identified & modeled > 400 transitions from 45 species.
  - A single, warm (40 - 60K) physical component works in most cases.
  - 2 components (cool/narrow + warm/broad) needed in some instances.
- Warm gas is extended and possibly externally heated.
- Orion S has chemical composition most similar to Orion KL Extended & Compact Ridges (except for $H_2{}^{18}O$).
  - no complex organics & poor fit to Hot Core ➡ no Hot Core chemistry.
  - poor fit to Plateau & low SiO, SO, $SO_2$ ➡ weak shock chemistry.
  - Evidence for UV chemistry?

## 2. Background & Goals:

- Spectral surveys allow us to:
  - use the rich variety of chemical species & transitions to understand the physical conditions in molecular clouds.
  - compare chemical abundances in high vs low mass star forming regions at different stages of evolution.
- Why Orion South?
  - It's a known region of massive star formation (embedded IR sources, outflows (Zapata et al. 2005;2006).
  - but has an IR luminosity x10 lower than Orion KL.
  - Narrower and fewer spectral lines (McMullen et. al 1993) indicate it may be a more quiescent star formation region at an earlier stage of its chemical evolution.
  - Provides an opportunity to directly compare the chemical abundances in a more evolved (Orion KL) vs less evolved (Orion S) star forming region.

## 3. Observations:

- HIFI Spectral scan mode.
- Covered 460-1900 GHz with resolution of 1.1 MHz.
- 36.7 hours.
- $T_{rms}$ = 0.1 - 0.7 K

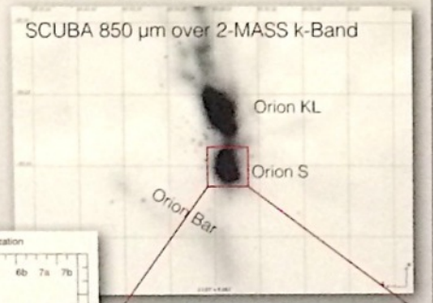


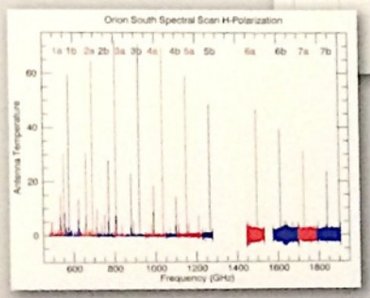


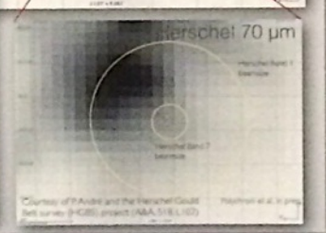


## 5. Spectral Line Modeling:

- Utilized CASSIS's to adjust $N_{tot}, T_{ex}, V_{LSR}, \Delta V_{FWHM}$, size($\theta$) iteratively to produce the best model that fits the data (via a chi-square fit).

Most species well fit by a single component.

Some species required a two-component fit.

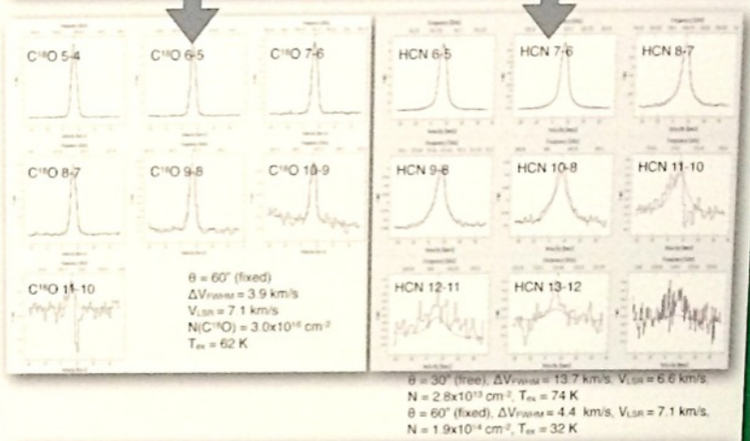


## 6. Chemical Abundances:

- Emission Properties (% of emission from each species):
  - Orion S - CO+$^{13}$CO+C$^{18}$O (70%), $CH_3OH$ (9%), $HCO^+$ (5%), $SO_2$ (<1%), $H_2O$ (1%), SO (1%).
  - Orion KL - CO+$^{13}$CO+C$^{18}$O (17%), $CH_3OH$ (33%), $HCO^+$ (10%) $SO_2$ (18%), $H_2O$ (10%), SO (7%).
- Comparison of shock tracers :
  - SiO/$HCO^+$ =0.1 (Orion S) = 5 (KL Plateau).
  - $SO_2$/$HCO^+$ =2.2 (Orion S) = 183 (KL Plateau).
  - SO/$HCO^+$ =15.5 (Orion S) = 187 (KL Plateau).
    - ➡No evidence for strong shock chemistry in Orion S despite the presences of CO and SiO Outflows.
- Comparison of UV Chemistry tracers:
  - CN/HCN=4.75 (Orion S) = 4 (KL Ext. Ridge).
  - $C_2H$/$HCO^+$ = 12.5 (Orion S)= 11 (KL Hot Core) = 3 (KL Ext. Rdg).
    - ➡Some evidence for UV chemistry in Orion S.

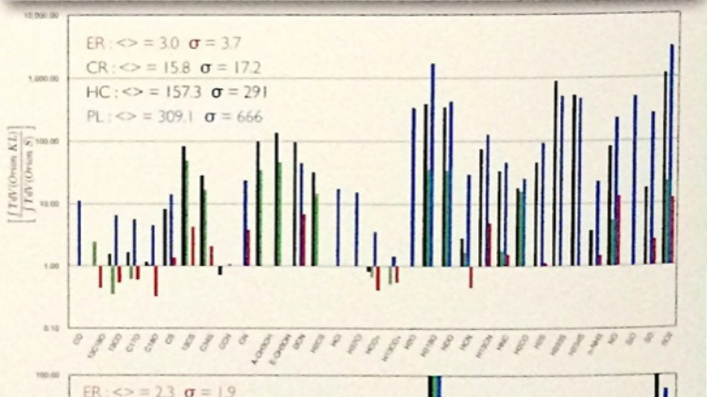


René Plume

# Star Formation in the Norma Cloud

Markus Nielbock[1], Jouni Kainulainen[1], Hendrik Linz[1], Rolf Chini[2]

[1]Max-Planck-Institut für Astronomie, Königstuhl 17, 69117 Heidelberg, Germany
[2]Astronomisches Institut der Ruhr-Universität Bochum, Universitätsstraße 150, 44801 Bochum, Germany

## Facts

The Norma Cloud is a filamentary dark cloud that is comprised of two distinct clouds, Sandqvist 187 and 188.

It is a site of low to medium mass star formation with the FU Ori star V346 Nor as its most prominent representative.

Sa 187/188 is located at a galactic latitude of +1.9° with R.A. (J2000) = 16°34ᵐ, Dec. (J2000) = -45°00' and at a distance of approximately 500 pc to 700 pc.

The filament covers an area of 36' x 12' or 7.4 pc x 2.4 pc for an assumed distance of 700 pc.

Only a few studies are available so far, mostly done at low angular resolution.

## Main goals

- to analyse data of a Herschel Key Programme as a follow-up to previous studies
- to investigate the properties of the filament/cloud (density, temperature, dimensions)
- to create a census of the embedded prestellar and protostellar population
- to derive source properties by SED fitting/modelling
- to establish the evolutionary stages of the cores and protostars



NICEST
(Lombardi et al. 2005, 2009)

NIR + MIR dust extinction mapping
(Kainulainen et al. 2013)

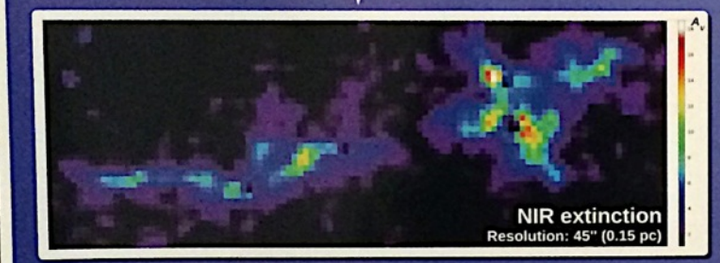


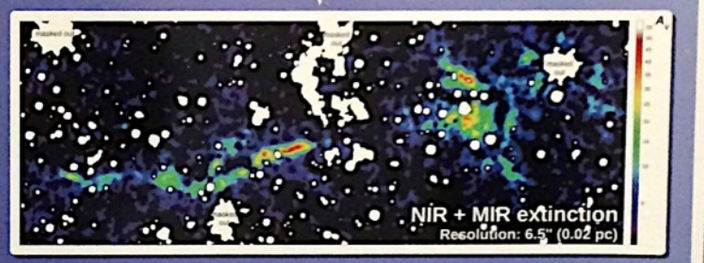


### Herschel/PACS 70 µm
**Resolution: 5.6" (4000 au)**

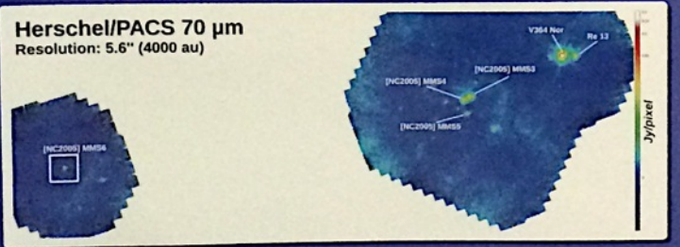


### Herschel/SPIRE 250 µm
**Resolution: 18" (12600 au)**

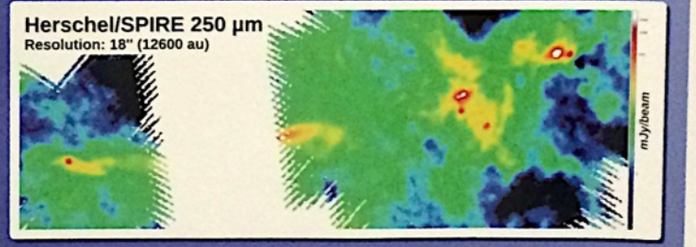


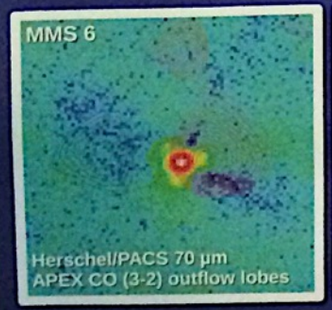


## Extinction at 70 µm

We observed MMS 6 with APEX by mapping the $^{12}$CO(3-2) line in order to find out, if the bipolar structure of reduced emission at 70 µm can be explained by an outflow cavity.

The red and blue outflow lobes do not match the bipolar structure. When compared with the other continuum data at hand, we conclude that this pattern can be explained by extinction at FIR wavelengths caused by the filament.

## Preliminary results

Based on NIR and MIR extinction measurements, the total gas mass of the Norma Cloud ranges between 500 and 1000 $M_\odot$.

The FWHM of the filament in $A_V$ is ~ 1' or (0.21 ± 0.02) pc at a distance of 700 pc.

The extinction attains values of up to $A_V$ = 50 mag in the eastern filament and up to $A_V$ = 60 mag in the western part of the Norma Cloud.

The number of candidate protostars was increased from a handful to some 40 objects.

There appears to be a wide spread in evolutionary stages.

Background source contamination cannot be ruled out for now.

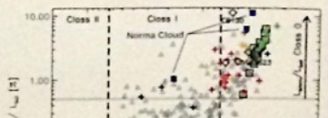


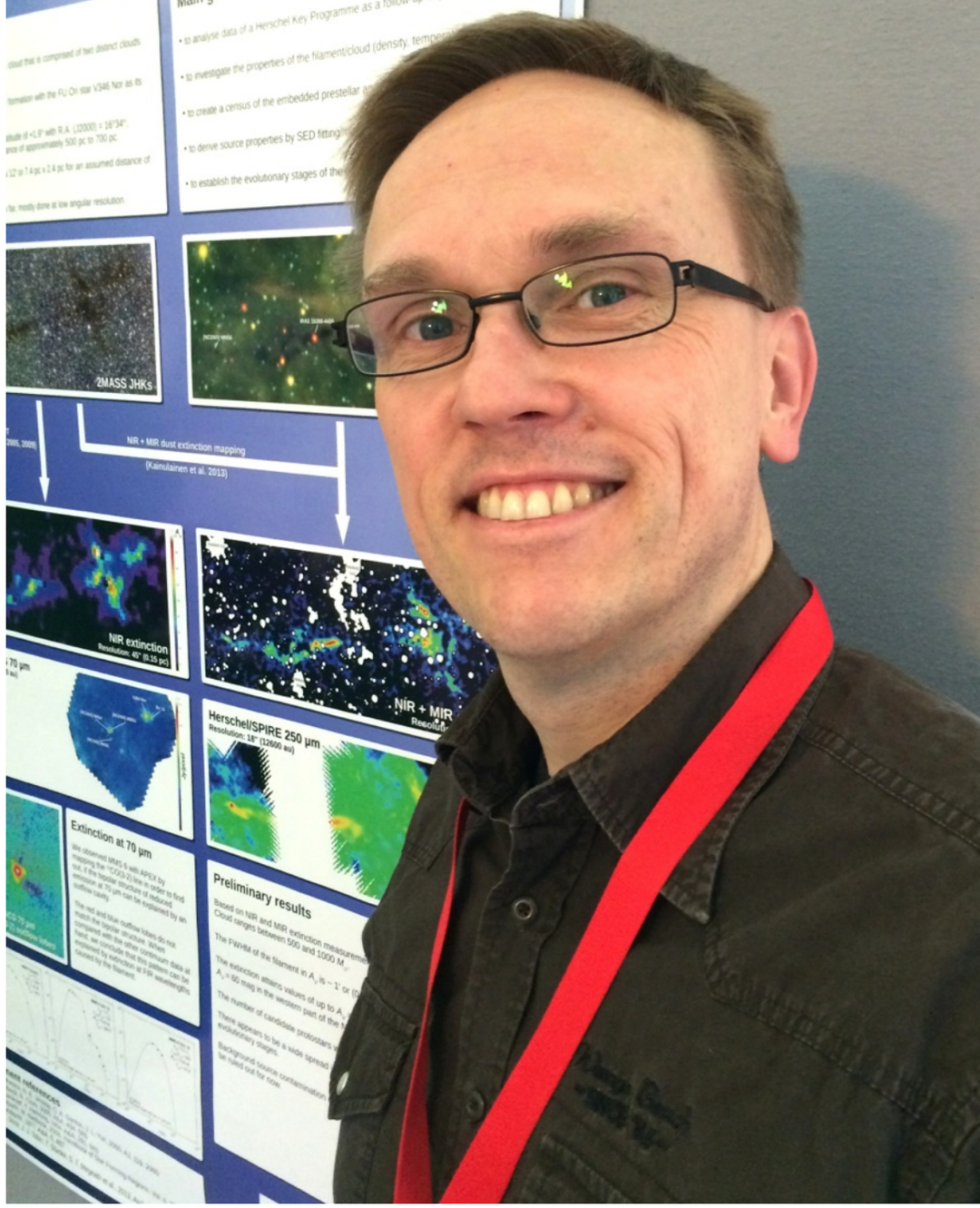

Markus Nielbock

# The fate of ionization triggered stars - Is Orion too dense?

Alexander von Humboldt

Matthias Gritschneder[1], Andreas Burkert[1,2], Doug Lin[3]

[1]University Observatory, Munich, [2]Max-Planck Institute for Extraterrestrial Physics, Munich, [3]University of California, Santa Cruz

## Abstract

We present a novel implementation of ionizing radiation into the SPH code SEREN. By using a Monte Carlo ray-shooting technique we are able to achieve a scaling which is independent of the number of sources. As a first application, we simulate the evolution of an Orion-like HII-region. The front position and speed develop as expected. However, the shock density in the simulations is lower than anticipated. Consequently, star formation is delayed and less efficient.

## Introduction

HII-regions and their constituents have been at the forefront of astronomic research for a long time. Generally, the morphology and idealized evolution of HII regions are well understood (e.g. Spitzer 1978). The location of young stellar objects (YSOs) in HII regions provide important information on their origin. However, up to now, little attention has been given to the question of how the YSOs have reached their current location. Among the YSOs, the so-called proplyds (short for protoplanetary disks) are particularly interesting. These are young protostellar disks, illuminated by an O-star in direct proximity. In Gritschneder & Burkert (2014), we used an analytic approach to investigate the heritage of the YSOs.

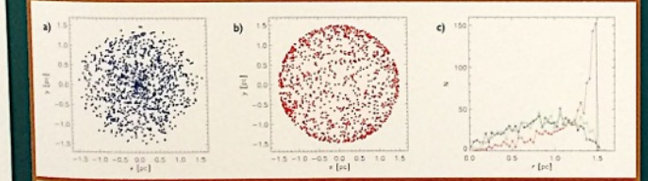

*Figure 1: a) Distribution of stars formed in a homogeneous sphere, b) distribution of stars triggered in a shell swept up by ionized gas, and c) comparison in radial bins.*

## Analytical Results

We use an analytical prescription for the position of the ionization front and assume that stars form at a constant rate in the swept up shell during 200-500 kyr after the ignition of the source. Then, we follow the trajectories of the formed stars under the influence of the gravity of the gas. We find that in general the stars inside HII-regions are likely not stars triggered within the shell of the ionisation front, as they would have formed with too high radial velocities to have returned yet. However, when compared to in situ star formation, the triggered component shows a ring-structure, making it possible to distinguish the two cases (Fig. 1).

## Method

We present a fully parallel implementation of ionization in the SPH code SEREN (Hubber et al 2013) via Monte-Carlo rays. The rays are shot in random directions, the number of rays per source is selected according to the luminosity of the source. The main advantage of this method is that the computation scales independent of the number of sources. Instead, the number of rays depends on the size of the ionized domain. Along these rays the photons are deposited. As a particle can be intersected by multiple rays, it is necessary to calculate two sweeps, one where the incoming photons are deposited and one where the new ionization degree is calculated as deposited photons divided by required photons.

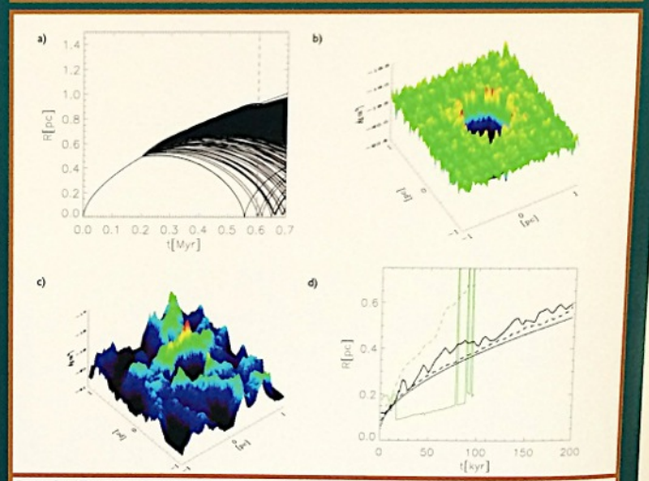

*Figure 2: a) Trajectories for triggered stars in Orion, b) simulation of the ionization of a constant density medium at t=100kyr, c) ionization of a turbulent cloud at t=100 kyr, and d) comparison of the ionization front (dashed) and shock front (solid) in both cases with the analytical predictions (blue: analytic, black: homogeneous, green: turbulent).*

## Numerical Results

To investigate the formation of Orion, we perform simulations with either a constant medium or a turbulent medium (Mach 5) with a mean number density of $n=4x10^4$ cm$^{-3}$. These setups get ionized by an Orion-like source with $10^{49}$ UV-photons per second. Whereas the evolution in both cases is as expected for an HII-region (Fig. 2b-d), the shocked density is quite small, as the initial high pressure region is very small. Therefore, star formation is less effective than predicted and in the turbulent case dominated by in situ stars.

## Conclusions

In the homogeneous case, star formation occurs later and is less efficient than previously estimated. In the turbulent case, star formation is mostly in situ and not triggered. Altogether, Orion seems to be too dense to be the ideal testbed to study ionization triggered star formation.

## References

Gritschneder, M. & Burkert, A., 2014, MNRAS, 438, 1318

Hubber, D.A.; Batty, C. P.; McLeod, A.; Whitworth, A. P., 2011, A&A, 529, 28

Spitzer L., 1978, Physical processes in the interstellar medium, Wiley-Interscience, New York

Matthias Gritschneder

# TADPOL polarization in protostellar cores

Chat Hull
UC Berkeley
chat@astro.berkeley.edu

## agnetic fields are (sometimes) consistent from core to envelope scales...


Sources with LOW polarization fraction (< 3%) have B-fields that are inconsistent from large to small scales

**B-field consistency from 10,000 → 1000 AU**

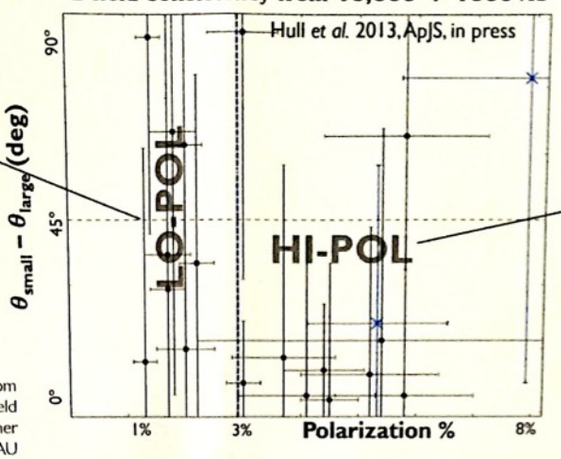


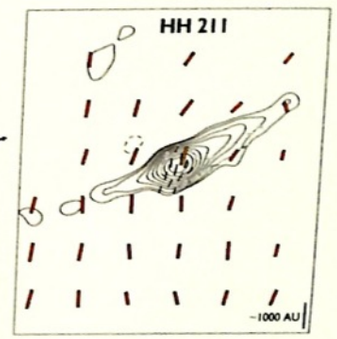


Sources with HIGH polarization fraction (>3%) have consistent large- and small-scale B-fields

Above/right: comparison of B-field orientations at large-scales (~10,000 AU, from SCUBA/CSO) and small-scales (~1000 AU, from CARMA). Center: B-field consistency vs. average dust polarization fraction in the core. Sources with higher polarization fractions have more consistent B-fields from 10,000 – 1000 AU scales. From Hull et al. 2014, ApJS, in press (arXiv:1310.6653)

## Yet...

### LO-POL sources have outflows and B-fields that are preferentially perpendicular

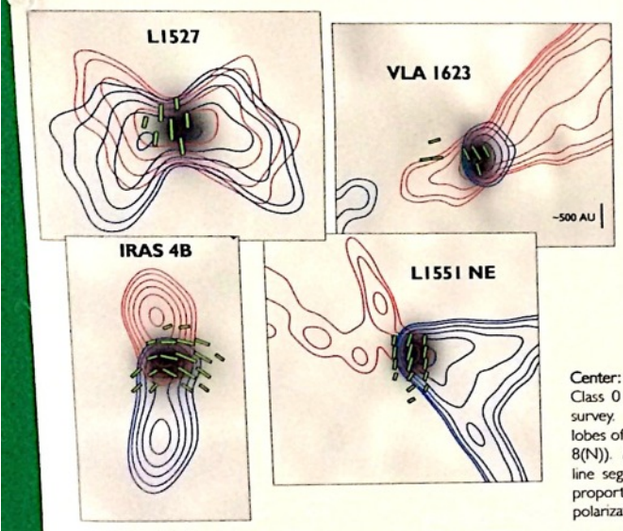


**Outflow vs. B-field orientations**

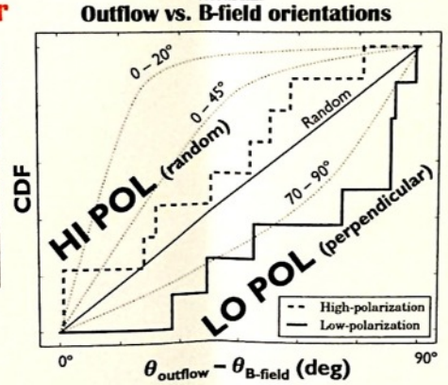


### HI-POL sources have outflows and B-fields that are randomly aligned

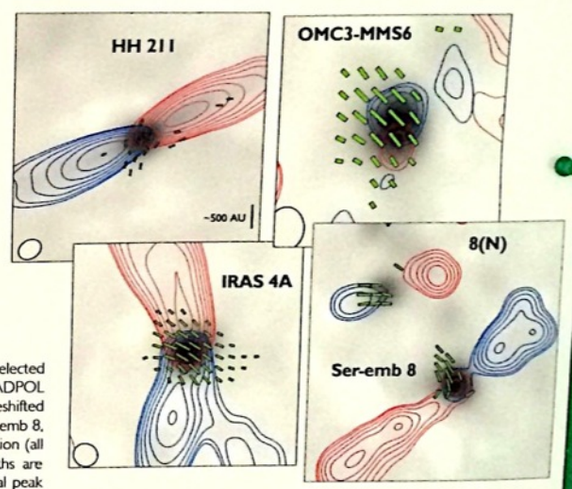


Center: comparison of outflow vs. small-scale B-field orientations. Left/right: selected Class 0 protostellar cores mapped at 1.3 mm as part of the CARMA TADPOL survey. *Grayscale:* Stokes *I* thermal dust emission. *Contours:* red- and blueshifted lobes of the sources' bipolar outflows, mapped in CO(2–1) or SiO(5–4) (Ser-emb 8, 8(N)). *Line segments:* magnetic field orientations inferred from dust polarization (all line segments are rotated by 90° to indicate the B-field). Segment lengths are proportional to the square root of polarized intensity, not percentage (typical peak polarization is a few percent). From Hull et al. 2014, ApJS, in press (arXiv:1310.6653)

## Future = 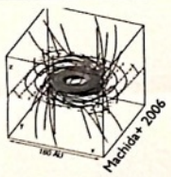 ?



Will ALMA see toroidally wrapped B-fields at ~100 AU disk scales in both low- and high-polarization sources?

Stay tuned for **ALMA Cycle 2** data!

Proposal **2013.1.00726.S**
PI: Hull, highest priority

**0.3" (~150 AU)** resolution dust polarization (@ Band 7)
Outflows & dense tracers (@ Band 6)

## Conclusions

- **LO-POL:** B-fields may be wrapped up by envelope rotation
  - This could aid in disk formation
- **HI-POL:** B-fields may be remnants of the "global field" drawn in by gravitational collapse
  - Outflows are not tightly aligned with the B-fields in the cores out of which they formed (see Hull et al. 2013, ApJ, 768, 159)

**Observations powered by the CARMA 1.3 mm full-Stokes system**

Hull et al. 2014, in prep


Chat Hull

# Things we should do

# Be concrete

## Things we call filaments:

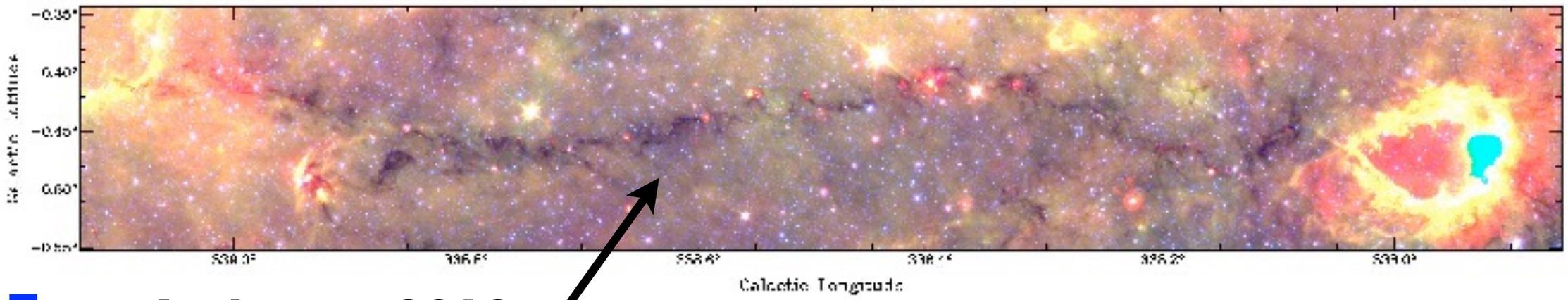


entire clouds

**Jackson+ 2010**:
L ~ 80 pc ; M ~ 10,000-40,000 $M_\odot$

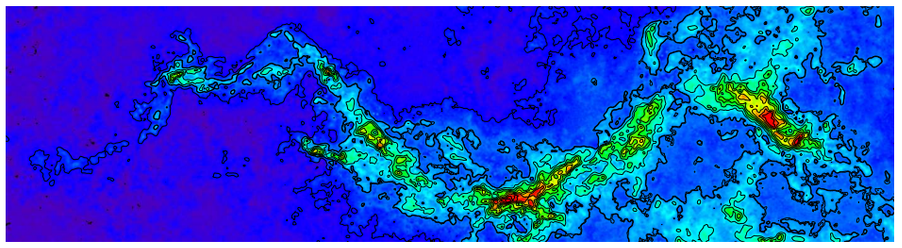

**Kainulainen+ 2013**:
L ~ 30 pc ; M ~ 18,000 $M_\odot$

parts of a cloud

**Schmalzl+ 2010**: L ~ 10 pc ; M ~ 700 $M_\odot$

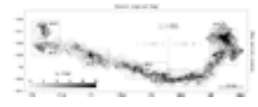

**(original Barnard's "dark lanes")**

**Hacar+ 2011**: L ~ 0.5 pc ; M ~ 10 $M_\odot$

**Tobin+ 2012**: L ~ 10,000 AU; M < 1 $M_\odot$

(slide from Alvaro Hacar)

# But what is actually a filament?

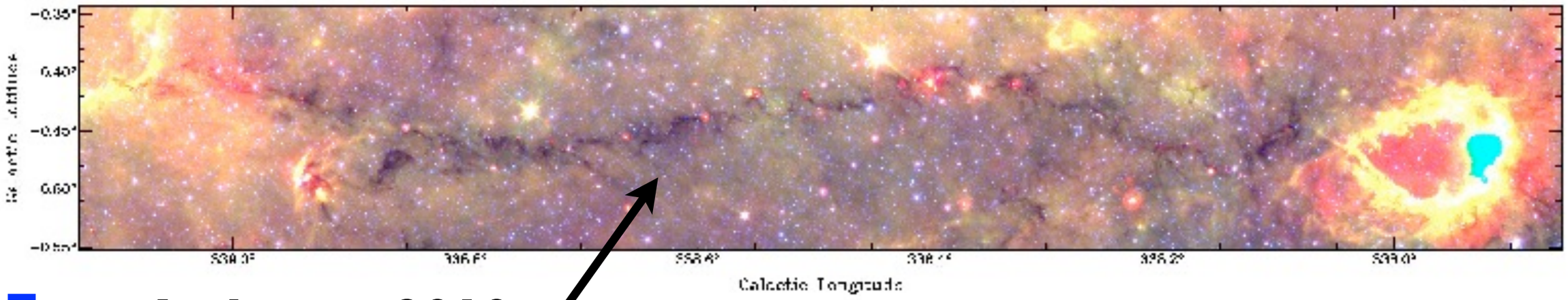


entire clouds

**Jackson+ 2010**:
L ~ 80 pc ; M ~ 10,000-40,000 $M_\odot$

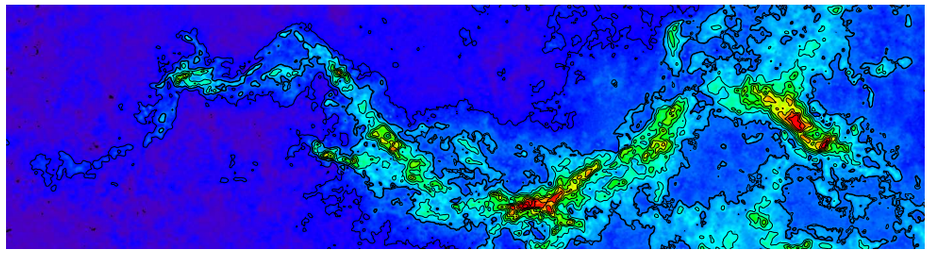

**Kainulainen+ 2013**:
L ~ 30 pc ; M ~ 18,000 $M_\odot$

parts of a cloud

**Schmalzl+ 2**
**(original Bar**

**Hacar+**

**Tobin+ 2**

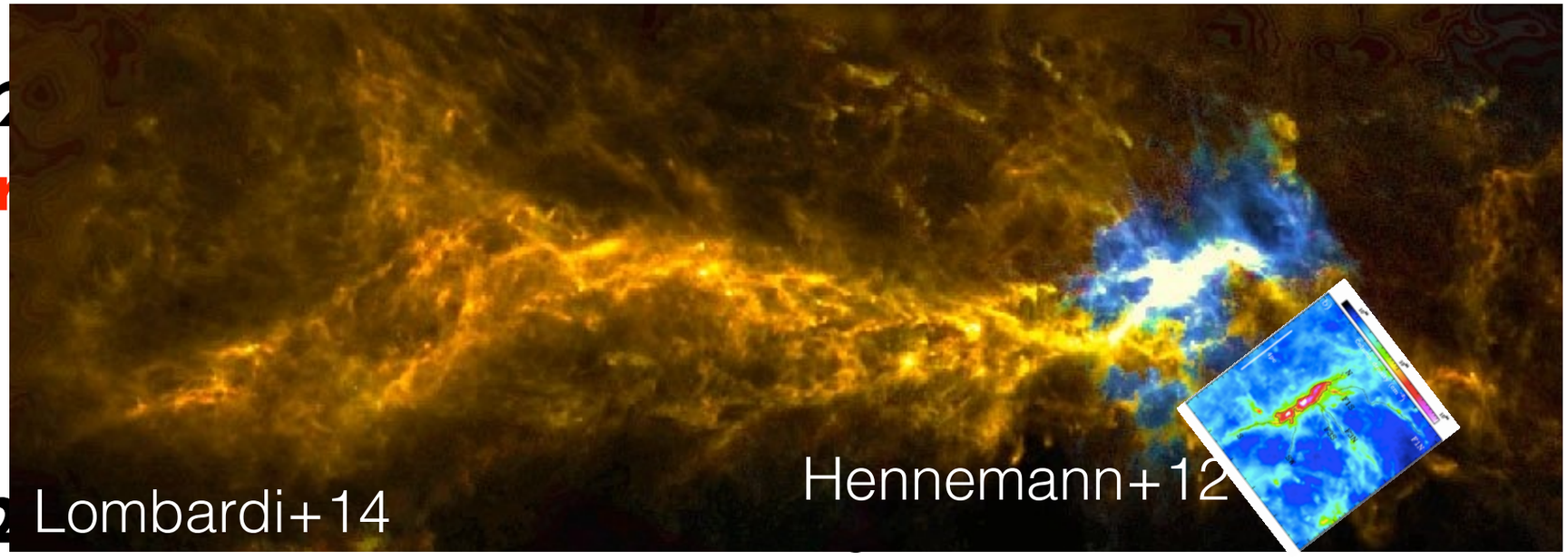

# Be educational

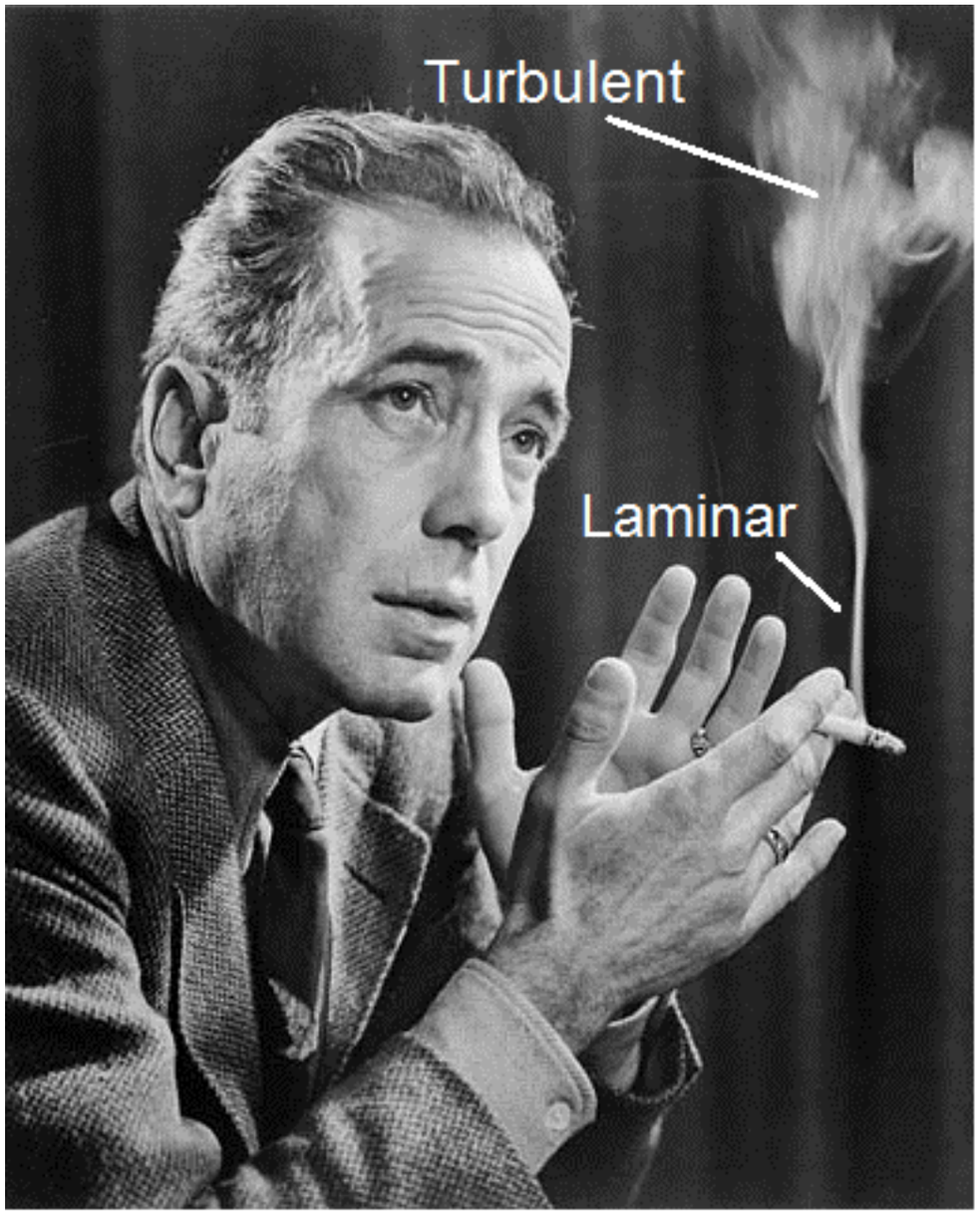


Good

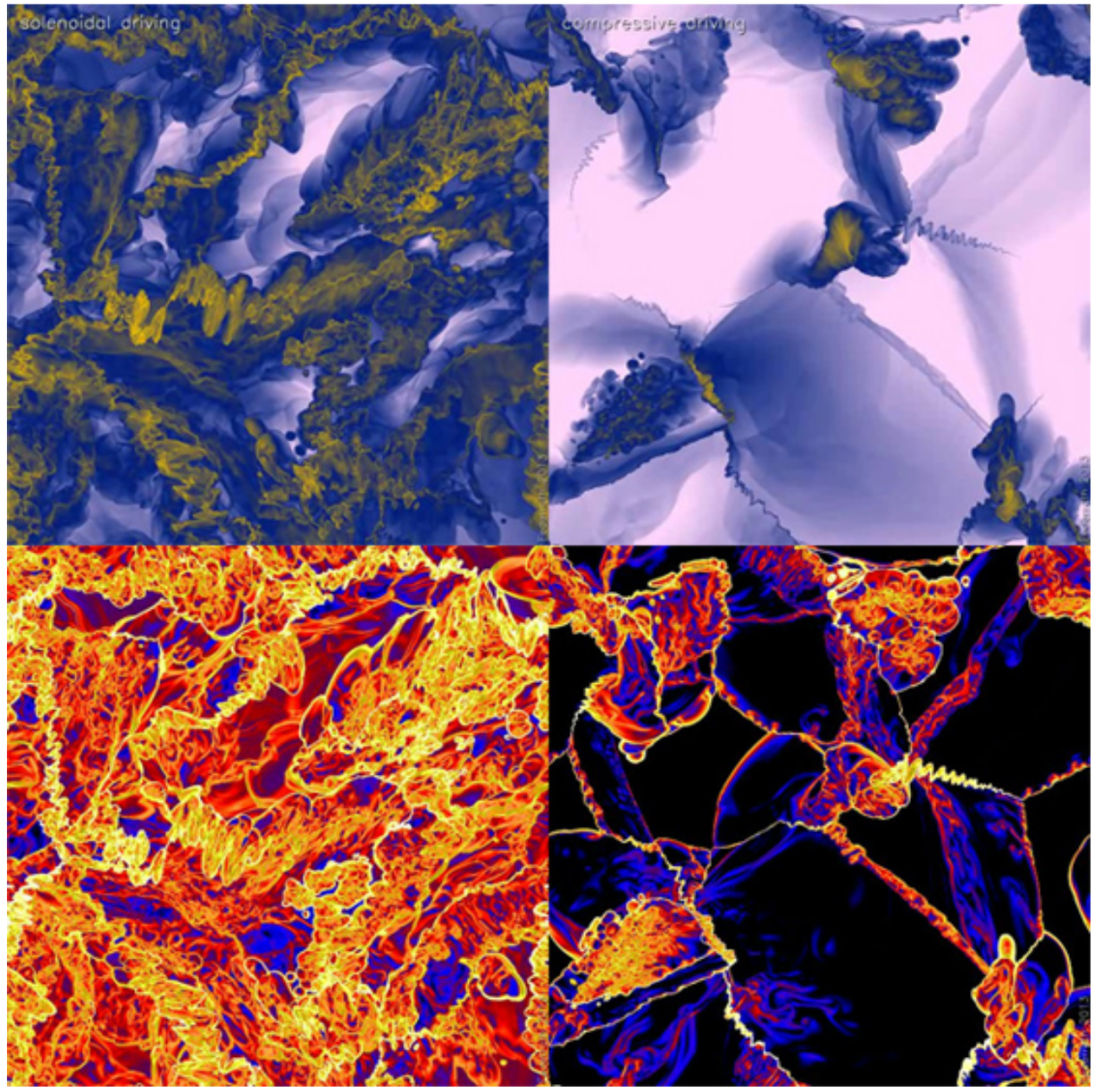


Bad

# Final thoughts

- Are we making progress?

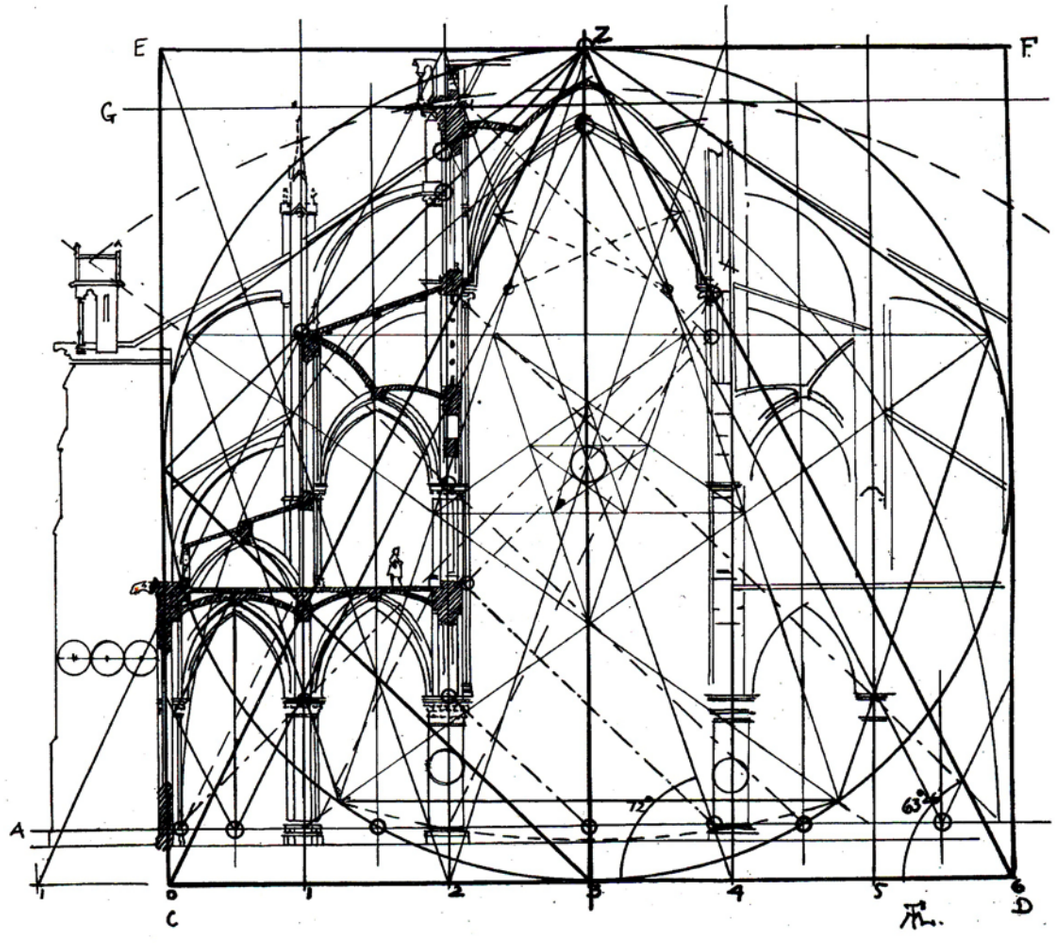

“We always have to be prepared for new perspectives that are now beyond our imagination”

-Adriaan Blaauw

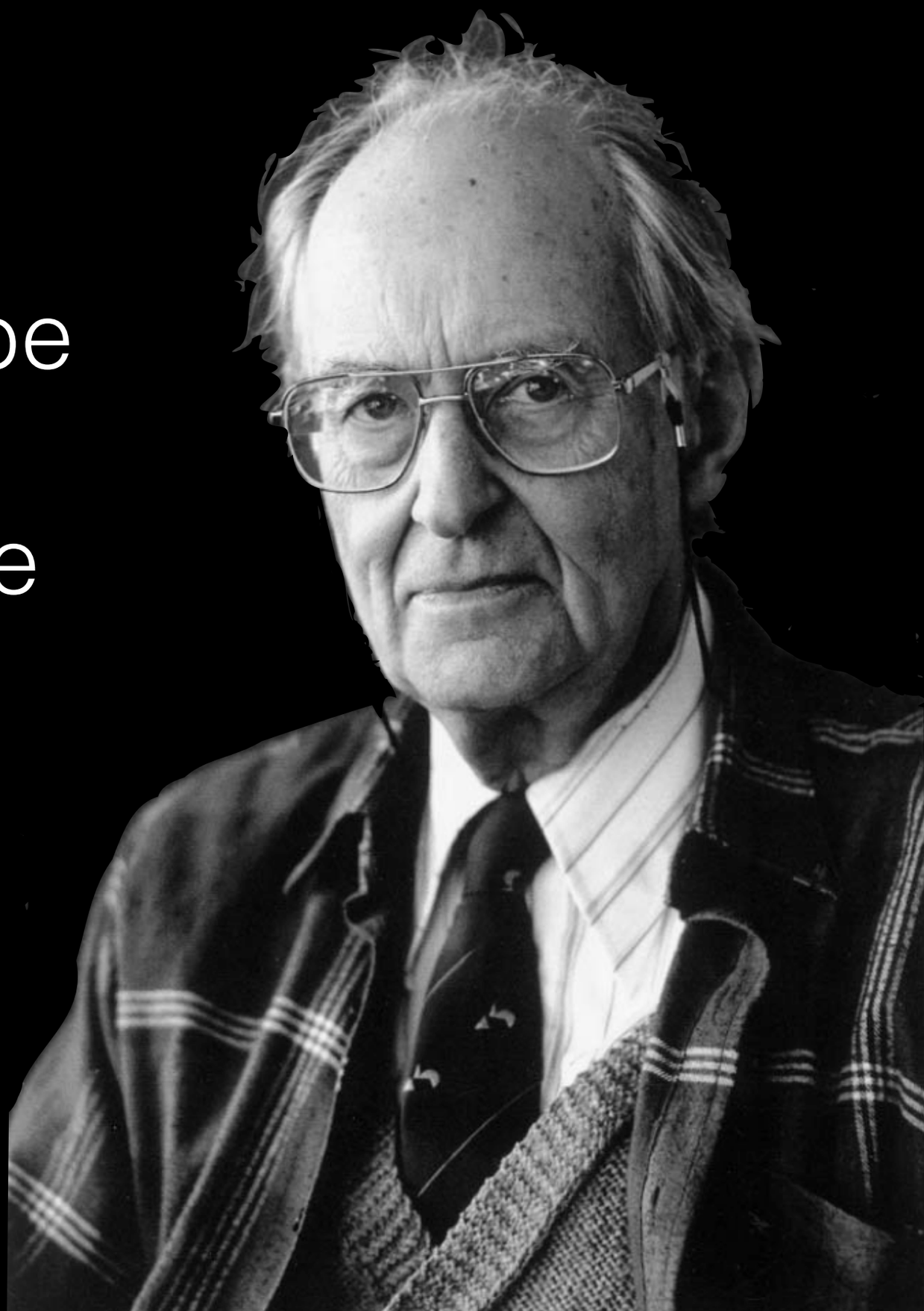

# The quotable EPoS 2014

- The paper should be out in a month (Molinari++)

- The clue is to understand the slides I skipped (Falgarone)

- If the rad. pressure problem was at 18 Msun, it would be a solved problem in 1977 (Kuiper)

- I left the Chemistry slides to the end in case I would run out of time (Arce)

- Gritschneder: If the interpretation of your simulation takes longer than running the simulation, you’re doing something wrong.

# The quotable EPoS 2014

- It's so easy to be the arrogant male theorist (Anon.)

- B-fields are NOT complicated (Basu)

- They are still blobs, but these were the smallest blobs I ever observed (Friesen)

- Accreting dense gas is good (Smith)

- EPoS, would this work? Would people put science politics aside and discuss weak points? (Steinacker)

# The Ringberg Muse

(fibers and cores?)

# The Ringberg Muse

(role of filaments in cluster formation?)

# The Ringberg Muse

(mass loading?)

# The Ringberg Muse

(binary ejection from a puffed-up disk?)

# The Ringberg Muse

(toroidal magnetic field?)

Oh Ringberg Muse! You revealed so much since 2006. Can't you reveal me the very last secret?


I mean, is it Turbulence? B? or Jeans? Do I really need all of them?

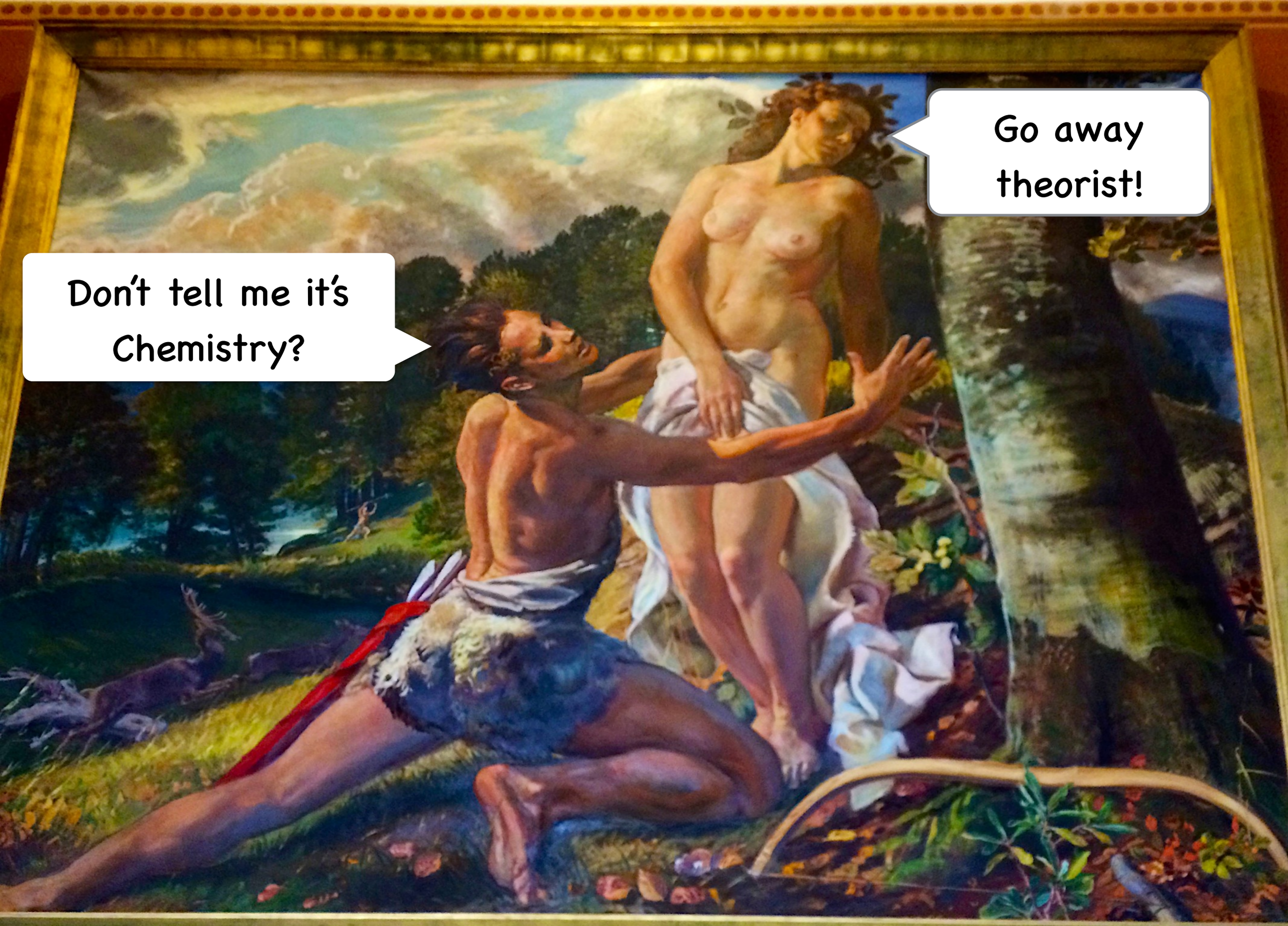
Don't tell me it's Chemistry?
Go away theorist!

*sigh*

But Muse,
we were never this
close to the truth.
Can't I just peek?

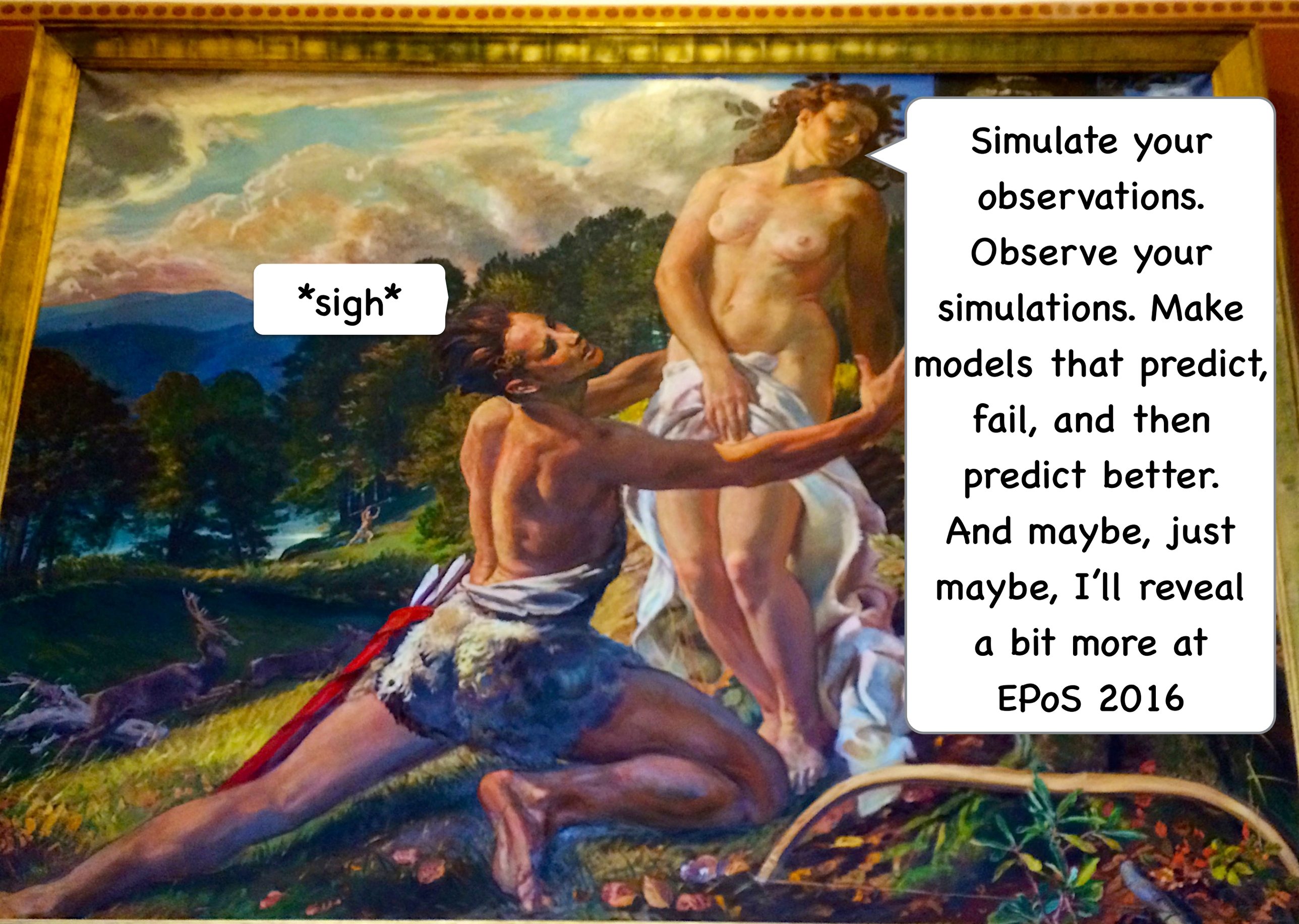
*sigh*
Simulate your observations. Observe your simulations. Make models that predict, fail, and then predict better. And maybe, just maybe, I'll reveal a bit more at EPoS 2016